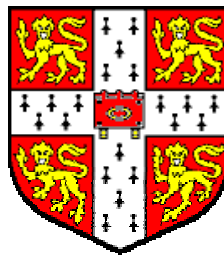


Equalization and Space-Time Processing for Fixed Broadband Wireless Access Systems

Ernst Karl Bartsch

Churchill College
University of Cambridge



A dissertation submitted for the degree of
Doctor of Philosophy

October 2002

to my parents

Rosemarie and Kurt Bartsch

for their encouragement, support and their belief in me

Abstract

This research investigates the performance of adaptive equalization and adaptive space-time processing for fixed broadband wireless access systems (FBWA).

Firstly equalization for single-antenna FBWA systems is considered. Linear equalizer and decision feedback equalizer (DFE) architectures are studied. Three types of tap-update algorithms are considered for systems operating in the multi-channel multipoint distribution services (MMDS) band, namely: (i) the least mean square (LMS) algorithm, (ii) the recursive least square (RLS) algorithm and (iii) the recursive least square lattice (LSL) algorithm. The equalization performance study shows the tradeoff between complexity and performance in terms of probability of symbol error (P_s) and convergence time. The LSL algorithm is shown to have a similar convergence time and P_s performance to the conventional RLS algorithm, but with greatly reduced computational complexity. In particular the LSL algorithm is nearly 3 times less computationally complex than the RLS algorithm for the SUI-3 channel. Secondly the performance of a space-time DFE trained with the LMS algorithm for the MMDS band is investigated employing single user detection. The improvement in performance gained with the use of multiple antennas at the base station (BS) is particularly demonstrated by the achievement of low P_s at low SNR values. It is observed that the minimum mean square error (MMSE) is significantly reduced as the number of BS antennas is increased. The MMSE values achieved with 1, 2, 4 and 8 antennas are $1.2 \cdot 10^{-2}$, $6.2 \cdot 10^{-3}$, $3.3 \cdot 10^{-3}$ and $2.0 \cdot 10^{-3}$ respectively for the SUI-2 channel model with a SNR of 20dB.

The performance of space-time algorithms strongly depends upon the underlying channel model. This research uses the Gaussian Wide Sense Stationary Uncorrelated Scatter (GWSSUS) channel modelling approach to assess the performance of the proposed systems. A closed form expression for the cross-correlation coefficient ρ is derived, which allows easy evaluation of the cross-correlation of the fading envelopes when a strong specular component (i.e. Rician fading) is present.

Many space-time equalization algorithms require a good estimate of the channel impulse response. Additional when FBWA systems are considered, low complexity is another design goal. Therefore a new low complexity cross-correlation based channel estimation method, which is based on cyclically shifting optimal sounding sequences to generate a set of zero correlation zone (ZCZ) sequences is proposed. With the proposed sequences one correlator is capable of estimating up to M SDMA/TDMA user channels. It is shown that the proposed cross-correlation channel estimation has the same performance than a full-rank maximum likelihood (FR-ML) channel estimation.

In addition to the performance study of standard adaptive time-domain and space-time adaptive equalizers, a novel multi-user space division multiple access (SDMA)/time division multiple access (TDMA) approach is presented. This approach combines adaptive filtering with successive interference cancellation (SIC). The space-time DFEs are either trained with the LMS algorithm or the RLS algorithm. The proposed SDMA/TDMA FBWA architecture consists of single antenna subscriber units (SUs) and BSs with multiple antennas. The architecture and training algorithms are of low computational complexity and are therefore a good candidate for FBWA systems. The performance of the proposed architecture is investigated for a number of different FBWA channels and BS antenna array configurations. Additionally the effect of symbol error propagation through the successive space-time DFE stages is studied and its implications are discussed. Finally the proposed combined space-time DFE/SIC system is compared with a MIMO DFE. For this purpose both systems are trained with the RLS algorithm. It is shown that the proposed combined space-time DFE/SIC system has a superior P_s performance to that of the MIMO DFE system.

Declaration

I hereby declare this thesis and the work reported herein is the result of my own work during my PhD study at the Cambridge University Engineering Department.

Except as indicated in the thesis, the contents are entirely original and are not the outcome of any work done in collaboration.

This dissertation is not substantially the same as any that I have previously submitted for a degree or diploma or any other qualification at other universities. Further no part of this thesis has already been, or is currently submitted for any such degree or diploma or other qualification.

This Ph.D. dissertation does not exceed 65,000 words, including appendices, bibliography, footnotes, tables and equations and does not contain more than 150 figures.



Ernst Karl Bartsch

Acknowledgements

I owe special thanks to my supervisor, Ian Wassell, for his guidance and encouragement during my research. His comments and suggestions are greatly appreciated.

I would also like to thank Adaptive Broadband Corp. for sponsoring this research. Special thanks also to Paul Hiscock for coding a very powerful simulator in C++, which facilitated the computational intensive Monte-Carlo simulations.

I am indebted to Malcolm Sellars for many interesting discussions about equalization techniques for high data-rate wireless systems.

Thanks are also due to Simon Godsill for many useful discussions and for being my PhD advisor.

I would like to express my gratitude to Jochen Hammerschmidt and Christopf Farsak from the TU-München and Siemens AG, Munich, respectively, as well as to Per Zetterberg from Radio Design AB in Sweden, for many fruitful discussions regarding space-time channel modelling using the Gaussian wide sense stationary uncorrelated scattering channel model.

Special thanks also to Ali Abdi from the New Jersey Institute of Technology for many constructive email discussions regarding modelling the cross-correlation in case of Rician fading space-time channels.

Last but not least, I would like to express my gratitude to Prof. Andy Hopper from the University of Cambridge for setting up an excellent research environment, the Laboratory for Communications Engineering and giving me the opportunity to do my Phd in this group.

I am also indebted to a number of people for proof reading this dissertation. Thanks to Malcolm Sellars and Ian Wassell.

Finally thanks to all those people, who I forgot to include and all my friends at the University of Cambridge, who made my stay here very pleasant and enjoyable.

Publications

Parts of this thesis have been published in the following papers:

1. E.K. Bartsch, I.J. Wassell and M.P. Sellars
Equalization Requirement Study For Broadband MMDS Wireless Access Systems
International Symposium on Communications (ISCOM), November 2001
2. E.K. Bartsch and I.J. Wassell
Multiuser cross-correlation channel estimation for SDMA/TDMA systems
35th Asilomar Conference on Signals, Systems and Computers, November 2001
3. E.K. Bartsch and I.J. Wassell
An Adaptive Space-time DFE Combined with Successive Interference Cancellation
IEEE Wireless Communications and Networking Conference (WCNC), March 2002

Table of Contents

Chapter 1: Introduction	1
1.1 Standardization and frequency bands	3
1.2 Last mile problem	3
1.3 Broadband access technologies	4
1.3.1 Digital subscriber line	5
1.3.2 Cable modem	6
1.3.3 Optical fibre networks	6
1.3.4 Satellite	7
1.3.5 Fixed broadband wireless access	7
1.4 The unique possibilities FBWA can offer.	8
1.5 Challenges of FBWA system design	8
1.6 Motivation	9
1.7 Novel achievements	9
1.8 Overview	12
Chapter 2: State of the Art Equalization and Space-Time Processing for High Data-Rate Wireless Systems	14
2.1 Equalizer Architectures	17
2.1.1 Linear Equalizer and DFE	17
2.1.2 Lattice DFE	19
2.1.3 Space-time DFE	20
2.1.4 MIMO DFE	21
2.2 Optimal equalizer settings	22
2.3 Adaptive equalization tuning algorithms	24
2.3.1 Least mean square algorithm	25
2.3.2 Recursive least squares algorithm	26
2.4 Complexity reduction techniques	28
2.5 Multiple antennas at the base station	29
2.5.1 Space-time processing in the uplink	31
2.5.2 Space-time processing in the downlink	32
Chapter 3: Channel Modelling for Fixed Broadband Wireless Access Systems	33
3.1 FBWA environments	33
3.2 Channel modelling for single antenna FBWA systems	35

3.3	Channel modelling for space-time processing in the uplink	36
3.3.1	Ideal diversity channel	37
3.3.2	Statistical channel models	37
3.3.2.1	‘One-ring’ spatial model	37
3.3.2.2	Gaussian wide sense stationary uncorrelated scatterer model	38
3.3.2.3	Gaussian angle of arrival model	47
3.3.2.4	Model parameters and assumptions for simulating a FBWA uplink	47
3.3.2.5	Numerical examples of ρ	49
3.3.3	Ray tracing simulation	52
3.4	Conclusions	53
Chapter 4: Equalization Requirement Study for Single Antenna MMDS FBWA Systems		54
4.1	Introduction	54
4.2	Algorithms studied	55
4.3	Simulation model and simulation parameters	55
4.4	Performance	56
4.5	Complexity	60
4.6	Conclusions	62
Chapter 5: Cross-Correlation Channel Estimation for Multi-Antenna Fixed Broadband Wireless Access Base Stations		63
5.1	Introduction	63
5.2	Single-user cross-correlation channel estimation	64
5.3	Multi-user cross-correlation channel estimation	65
5.3.1	System	65
5.3.2	Cross-correlation method	67
5.3.3	Definitions	68
5.3.4	ZCZ sequence set construction	70
5.4	FR-ML channel estimation	73
5.5	Performance	73
5.6	Conclusions	76
Chapter 6: Space-Time Processing in the Uplink for Fixed Broadband Wireless Access		77
6.1	Introduction	77
6.2	Proposed SDMA/TDMA FBWA system	78
6.2.1	System model	80
6.2.2	Successive interference cancellation	81

6.2.3	Signal ordering	82
6.3	Simulation Results	83
6.3.1	Single-user detection	84
6.3.1.1	Convergence investigation	84
6.3.1.2	Probability of symbol error	85
6.3.2	Multi-user detection	87
6.3.2.1	Convergence investigation	87
6.3.2.2	Error Propagation through the successive detection stages	90
6.3.2.3	Probability of symbol error performance	91
6.3.2.4	2 SIC stages for 2 users	99
6.3.2.5	Space-Time DFE/SIC compared with MIMO DFE	101
6.4	Conclusions	102
Chapter 7: Conclusions		105
Chapter 8: Future Work		108
8.1	Channel Modelling for FBWA MIMO channels	108
8.2	Performance Study of the LSL algorithm	108
8.2.1	Fractionally symbol spaced taps	108
8.2.2	High-order modulation schemes	108
8.3	Cross-Correlation channel estimation for MIMO FBWA systems	109
8.4	Space-time processing for the FBWA downlink	109
8.4.1	MIMO pre-coding	109
8.4.2	Space-time coding	109
8.5	Improvements for the proposed SDMA/TDMA system	110
8.5.1	Signal ordering based on the post-detection SNR	110
8.5.2	Techniques for preventing error propagation through the SIC stages	110
8.5.3	Antenna array at the SU and at the BS	110
Appendix A: Spatial fading cross-correlation for Rician channels using the GWSSUS channel model		111
References		123

Table of Figures

Fig. 1-1:	FBWA deployment scenario	2
Fig. 1-2:	Broadband access technologies	4
Fig. 2-1:	LE and DFE	18
Fig. 2-2:	LSLDFE	19
Fig. 2-3:	Lattice stage	19
Fig. 2-4:	Space-time DFE	20
Fig. 2-5:	MIMO DFE	21
Fig. 2-6:	Temporal and spatial processing for FBWA systems	29
Fig. 3-1:	Typical FBWA environment	33
Fig. 3-2:	SUI-2 channel model	35
Fig. 3-3:	SUI-3 channel model	35
Fig. 3-4:	FBWA system with BS equipped with dual antenna array	37
Fig. 3-5:	GWSSUS channel model	39
Fig. 3-6:	Modelling the frequency-selective channel with a 2D FIR filter structure	41
Fig. 3-7:	SIMO channel modelling according to Abdi [Abdi02]	43
Fig. 3-8:	LOS paths when SU is located in the far field	44
Fig. 3-9:	Fading cross-correlation ρ for a mean DOA of 30° for the diffuse component and a mean DOA of 60° for the LOS component with a K-factor of 10	49
Fig. 3-10:	Closed-form expression for ρ and numerical evaluation for a DOA spread of 3° for scenario of Fig. 3-9	50
Fig. 3-11:	Closed-form expression for ρ and numerical evaluation for a DOA spread of 40° for scenario of Fig. 3-9 (max. error = 2.2%)	50
Fig. 3-12:	Fading cross-correlation ρ for a mean DOA of 30° for the diffuse component and a mean DOA of 60° for the LOS component with a K-factor of 3	50
Fig. 3-13:	Closed-form expression for ρ and numerical evaluation for a DOA spread of 3° for scenario of Fig. 3-12	51
Fig. 3-14:	Closed-form expression for ρ and numerical evaluation for a DOA spread of 40° for scenario of Fig. 3-12 (max. error = 8%)	51
Fig. 3-15:	Fading cross-correlation ρ for a mean DOA of 30° in azimuth for the diffuse component and a mean DOA of 60° in azimuth for the LOS component with a K-factor of 3, the mean DOA in elevation for both components is 10°	51
Fig. 3-16:	Closed-form expression for ρ and numerical evaluation for a DOA spread of 3° for scenario of Fig. 3-15	52

Fig. 3-17:	Closed-form expression for ρ and numerical evaluation for a DOA spread of 40° for scenario of Fig. 3-15 (max. error = 4%)	52
Fig. 4-1:	Simulation model	56
Fig. 4-2:	Convergence rate for channel SUI-2: a) RLSDFE, b) LSLDFE c) LMSDFE and d) LMSLE	57
Fig. 4-3:	Probability of symbol error for channel SUI-2: a) matched filter bound for AWGN channel, b) RLSDFE, c) LSLDFE, d) LMSDFE and e) LMSLE	58
Fig. 4-4:	Convergence rate for channel SUI-3: a) RLSDFE, b) LSLDFE c) LMSDFE and d) LMSLE	59
Fig. 4-5:	Probability of symbol error for channel SUI-3: a) matched filter bound for AWGN channel, b) RLSDFE, c) LSLDFE, d) LMSDFE and e) LMSLE	60
Fig. 4-6:	Complexity: a) LMS, b) LSL and c) standard RLS (for equations see Table 4-1)	61
Fig. 5-1:	SDMA/TDMA system model	66
Fig. 5-2:	SDMA packet	66
Fig. 5-3:	Correlator output on antenna 1	67
Fig. 5-4:	Autocorrelation of optimum sounding sequence of length $N=16$	69
Fig. 5-5:	Mothersequence s_1	70
Fig. 5-6:	Correlation functions of a sequence set of size 4	71
Fig. 5-7:	Channel estimate of antenna 1 $\hat{h}_{est,1}$ without AWGN	74
Fig. 5-8:	Channel estimate of antenna 1 $\hat{h}_{est,1}$ with a SNR of 20dB	75
Fig. 5-9:	MSE vs. SNR	75
Fig. 6-1:	Proposed SDMA/TDMA FBWA system for 2 SDMA users	78
Fig. 6-2:	Convergence curves for space-time DFE (8,7), ULA(0.5λ spacing), DOA spread 3° for SUI-2 channel with: a) 1 antenna, b) 2 antennas, c) 4 antennas and d) 8 antennas	84
Fig. 6-3:	Convergence rate for SUI-3 using space-time DFE(8,7), ULA(0.5λ spacing), DOA spread 40° : a) 1 antenna, b) 2 antennas, c) 4 antennas and d) 8 antennas	85
Fig. 6-4:	Convergence rate for SUI-3 using space-time DFE(15,10), ULA(0.5λ spacing), DOA spread 40° : a) 1 antenna, b) 2 antennas, c) 4 antennas and d) 8 antennas	85
Fig. 6-5:	P_s for SUI-2 channel	86
Fig. 6-6:	P_s for SUI-3 channel	87
Fig. 6-7:	Convergence plot for SUI-2, ULA(10λ spacing), DOA spread 3° : a) noSIC user ₂ , b) corSIC user ₂ , c) idealSIC user ₂ and d) noSIC user ₁	89
Fig. 6-8:	Convergence plot for SUI-3, ULA(0.5λ spacing), DOA spread 40° : a) noSIC user ₂ , b) corSIC user ₂ , c) idealSIC user ₂ and d) noSIC user ₁	90

Fig. 6-9:	Ps for SUI-2 channel, SIR=5dB, 2 antennas, $10\cdot\lambda$, 2 users	92
Fig. 6-10:	Ps for SUI-2 channel, SIR=5dB, 2 antennas, $0.5\cdot\lambda$, 2 users	94
Fig. 6-11:	Ps for SUI-3 channel, SIR=5dB, 2 antennas, $0.5\cdot\lambda$, 2 users	94
Fig. 6-12:	Ps for SUI-2 channel, SIR=5dB, 4 antennas, $0.5\cdot\lambda$, 2 users	95
Fig. 6-13:	Ps for SUI-2 channel, SIR=5dB, 4 antennas, $10\cdot\lambda$, 2 users	95
Fig. 6-14:	Ps for SUI-3 channel, SIR=5dB, 4 antennas, $0.5\cdot\lambda$, 2 users	96
Fig. 6-15:	Ps for SUI-2 channel, SIR=0dB, 2 antennas, $10\cdot\lambda$, 2 users	97
Fig. 6-16:	Ps for SUI-3 channel, SIR=0dB, 2 antennas, $0.5\cdot\lambda$, 2 users	97
Fig. 6-17:	Ps for i.i.d. SUI-2 channel, SIR=5dB, 2 antennas, 2 users	98
Fig. 6-18:	Ps for i.i.d. SUI-2 v2 channel, SIR=5dB, 2 antennas, $10\cdot\lambda$, 2 users	98
Fig. 6-19:	Ps for i.i.d. SUI-3 channel, SIR=5dB, 2 antennas, 2 users	99
Fig. 6-20:	Ps for SUI-3 channel, SIR=5dB, 2 antennas, $10\cdot\lambda$, 2 users	99
Fig. 6-21:	Ps for SUI-2 channel, SIR=5dB, 2 antennas $10\cdot\lambda$ apart, 2 SIC stages, 2 users	100
Fig. 6-22:	Ps for SUI-3 channel, SIR=5dB, 2 antennas $0.5\cdot\lambda$ apart, 2 SIC stages, 2 users	100
Fig. 6-23:	Space-time DFE/SIC compared with MIMO DFE for SUI-2 channel, SIR=5dB, 2 antennas $10\cdot\lambda$ apart, 2 users	101
Fig. 6-24:	Space-time DFE/SIC compared with MIMO DFE for SUI-3 channel, SIR=5dB, 2 antennas $0.5\cdot\lambda$ apart, 2 users	102

Glossary

ADSL	asymmetric digital subscriber line
ARQ	automated repeat request
ATM	asynchronous transfer mode
AWGN	additive white Gaussian noise
BER	bit error rate
BLAST	Bell Laboratories Layered Space-Time
BS	base station
CCI	co-channel interference
CDMA	code division multiple access
CRC	cyclic redundancy check
dB	decibells
DFE	decision feedback equalizer
DOA	direction of arrival (equivalent to angle of arrival)
DSL	digital subscriber line
FB	feedback
FBWA	fixed broadband wireless access
FCC	federal communications commission
FDMA	frequency division multiple access
FEXT	far end crosstalk
FF	feedforward
FIR	finite impulse response
GWSSUS	Gaussian wide sense stationary uncorrelated scatterer
HDSL	high bit rate digital subscriber line
HIPERLAN	high performance radio local area network
IEEE	institute of electrical and electronics engineers
ISI	intersymbol interference
kb/s	kilo bits per second
LAN	local area network
LOS	line-of-sight
LMCS	local multipoint communication systems
LMDS	local multipoint distribution service
LMS	least mean square
LMSDFE	decision feedback equalizer trained with the LMS algorithm
LMSLE	linear equalizer trained with the LMS algorithm

LSL	least square lattice
LSLDFE	decision feedback lattice equalizer trained with the LSL algorithm
MAC	medium access control
MAI	multi-access interference
Mb/s	mega bit per second
MEA	multi-element antenna array
MIMO	multiple input multiple output
MLSE	maximum likelihood sequence estimation
MMDS	multi-channel multipoint distribution services
MMSE	minimum mean square error
MSE	mean square error
MS/s	mega symbols per second
NEXT	near end crosstalk
NLOS	non line-of-sight
POTS	plain old telephony service
P_s	probability of symbol error
QAM	quadrature amplitude modulation
QPSK	quadrature phase shift keying
RF	radio frequency
RLS	recursive least square
RLSDFE	decision feedback equalizer trained with the RLS algorithm
RRC	square-root raised cosine
SDMA	space division multiple access
SIC	successive interference cancellation
SIMO	single input multiple output
SIR	signal to interference ratio
SNR	signal to noise ratio
SU	subscriber unit
SUI	Stanford University
SUI-2	Stanford University channel model for fixed broadband wireless access number 2
SUI-3	Stanford University channel model for fixed broadband wireless access number 3
TDD	time division duplex, e.g. ping-pong system
TDMA	time division multiple access
ULA	uniform linear array
UNII	unlicensed national information infrastructure
VDSL	very high bit rate digital subscriber line

Mathematical Notations

\mathbf{e}	small bold face letters denote vectors
\mathbf{X}	capital bold face letters denote matrices
pdf	probability density function
i.i.d.	independent identically distributed
$\exp\{ \}$	exponential function
$N(\mu, \sigma^2)$	standard (Gaussian) pdf with parameter μ and σ^2 ; μ =mean and σ^2 =variance
$U(\mu, \sigma^2)$	uniform pdf with parameter μ and σ^2 ; μ =mean and σ^2 =variance
$R(B)$	Rayleigh distribution with parameter B
\Re	denotes the set of real numbers
\mathbb{C}	denotes the set of complex numbers
$\sqrt{\quad}$	square root
j	imaginary unit, i.e. $j = \sqrt{-1}$
z^{-1}	unit delay
T	superscript T denotes transpose
H	superscript H denotes Hermitian transpose
\bullet	vector dot product, e.g. $\mathbf{a} \bullet \mathbf{b} = \mathbf{a}^T \cdot \mathbf{b} = a_1 \cdot b_1 + a_2 \cdot b_2 + \dots + a_n \cdot b_n$, where n is the number of components of vector \mathbf{a} and vector \mathbf{b}
φ	azimuth
θ	elevation
λ	wavelength
$E6$	short hand notation for, e.g. 10^6
$E[X]$	expected value of random variable X
$\ \mathbf{A}\ $	Frobenius norm, i.e. $\ \mathbf{A}\ = \sqrt{\sum_{i=1}^m \sum_{j=1}^n a_{ij} ^2}$, m =number of rows, n =number of columns
$ \mathbf{a} $	length of vector \mathbf{a} , i.e. $ \mathbf{a} = \sqrt{\mathbf{a} \bullet \mathbf{a}}$
$ z $	absolute value of z
\mathbf{I}	identity matrix
\mathbf{X}^{-1}	denotes inverse of matrix \mathbf{X}
$((a))_N$	denotes a modulo N
$O(N)$	order of N
T^r	denotes cyclical shift to the right by r places, e.g. $T^r \mathbf{x} = [x_{((N-r+n))_N+1}]$, where N is the number of components of the vector \mathbf{x} and $n=1 \dots N$

- T^r denotes cyclical shift to the left by r places
- \hat{y} the circumflex denotes an estimated quantity, i.e. \hat{y} is estimated transmitted symbol
- y known quantity, i.e. y is transmitted symbol

Chapter 1

Introduction

Fixed Broadband Wireless Access (FBWA) systems have received much interest recently. They provide an elegant solution to the ‘last mile’¹ problem. FBWA systems use microwave frequencies to provide high speed data and multimedia services. Fig. 1-1 depicts a typical FBWA deployment.

Currently a number of such systems are on the market. Whereas some systems integrate different services like telephony, data, video and internet services, other FBWA systems concentrate solely on one service. Most FBWA systems at the moment do not support mobility, although portability is supported. FBWA has attractive features such as ease and speed of deployment, fast revenue, low infrastructure cost and flexibility in changing and deploying subscriber units (SU) compared to other access technologies.

In order to compete with wireline technologies, FBWA systems must support comparable data rates. One major obstacle in achieving high data rates are the effects that the radio channel introduces. Radio links have higher bit error rates (BER) compared to wireline systems and further are susceptible to a number of interferences, namely intersymbol interference (ISI), co-channel interference (CCI), multi-access interference (MAI) and interference from other systems that operate in the same frequency band.

ISI is caused by the dispersive nature of the channel. The delay spread associated with FBWA radio channels is particularly detrimental when high data rates (100MB/s and above) and non-line of sight operation (NLOS) are considered. NLOS channels exhibit far more severe ISI than line of sight (LOS) channels. In order to combat ISI, the receiver has to use some form of equalization.

It is CCI that limits the capacity of a FBWA network employing a cellular style of frequency re-use. In order to increase the capacity, the cell size and therefore the re-use distance has to be decreased. However this leads to additional CCI, which is very detrimental, since it has the same frequency as the wanted user signal. CCI suppression can be achieved if multiple antennas (space diversity) are employed.

MAI is caused by the multi-access method. In time division multiple access (TDMA) and frequency division multiple access (FDMA), MAI is caused by bandwidth limitations of receive

¹ The ‘last mile’ means the connection from the service provider to the customer (e.g. residential homes)

and transmit filters and is commonly known in this context as adjacent channel interference. In code division multiple access (CDMA), MAI is caused by non-ideal code orthogonality.

In order to increase the capacity and the data rate of FBWA systems, methods are needed, both at the physical and the system level to combat these interferences. Equalization is the primary physical layer technique used to combat these performance limiting interferences. Time-domain equalization deals with ISI, whereas the extension of time-domain equalizers into the spatial domain, known as space-time equalizers [Ariya99, Lind99] and multiple-input multiple-output (MIMO) equalizers [Duel92, Tide99, Al-Dha00] are capable of suppressing ISI, CCI and MAI. The majority of the available processing power is consumed by the equalizer in FBWA systems and so efficient algorithms with good performance are proposed in this work.

The treatment of interference from other systems operating in the same band is outside the scope of this study. The institute of electrical and electronics engineers (IEEE) co-existence workgroup is currently investigating this issue [IEEE8022].

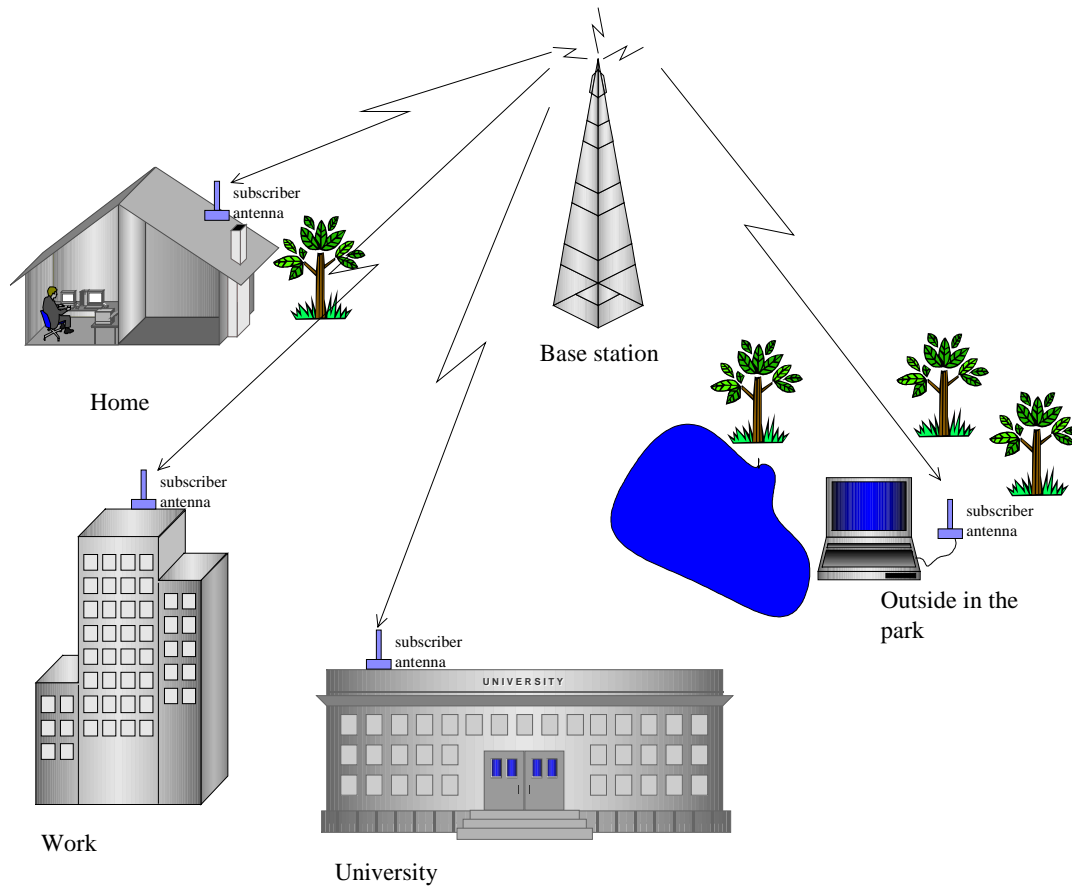


Fig. 1-1: FBWA deployment scenario

1.1 Standardization and frequency bands

Standardization of FBWA networks is carried out by various organizations (IEEE 802.16, ETSI BRAN HIPERMAN, ITU-R). The following frequency bands have been identified as being the most suitable for such fixed broadband wireless access systems:

- LMDS/LMCS (29 GHz)
- MMDS (2.5GHz)
- UNII (5GHz)
- and 3.5GHz in Europe

The local multipoint distribution service/local multipoint communication systems (LMDS/LMCS) band offers huge bandwidth, but radio frequency (RF) devices are expensive at such high frequencies. Research in these bands has shown that multipath can be successfully combated with relatively basic equalization architectures and highly directional antennas [Falc99]. Further, these systems rely mainly on LOS propagation. The bands at lower frequencies are expected to exhibit more detrimental multipath, but are less susceptible to rain attenuation. Furthermore the unlicensed national information infrastructure (UNII) band is an unlicensed band and restrictions to transmitted power levels are tight. This work concentrates on the multi-channel multipoint distribution services (MMDS) band. This is primarily because equalization for LMDS/LMCS systems has been shown to be relatively simple due to the low delay spread [Falc99], and secondly because channel models and propagation measurements for the UNII band are not available at this time. For the MMDS band, channel models are available and propagation measurements have been performed. Equalization is still one of the major obstacles to be overcome in MMDS systems.

1.2 Last mile problem

Despite improvements already made in the capacity of the internet backbone, the access network remains a bottleneck. The situation of access networks compared to backbone networks is quite different. The ever increasing data traffic on the backbone network has led to sustained progress in switching and carrier technology and so expensive and high performance equipment is used. This is because in backbone networks the resource is shared among a large number of users, whereas in the case of access networks only a relatively small number of users share the resource. Thus more money is available for the backbone, whereas in the case of access networks low cost solutions are required.

In order to harvest the possibilities offered by advanced internet technologies, fast access is necessary. FBWA is such a technology, which is capable of solving this imbalance. FBWA has

certain unique features compared to other broadband access technologies, which will be described in the next section.

1.3 Broadband access technologies

Due to the enormous growth in popularity of the Internet and multimedia services, residential customers demand higher data rates than the traditional analogue modem can offer.

Most people access the internet at home via a telephone line and a modem. Ordinary modems, even V.90 devices rated at 56.6kb/s, are not sufficient for today's data communication needs. Users who want to download large files (image, audio) get frustrated by the long delays, and streaming video is not feasible.

The so called 'last mile' is still a bottleneck in realising fast internet access with modern technologies. Consequently there is a great need for fast broadband access. Various types of broadband access, namely: digital subscriber line (DSL), cable modem, fibre, satellite, FBWA are illustrated in Fig. 1-2.

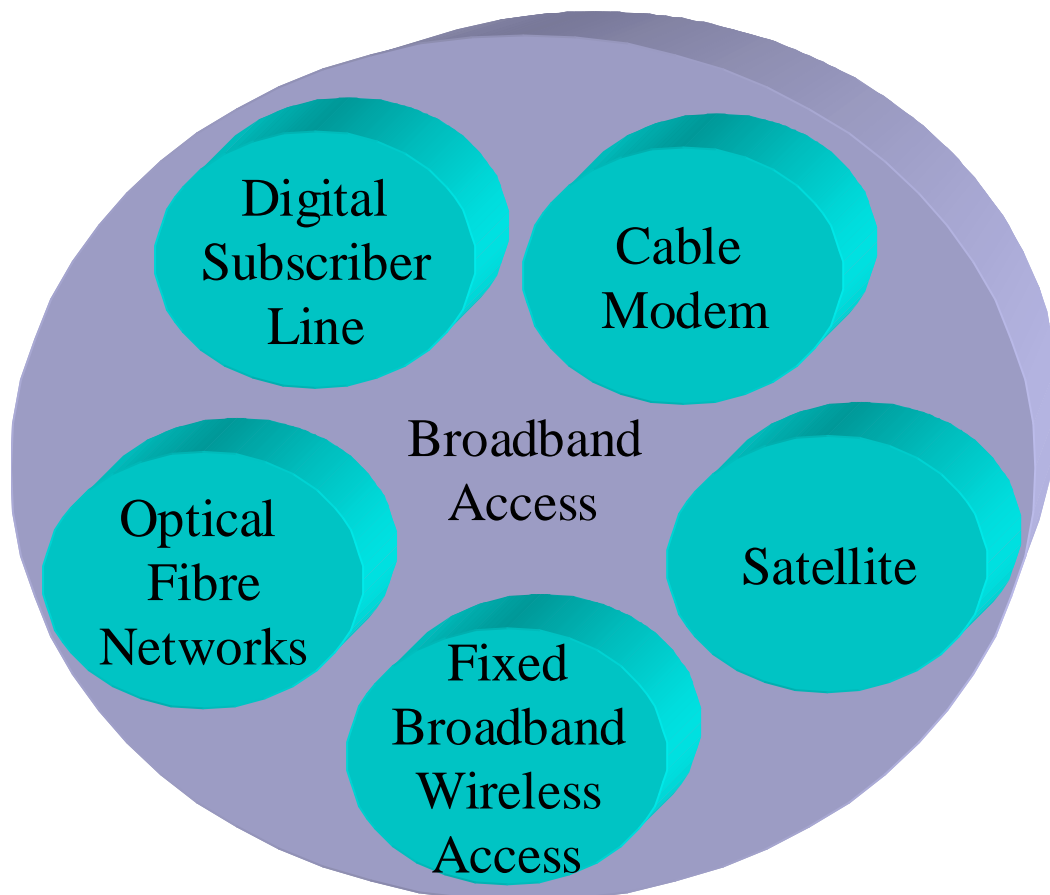


Fig. 1-2: Broadband access technologies

In the following sections, different technologies for high data rates in ‘the last mile’ are reviewed, with the exception of voice-band analogue modem technology. Analogue voice-band modems are not considered, since their potential to deliver higher data rates has been exhausted.

1.3.1 Digital subscriber line

Digital subscriber line (DSL) techniques utilise the existing telephone copper lines for high-speed communication. DSL techniques for example include high bit rate DSL (HDSL), asymmetric digital subscriber line (ADSL) and very high bit rate DSL (VDSL).

According to [Dut99] ADSL can offer data rates up to 768kb/s in the uplink and 6-8Mb/s in the downlink depending on the length and the condition of the local loop. DSL technologies coexist with the telephone service on a twisted pair copper wire, consequently it is usual to employ a plain old telephone service (POTS) splitter comprising a highpass and lowpass filter [Chen98] at the customer premises. Sophisticated modulation schemes are employed for DSL to overcome the impairments of the twisted pair channel.

The capacity of DSL systems is limited by crosstalk noise. Near-end crosstalk (NEXT) is usually dominant compared to far-end crosstalk (FEXT) [Chen98]. Although, additive white Gaussian noise (AWGN) is present, NEXT is usually the dominant noise impairment in DSL channels.

The next step in the DSL market is VDSL. VDSL modems are targeted to feed data at about 53Mb/s over a range of 300m [Pap99]. The data rates achievable by all DSL systems strongly depends on the condition of the telephone lines and the transmission distance. Therefore the data rate can vary to a high degree: assuming 30MHz bandwidth and a loop length of only 500m the theoretical capacity could be 110 Mb/s with an efficiency of approximately 3.7 b/s/Hz. However the same calculation with a loop length of 1400m leads to only 20Mb/s and an efficiency of only 0.7 b/s/Hz [Pap99].

The clear advantage of DSL is that the investment in installing this system is very low, since copper cables are already connecting most homes. Further, the bandwidth can be varied over a wide range to suit business and private demand.

The main drawback of DSL technologies is that it can be only used for short distances, typically up to a few kilometres. However in rural areas, copper lines often span much greater distances. Although the low costs of the digital subscriber loop makes it very attractive, the marked dependency of the data rate upon the quality and the length of the copper cable is a major drawback.

1.3.2 Cable modem

Cable modems can usually use a variety of cables from all-coaxial to hybrid fibre/coax systems. The interest in these technologies is demonstrated by the fact that in the US many major telecommunication companies are buying cable companies. However cable TV is designed intentionally for broadcasting and not for full duplex operation. Therefore one-way cable television systems must be upgraded into modern two-way networks to support advanced communications services, which is a technically-complex and capital-intensive proposition. Therefore the upstream path is often realized over the POTS. This is acceptable for asynchronous Internet traffic, where the downlink traffic exceeds the uplink traffic, but for future multimedia networks, which will support different services such as data, voice, video and audio, the uplink will become a bottleneck.

Today, commercial cable modems offer data rates up to 512kb/s. Dutta-Roy says that realistically cable modems are capable of delivering 200kb/s to 2Mb/s upstream and about 10Mb/s downstream [Dut99]. Although, the downlink speed exceeds that of ADSL, one has to note that the link is shared between many users and contention will cause the data-rate to plunge.

1.3.3 Optical fibre networks

Although it was the first approach used to deliver high speed internet access, fibre never reached the residential customer because of the high investment required to build up a fibre infrastructure. Upgrading the local loop plant to a purely optical fibre infrastructure is not seen as being an economically viable solution in the near term [Dut99]. Optical fibre networks are therefore mainly used for backbones and not for the last mile. However very high data rates can be achieved with fibre, and optical fibre networks are immune to electromagnetic interference. WDM transmission systems with a capacity of 40Gb/s are now being introduced, particularly in North America [Yos99]. Still the capacity to handle future demands on the backbone may be much higher than this. In today's backbone networks, electronic processing is done at every node. Yoshimura predicts in his paper that in the future, electronic processing will be removed from the core network and instead photonic networks will be deployed using direct optical connections [Yos99]. Electronic processing, if used, will be performed only in the edge network.

It is seen that optical networks have great potential for high-speed backbone networks, however their deployment to the residential customers will not be seen in the near future, because of the high costs involved.

1.3.4 Satellite

Another way of delivering high-speed Internet access to the home is via satellite networks. The “DirectPC” service from Hughes Network Systems for example currently offers 400kb/s downlink via a KU-band satellite link and 56kb/s uplink via a terrestrial telephone line [Dut99, Evans01]. Broadband Satellite systems offer another interesting approach to solve the last mile issue. However the investments in the infrastructure can be immense and the latency of GEO stationary satellite links is excessive. Another drawback is that although the downlink usually has a high capacity, the uplink is often realised with an analogue modem connection [Dut99].

1.3.5 Fixed broadband wireless access

FBWA is often seen by many as a niche technology. However certain systems can provide a data rate of up to 25Mb/s downstream [ADAP99]. For example the ‘AB-Access’ system provides Internet access at 25 Mb/s. Note that 25 Mb/s is the gross bit rate (not including overhead due to synchronization and equalization) and is shared among up to 254 users, so each user’s data-rate will go down respectively. The network manager can set a minimum throughput threshold, e.g. 384kb/s for residential and small businesses and 1.5Mb/s for medium and large businesses. Note, this minimum threshold is guaranteed, however the actual data-rate can be far in excess of that.

Fixed wireless broadband access systems can be implemented with less effort, faster and more cheaply than with wired technologies. Therefore, it is the technology of choice for rural areas or areas with a bad telecommunication infrastructure or where new operators wish to compete with an incumbent operator. The major obstacle in wireless access is that the channel is more hostile, and consequently the signal processing task is immense. However there are clear advantages in using wireless access methodologies instead of wired ones. A wireless system can be more easily maintained and provides rapid provisioning.

A number of solutions for broadband network access have been discussed. Each system has certain limitations and certain unique advantages. However, it is unlikely that in the future only one technology will dominate the access market. Rather all of them will play an important role, and systems may be designed where more than one technology is used, e.g. hybrid satellite microwave radio systems may evolve.

1.4 The unique possibilities FBWA can offer.

Portability is a unique feature of the wireless alternative. It would be possible for example to sit on a bench in Regents Park surfing the Internet and/or check your emails during your lunch break.

Third world countries do not have the resources to install a wired infrastructure for internet access. However a wireless internet access network will be more cost effective and feasible for these countries. A similar trend can already be observed in those countries with the telephone service: These countries often have a wireless telephone system and a significant proportion of the population has mobiles.

FBWA also offers an interesting business model for small business to gain access to the internet access market without a major initial investment. With FBWA systems costs are incremental and no full-blown wired access network is necessary to commence service.

Another example, which would benefit from a FBWA system, would be marketing campaigns or remote TV shows, which need fast internet access to either respond to emails and/or for live broadcasting of the show on the internet. Wireless has the unique advantage that no cabling is necessary and setting up the information infrastructure will be fast and cost effective for such portable short-term solutions.

1.5 Challenges of FBWA system design

Complexity is a major challenge in FBWA systems. FBWA has much faster data-rates than current mobile phone systems and so low complexity algorithms and architectures with good performance are needed. The high symbol rates required and the dispersive nature of the FBWA channel makes this a difficult task.

Very high throughput and *very high capacity* is required to make FBWA competitive compared to their wireline counterparts. Multiple element antenna (MEA) techniques offer a solution to this problem. MEAs and space-time processing is investigated here to evaluate the advantages of installing multiple antennas at the base station (BS).

Another challenge is to deliver a *very low BER* (of the order of 10^{-6}) in order to guarantee a low packet error rate. Such low BERs are required for reliable data transfer. This could lead to a substantial signal to noise ratio (SNR) requirement at the receiver and therefore limit the cell size. Again MEA techniques can offer a solution.

Low latency is another requirement. The latency should be comparable to DSL. The equalizer convergence time strongly influences the latency and hence *fast converging equalizer tap update algorithms* with low complexity are required for FBWA systems. Thus, convergence speed is another important design goal for bandwidth efficient FBWA systems. The length of

the training sequence is in essence wasted bandwidth. However, there is the trade-off between fast convergence and complexity, which has to be evaluated for FBWA propagation environments.

1.6 Motivation

Current single-carrier FBWA systems use single antennas at the SU and the BS. The next step in FBWA will be the use of MEAs at the BS to combat fading, to suppress CCI and/or to enable space division multiple access (SDMA).

Further, equalization is a problem owing to its complexity. The equalizer is an integral part of the physical layer of these systems. Owing to complexity issues more simple, but less powerful equalization methods are used.

The main theme of this research is to propose computationally efficient yet powerful equalization techniques for FBWA systems, both in the time-domain (traditional equalization) and in the space-time domain (space-time processing) via the introduction of MEAs at the BS.

Efficient implementations are explored to show that sufficiently effective equalization methods can be employed while achieving reasonable complexity for FBWA systems.

Equalization for FBWA in the time-domain only and also equalization in both space and time domains, known as space-time processing or space-time equalization are investigated. First, investigations are conducted to determine the equalization approach that is most suitable for FBWA systems and secondly the possibilities offered by the use of MEAs at the BS are investigated. In this context a novel FBWA system based on MEAs at the BS is proposed, which is capable of either single-user detection or multi-user detection.

1.7 Novel achievements

In summary the following new achievements are presented in this thesis:

1. A closed-form expression for the fading envelope correlation coefficient using the Gaussian wide sense stationary uncorrelated scatterer (GWSSUS) channel model for Rician-fading – chapter 3
2. An equalizer performance study for MMDS fixed broadband wireless access systems (study of recursive least square (RLS), least mean square (LMS) and lattice algorithms for the MMDS band) – chapter 4
3. A Low-complexity cross-correlation channel estimator using only one correlator per antenna branch – chapter 5

4. A Multi-user detection SDMA/TDMA fixed broadband wireless access system using a space-time decision feedback equalizer (DFE) combined with successive interference canceling (SIC) – chapter 6

1. Fading envelope correlation coefficient

Based on theoretical derivations from Asztély [Aszt96] and Abdi [Abdi02] a closed-form expression is derived, which allows easy evaluation of the space-time correlation between fading envelopes using the GWSSUS channel model. A closed-form expression can be obtained when using Asztély's trigonometric approximation. This approximation is accurate up to a direction of arrival (DOA) spread of approximately 40° as demonstrated through numerical evaluation of the integral in the cross-correlation coefficient equation versus the closed-form expression. Asztely addressed Rayleigh fading only and Abdi developed a general framework for calculating the cross-correlation between fading envelopes for Rician fading, but did not consider the GWSSUS channel model. Combining the two approaches permits the cross-correlation between the fading envelopes when a strong specular component is present (i.e. Rician fading) to be calculated. Further, a closed-form expression is derived for 3D propagation (horizontal and vertical wave propagation).

2. Equalization performance study for the MMDS band

Processing complexity is a major bottleneck in FBWA. FBWA channels are slowly changing and usually short packet based burst-mode communication is employed. Consequently the channel can be considered constant (i.e. very slow Doppler fading) over the duration of one burst. However the delay spread of such channels can be severe. Single-carrier FBWA systems must therefore use an equalizer to combat the intersymbol interference (ISI) introduced by the dispersive fading channel. An equalizer performance study was therefore carried out to identify the most suitable equalizer architecture and algorithm for single-antenna FBWA systems. Maximum likelihood sequence estimation (MLSE) (e.g. implemented via the Viterbi algorithm) and Bayesian equalization approaches were eliminated from this study owing to their complexity. The study presented here concentrates on symbol based adaptive equalization algorithms using the LMS and RLS algorithm, as well as a fast lattice RLS algorithm (RLS algorithms with linear increasing complexity). It is shown that the least square lattice algorithm and architecture offers worthwhile complexity performance trade-off.

3. Channel estimation

From this point in the research onwards, the introduction of an antenna array at the BS is considered. This means that the BS is equipped with multiple antennas and the SU with a single antenna. Individual SUs may transmit at the same time and at the same frequency if multi-user

detection is employed. Space-time processing at the BS offers an interesting solution to combat the detrimental effects induced by the FBWA channel. Installing a MEA at the BS will be the first step to achieve higher capacity and give resilience to fading in future FBWA systems. A MEA at the BS improves the wireless link quality through receive diversity and antenna gain and further enables SDMA on the uplink. Multi-user communication on the same frequency channel and at the same time slot in the uplink (i.e. SDMA) is the key to improving the throughput of future FBWA systems.

Space-time adaptive algorithms at the BS typically require a good channel estimate. Further a channel estimate is also required, when considering successive interference canceling (see point 4). A low complexity channel estimation method is proposed, which requires only one correlator per antenna branch to estimate up to M SDMA user channels. This cross-correlation based channel estimation technique can also be used for packet synchronization. The heart of the proposed channel estimation method is the training sequence design. The sequence set is constructed by cyclically shifting complex optimal training sequences originally proposed by Ng [Ng98a]. Simulations show that the suggested method has very similar performance to full-rank maximum likelihood channel estimation, however it requires no matrix inversion.

4. Multi-user detection using a space-time DFE combined with SIC

Finally a completely new FBWA system (chapter 6) is proposed, which applies the previous channel estimation technique (chapter 5) to a detector employing a combination of a space-time DFE and SIC. The system uses the GWSSUS channel model (chapter 3) to assess the performance under realistic conditions. The performance of the proposed system is shown in terms of convergence speed and probability of symbol error (P_s). The space-time DFE in this research is trained with the LMS algorithm and/or with the RLS algorithm. It is shown that SIC improves the P_s of the weaker user towards that of the P_s of the stronger user. However the P_s of the weaker user reaches an irreducible level owing to error propagation through the SIC stages. This effect is investigated and it is seen that almost all symbol errors caused in the first stage propagate through to the final stage. It is shown that space-time processing at the BS enables a significant performance gain in terms of P_s performance. Furthermore it allows the use of SDMA, which leads to a linear increase in throughput for every antenna added at the BS.

1.8 Overview

chapter 2 - State of the art equalization and space-time processing for high data-rate wireless systems

Chapter 2 reviews equalization for high data rate wireless systems. Standard time-domain equalization architectures and tap-update algorithms are described. Further, hardware efficient implementation and complexity reduction techniques are discussed. Space-time equalization methods are also reviewed and it is shown that a space-time equalizer can be considered as an extension of a time-domain only equalizer into the spatial domain.

chapter 3 - Channel modelling for space-time processing in the uplink

Chapter 3 gives background information on spatial channel modelling and channel modelling for FBWA environments. Also new closed-form expressions for the fading cross-correlation in the case of Rician fading when employing the GWSSUS channel model are presented. These closed-form expressions for 2D (horizontal) and 3D (horizontal and vertical) wave propagation can be evaluated much more quickly than a numerical evaluation of the associated integral equations. Especially in case of 3D wave propagation the speed-up is significant. The closed-form expressions are based on trigonometric approximations, which are valid for BS reception. However, for reception at the SU it is likely that a larger DOA spread will be encountered and the proposed closed-form expressions will not be sufficiently accurate. In this case numerical evaluation of the integral equations is necessary.

chapter 4 - Equalization Requirement Study for MMDS fixed broadband wireless access systems

This chapter investigates different equalization algorithms and architectures for single carrier single antenna FBWA systems. Both linear equalizer (LE) and DFE architectures are used. The LMS, RLS or least square lattice (LSL) algorithms are employed for updating the equalizer taps. Specifically it is shown that the LSL algorithm offers an interesting performance complexity trade-off for FBWA systems.

chapter 5 - Low complexity channel estimation for fixed broadband wireless access systems

In Chapter 5 a novel low complex channel estimation technique is presented. The method requires only one correlator per antenna branch to estimate up to M SDMA user channels. The key innovation is the method used to construct the training sequence set. The training sequence set selected is a zero correlation zone (ZCZ) sequence set, which is constructed by cyclically shifting complex optimal training sequences.

chapter 6 - Space-time processing in the uplink for fixed broadband wireless access

Chapter 6 uses the GWSSUS channel model of chapter 4 and the computationally efficient channel estimation method of chapter 5 in conjunction with a space-time DFE combined with successive interference cancelling (SIC) to form a new FBWA system. The proposed system is capable of either single-user or multi-user detection. Depending on the environment the network operator could configure the system accordingly. The effects of error propagation in the successive detection stages are also investigated.

chapter 7 – Conclusions

In chapter 7 conclusions are drawn and the main findings in this thesis are summarized.

chapter 8 – Future work

Chapter 8 is devoted to future work. Potential research activities are discussed and the extension of the ideas presented in this thesis to MIMO systems is proposed. Space-time processing and multiple antennas at the BS and at the SU (i.e., a MIMO system) have the capability to solve the capacity bottleneck. Highlighted areas include space-time equalization techniques and channel estimation for MIMO channels.

Chapter 2

State of the Art Equalization and Space-Time Processing for High Data-Rate Wireless Systems

Adaptive equalization has been an active area of research for many years. It started with the invention of the zero forcing (ZF) equalizer by Lucky in 1965 [Luck65, Luck66]. Lucky's equalizer is based on the peak distortion criterion. Lucky also introduced decision-directed learning [Luck66] to train an adaptive equalizer. The decision directed mode is also able to track channel variations. Later on it was seen that the ZF equalizer is inferior to equalizers based on the mean square error (MSE) criterion in terms of noise enhancement. A celebrated adaptive algorithm for tuning an equalizer based on the MSE criterion is known as the LMS algorithm [Wid66]. The LMS algorithm belongs to the family of stochastic gradient algorithms. Widrow later applied the LMS algorithm to adaptive antenna arrays [Wid67]. An adaptive antenna array using beamforming can be viewed as a spatial equalizer. Unfortunately the LMS algorithm's convergence behaviour strongly depends on the eigenvalue spread of the correlation matrix of the input samples. Many variants of the original LMS algorithm exist, for example the normalized LMS algorithm [Nagu67, Albert67, Bitm80]. The normalized LMS algorithm has advantages compared to the original LMS algorithm in terms of gradient noise amplification and convergence rate. Although, the original version of the LMS and ZF algorithm are applied only to a linear transversal equalizer (LE), these algorithms can also be applied to a DFE. The DFE proposed by Austin [Aus67] uses decision-feedback to cancel the interference from previously detected symbols. The DFE outperforms the LE in the presence of spectral nulls in the channel.

Godard [Goda74] applied Kalman filter theory to the problem of setting the tap values of a transversal equalizer. In this work he treated the growing memory recursive least-square problem in a stochastic state-space framework. Later on it was recognized by Sayed and Kailath [Say94], that the RLS algorithm [Hay96] can be derived from Kalman theory, which lead to a correspondence between Kalman variables and RLS variables. The main advantage of the RLS algorithm [Hay96] compared to the LMS algorithm is that it is relatively insensitive to the eigenvalue spread of the correlation matrix of the input samples and so converges faster.

However, the main problem of the RLS algorithm is that the complexity is proportional to N^2 , where N is the number of taps in the equalizer. Therefore research has been devoted into finding new RLS algorithms that exhibiting a linear increase in complexity with the number of taps, leading to so called fast RLS algorithms. Falconer and Liung proposed the fast RLS Kalman algorithm in [Falc78] and later Ling and Proakis proposed the least square lattice DFE in [Ling85]. Also square-root RLS algorithms have been proposed [Say94, Hay96], which show better numerical stability than the standard RLS algorithm. A good tutorial review of these early adaptive equalization methods is given in [Qure85].

Another class of equalizers utilises a sequence-based method known as maximum likelihood sequence estimation (MLSE). Full MLSE is very complex, but using a dynamic programming technique known as the Viterbi algorithm [Vit67] allows a reduction in complexity, since only a fraction of all possible input sequences needs to be considered. The Viterbi algorithm was originally used for decoding convolutional codes. Only a few years later, Forney [Forn72] applied the MLSE via the Viterbi algorithm to the problem of signal detection in the presence of ISI.

In the following four paragraphs various equalization approaches, which were not considered in this work are summarized. *Bayesian equalizers* and *MLSE implemented via the Viterbi algorithm* are not considered here owing to their computational complexity. For FBWA channels in which the ISI spans many symbols, these probabilistic algorithms become impractical due to an exponential growth in computational complexity. The complexity trade-off can clearly be seen by considering a numerical example. For example, assuming the Stanford University (SUI)-3 channel (see Chapter 3, section 3.2), quadrature phase shift keying (QPSK) modulation at 5MS/s and root raised cosine (RRC) filtering at the transmitter and receiver with a roll-off factor of 0.35, the combined impulse response of transmit RRC, channel and receive RRC spans 15 symbol periods. Further the DFE architecture of chapter 4 for this scenario employs 16 feedforward (FF) taps and 12 feedback (FB) taps with a decision delay of 11 symbol periods. The computational complexity per iteration for the named equalizers is shown in Table 2-1: the DFE trained with the LMS algorithm (LMSDFE) [Hay96], the DFE trained with the RLS algorithm (RLSDFE) [Hay96], the decision feedback lattice equalizer trained with the LSL algorithm (LSLDFE) [Ling85], the Bayesian DFE [Chen93, Chen95a, Mulg96] and the MLSE implemented via the Viterbi algorithm [Qure85].

algorithm	operations per iteration	in numbers
LMSDFE	$2 \cdot N_{taps} + 1$	57
RLSDFE	$2.5 \cdot N_{taps}^2 + 4.5 \cdot N_{taps}$	2086
LSLDFE	$18 \cdot FF + 39 \cdot FB - 39$	717
Bayesian DFE	$O(S^{d+1})$	16.78E6
MLSE via the Viterbi algorithm	$O(S^{L-1})$	268E6

where:

N_{taps} = total number of taps

FF = number of taps of the feedforward filter

FB = number of taps of the feedback filter

S = alphabet size of the transmitted symbols, e.g. QPSK: $S=4$

d = decision delay

L = channel span in symbol periods

Table 2-1: computational complexity of different equalization structures

However, to increase the bit rate some FBWA systems will offer high-order modulation schemes such as quadrature amplitude modulation (QAM) (e.g. 64-QAM). Clearly in this situation the complexity of the Bayesian equalizer and the MLSE will grow enormously. In contrast the complexity of the conventional DFE stays more or less the same for high-order modulation schemes. The enormous increase in complexity of the Bayesian DFE with S is however dwarfed by that expected by the MLSE using the Viterbi algorithm. The Bayesian equalizer (also known as the MAP symbol-by-symbol equalizer) is the optimum symbol-by-symbol equalizer structure without decision feedback [Abend70], whereas the optimum sequence based equalization method is the MLSE. Interestingly the Bayesian DFE has a reduced complexity compared with a conventional Bayesian equalizer without decision feedback. This is achieved by reducing the number of states which have to be considered in the evaluation of the Bayesian decision function. For stationary channels, Chen [Chen93] showed that the optimum equalization performance in terms of symbol error rate is achieved with the MLSE, followed by the Bayesian DFE and then the conventional DFE. Very surprisingly, this changes with rapidly time-varying channels. In this case the Bayesian DFE can outperform the MLSE [Chen95a].

Also *blind equalization* will not be considered in this thesis and only training based methods are employed. Blind equalization methods often require much longer to converge than training based methods [Goda80, Chen95b]. In [Goda80] it is observed via computer simulations that Godard's blind algorithm needs 10000-20000 iterations to converge. Blind approaches require long processing times and suffer from poor robustness [Sell99b]. Thus blind equalization is not the preferred choice for high-rate FBWA systems.

Linear optimum filtering (i.e. Wiener filters) [Hay96] requires the inverse of the correlation matrix of the tap inputs to be calculated. The computational complexity of a matrix inversion is of $O(N^3)$, where N is the dimension of the matrix [Press92] and is therefore also not considered in this work. Recursive approaches based on either the LMS or RLS offer a less complex solution.

Adaptive equalization methods using the LMS algorithm [Hay96], the RLS algorithm [Hay96] and the recursive least square lattice (LSL) algorithm [Ling85] are however considered in this work. The equalizer architecture employed is either the linear equalizer or the conventional DFE. The theory regarding equalizer tuning algorithms and architectures will be reviewed later in this chapter. First, the equalization architectures studied in this chapter are reviewed. Following the consideration of time domain equalization in section 2.1, the extension to the spatial domain, known as space-time equalization is treated in sections 2.1.3 and 2.1.4. The optimum tap settings are discussed in section 2.2 and equalizer tuning algorithms appropriate for the FBWA system under consideration in this thesis are reviewed. Important topics with respect to equalization for FBWA systems include complexity reduction techniques, equalization methods for high data rate systems and space-time techniques for FBWA systems. Space-time equalization is used in conjunction with multiple antennas at the BS with the aim of improving the receive signal quality compared with a single antenna system. Furthermore, MEAs enable CCI suppression and SDMA at the BS. Receiver algorithms and architectures suitable for space-time processing in the FBWA uplink are reviewed. Finally space-time processing techniques appropriate for the downlink are discussed.

2.1 Equalizer Architectures

2.1.1 Linear Equalizer and DFE

Fig. 2-1 shows a linear transversal equalizer (LE) and a DFE in the direct form using finite impulse response (FIR) filters. The feedforward filter (FFF) section of the DFE is identical to a LE as depicted in Fig. 2-1. The only non-linear part in the DFE is the slicer or decision device. The idea behind the DFE is that the feedback filter (FBF) removes ISI caused by previously detected symbols. The pre-slicer data can be expressed as:

$$z(k) = \sum_{i=0}^{N_f-1} x(k-i) \cdot w_{f,i} - \sum_{i=0}^{N_b-1} \hat{y}((k-1)-i) \cdot w_{b,i} \quad (2.1)$$

where: N_f = number of feedforward taps
 N_b = number of feedback taps
 $w_{f,l}$ = feedforward coefficients
 $w_{b,l}$ = feedback coefficients

$\hat{y}(k)$ = equalizer output at time k

$x(k)$ = feedforward filter tap input vector

The decision device maps the pre-slicer data to the nearest constellation point. The constellation depends on the modulation used. For binary modulation and QPSK modulation the slicer can be realized without an automatic gain control (AGC), however higher order modulation schemes such as 64-QAM require an AGC circuit.

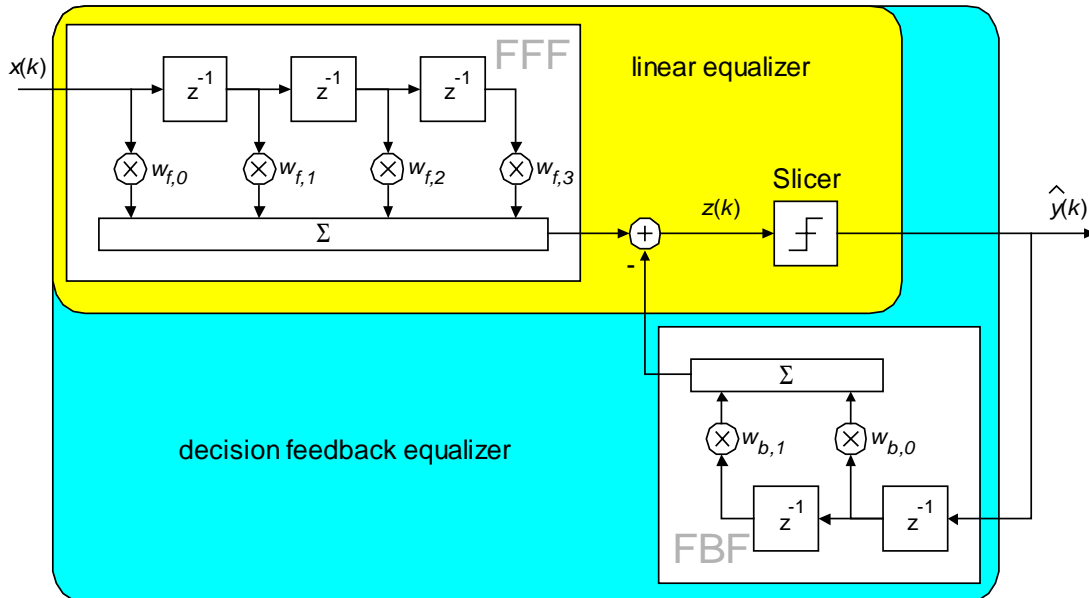


Fig. 2-1: LE and DFE

The input to the LE and DFE are the received symbols $x(k)$. The LE and DFE make memoryless decisions on a symbol-by-symbol basis. Both the LE and DFE can be trained using a variety of adaptive algorithms, e.g. LMS and RLS. The DFE is a good candidate for high-speed wireless data networks, e.g. high performance radio local area network (HIPERLAN) and is used extensively in this work, since it offers a good performance complexity trade-off. The main problem with the LE is its poor performance in presence of spectral nulls in the channel.

Here, all equalizer taps are symbol spaced. Both LE and DFE can also be realized with fractionally spaced taps [Pro91]. This may lead to improved performance at the cost of computational complexity. Unfortunately DFEs suffer from error propagation. This effect occurs when the slicer makes incorrect decisions and then these propagate through the FBF.

In theory one could realize the LE and DFE with IIR filters, however stability is then no longer guaranteed. On the other hand using lattice filters leads to an interesting computationally efficient architecture.

2.1.2 Lattice DFE

Fig. 2-2 shows the LSLDFE. The feedback section for the lattice structure is realized with N_2-1 two-channel lattice stages. Preceding the two-channel lattice stages are N_1-N_2 single channel lattice stages. This LSLDFE architecture was proposed by Ling and Proakis [Ling85] and it removes the requirement to have the same number of stages in each channel imposed by the previously proposed least square lattice algorithm [Lee81].

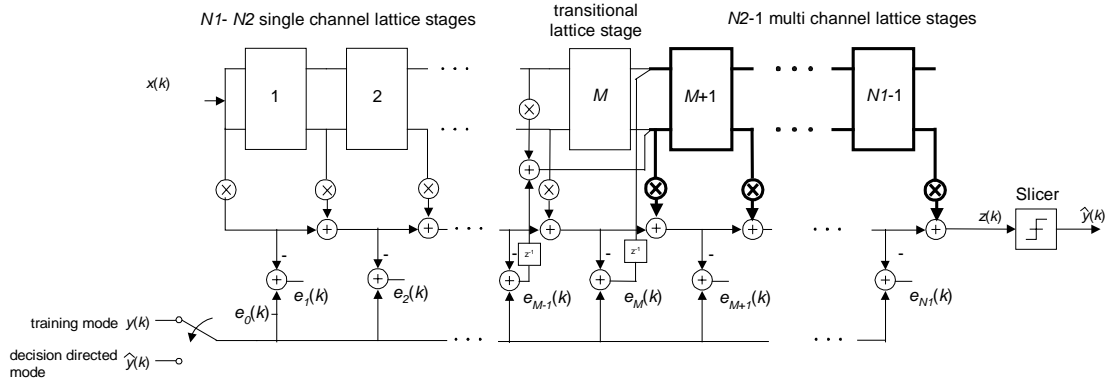
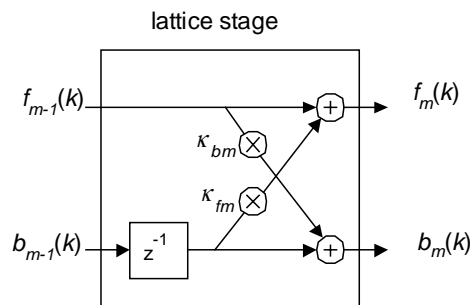


Fig. 2-2: LSLDFE

The main advantage of the LSLDFE is that its complexity increases linearly with the number of taps and not by a power of two as for the conventional RLS algorithm. Alternatively, the fast RLS Kalman algorithm [Falc78] can be used, which also has a computational complexity proportional to the number of stages. However the fast RLS Kalman algorithm is sensitive to roundoff noise [Ling85]. Lattice type equalizers are known to be less sensitive to this.

The lattice stage of the LSLDFE is depicted in Fig. 2-3. For the single-channel lattice stage all the quantities are scalars and for the two-channel lattice stage the dimensions of f_m and b_m are 2×1 and the dimensions of κ_{bm} and κ_{fm} are 2×2 .



where: b_m = backward prediction error
 f_m = forward prediction error
 κ_{bm} = backward reflection coefficient
 κ_{fm} = forward reflection coefficient

Fig. 2-3: Lattice stage

The LSLDFE was also applied recently in conjunction with selection diversity by Lee [Lee97]. The equalizer tuning algorithm proposed by Ling and Proakis is somewhat lengthy and therefore more specific details and the algorithm itself are described in [Ling85, Lee97].

2.1.3 Space-time DFE

Fig. 2-4 shows the extension of the time domain only DFE of Fig. 2-1 into the spatial domain. Instead of only one FFF the space-time DFE now has as many FFF as there are input channels available. These channels could come from multiple antennas or from antennas with different polarization.

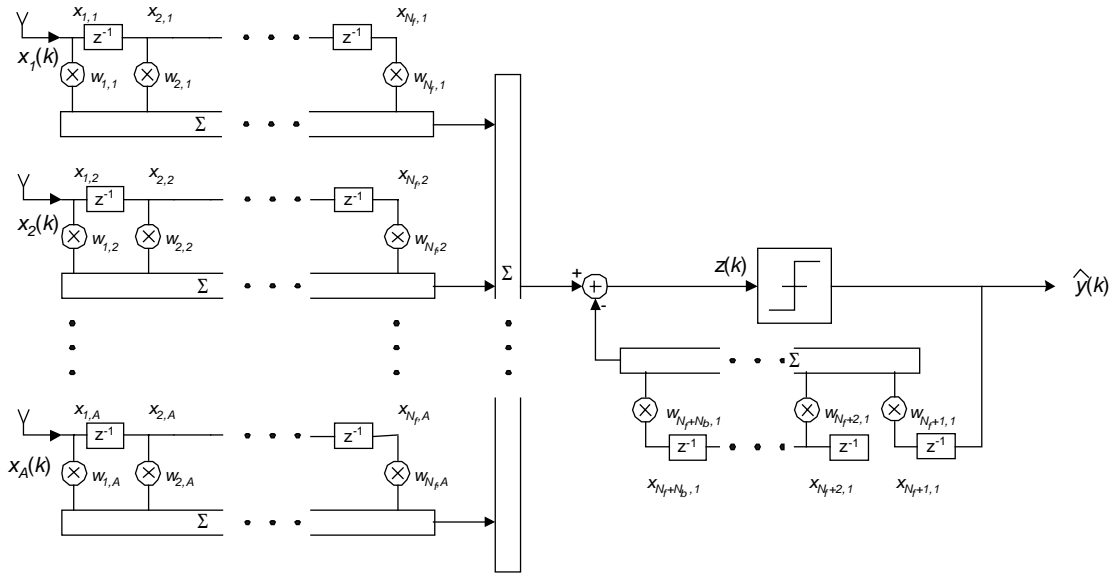


Fig. 2-4: Space-time DFE

In [Ham00] a space-time DFE is used for ISI and CCI suppression in frequency selective channels. The space-time DFE is trained with the QR-RLS algorithm. A comparison with selection combining clearly shows that joint optimization in the spatial and time domain outperforms the selection combining approach. The space-time DFE can also be tuned with the LMS algorithm, however the RLS algorithm converges much faster. Lindskog [Lind99] proposed the reduced-rank space-time DFE. By exploiting the rank of the channel, the space-time DFE can be realized with reduced complexity. The performance of the reduced rank space-time DFE is close to the performance of the conventional full-rank space-time DFE. Ng [Ng98b] presents another performance study of space-time DFEs in frequency selective environments and a theoretical treatment of the finite-length space-time DFE is presented in [Ariya99].

The previously referenced papers addressing space-time DFEs combat only ISI and CCI. The work of Choi and Lu [Choi99a, Choi99b] considers multi-user detection and SDMA using space-time DFEs and space-time LEs. Three different approaches are investigated in [Choi99a]:

a) pre-processing only using a general zero forcing criterion at the transmitter (i.e. an extension of single-user pre-equalization), b) post-processing using a space-time DFE or a space-time LE, c) a combination of a) and b). Approach c), which is a MIMO system, shows superior performance compared to the other two systems. The space-time DFE can be enhanced by an additional cross-decision feedback filter. The next subsection treats this DFE architecture, which is also known as the MIMO DFE.

2.1.4 MIMO DFE

The idea of a cross-decision feedback filter arises from the dual polarized antenna system that was first introduced by Kavehrad and Salz [Kav85]. This idea is used in the MIMO DFE, first introduced by Duel-Hallen in the context of spread spectrum systems [Duel92, Duel95]. However the MIMO DFE can be applied to many other systems as well, typically whenever the received signal is composed of several transmitted signals corrupted by ISI, MAI and additive noise. These scenarios arise not only in wideband asynchronous CDMA systems but also in broadband wireless communication systems with multiple antennas at the BS and/or SU and in wideband DSL systems due to cross-talk.

Fig. 2-5 shows the block diagram of a MIMO DFE. A MIMO DFE consists of a multidimensional FFF and a multidimensional FBF. For symbol spaced multi-antenna systems, the FFF has as many inputs as there are antennas and as many outputs as there are users. The number of inputs and outputs of the FBF corresponds to the number of users. A MIMO DFE can be viewed as a series of space-time DFEs, one for each user, where each individual space-time DFE is cross-connected with additional feedback filters to the output of all the others.

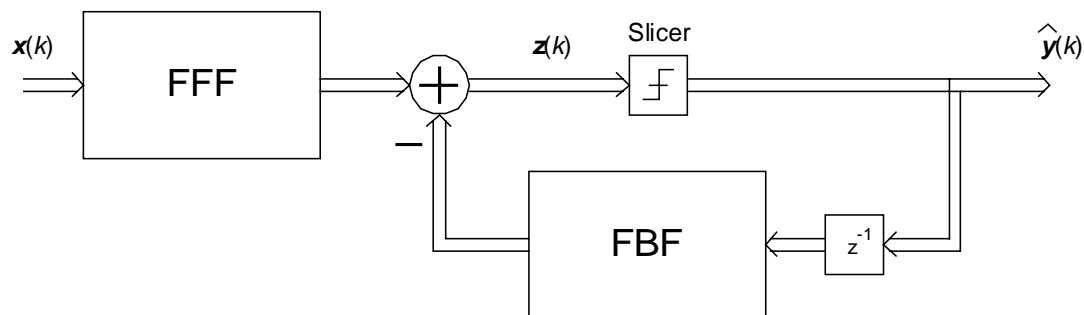


Fig. 2-5: MIMO DFE

Fig. 2-5 depicts a MIMO DFE where only previously detected symbols are available. But a MIMO DFE also allows for more elaborate choices: for example previously detected symbols and current symbols from all previously detected users in the current time frame are available or alternatively previously detected symbols and all current symbols are available (in this case a previous detection stage is necessary) [Al-Dha00].

The MIMO DFE can be optimized with the MSE criterion or with the ZF criterion. Similarly as for the time-only DFE (see section 2.1.1) the ZF MIMO DFE is inferior to the minimum mean square error (MMSE) MIMO DFE owing to noise enhancement.

The performance of a MIMO DFE for multiuser detection has been shown to be superior to the performance of a series of space-time DFEs for multiuser detection [Tide99]. This is because the MIMO DFE has the capability to effectively suppress interference from other users. However, the optimization of the MIMO DFE is quite complex [Al-Dha00]. Al-Dhahir's work concerns the MIMO DFE in the context of a digital TDMA system with multiple transmit and/or receive antennas. Optimum settings for finite-length MIMO DFEs are derived and fast algorithms are proposed for optimum finite MIMO DFE tuning in the MMSE sense.

2.2 Optimal equalizer settings

The optimal settings for the linear equalizer taps are given by the Wiener Hopf equations. This filter is also known as the Wiener filter. Let \mathbf{x}_k be the $N \times 1$ tap input vector at time $t=k \cdot T$:

$$\mathbf{x}_k = [x(k), x(k-1), \dots, x(k-N+1)]^T \quad (2.2)$$

The cost function J for the Wiener filter is given by the MSE criterion:

$$J = E[e(k) \cdot e^*(k)] \quad (2.3)$$

where: $e(k)$ = estimation error at time $t=k \cdot T$ and T is the symbol duration

The Wiener Hopf equations in matrix form are given by [Pro95, Hay96]:

$$\mathbf{R}_{xx} \cdot \mathbf{w}_{opt} = \mathbf{r}_{xy} \quad (2.4)$$

where: \mathbf{R}_{xx} = auto-correlation of received tap input samples \mathbf{x}_k , i.e. $\mathbf{R}_{xx} = E[\mathbf{x}_k \cdot \mathbf{x}_k^H]$

\mathbf{w}_{opt} = column vector of optimum tap settings in the MSE sense

\mathbf{r}_{xy} = cross-correlation of desired signal $y(k)$ and received tap inputs ' \mathbf{x}_k ', i.e.

$$\mathbf{r}_{xy} = E[\mathbf{x}_k \cdot y^*(k)]$$

$y(k)$ = desired signal at time $t=k \cdot T$

The optimal settings of the tap vector \mathbf{w}_{opt} involves the inversion of \mathbf{R}_{xx} :

$$\mathbf{w}_{opt} = \mathbf{R}_{xx}^{-1} \cdot \mathbf{r}_{xy} \quad (2.5)$$

By using the MSE criterion and a LE, the error-performance surface has a unique minimum in \mathbf{w}_{opt} . The dependence of J on the tap weights is a $N+1$ dimensional bowl-shaped surface, which is also known as the error performance surface [Hay96].

Another important principle, which can be used to check if the equalizer is operating at the optimum point and which can also be used to derive the Wiener Hopf equations is the principle of orthogonality: It states that the estimation error e_o when the filter operates with its optimum tap settings \mathbf{w}_{opt} is orthogonal to each tap input, i.e.:

$$E[x(k-n) \cdot e_o^*(k)] = 0, \quad n = 0, 1, 2, \dots, N-1 \quad (2.6)$$

There is also an interesting corollary to the principle of orthogonality. It can be shown using the principle of orthogonality that the filter output $\hat{y}(k)$ is orthogonal to the corresponding estimation error e_o , when it operates at its optimum point in the MSE sense [Hay96], i.e.:

$$E[\hat{y}(k) \cdot e_o^*(k)] = 0 \quad (2.7)$$

This corollary provides an easy way of checking if the equalizer has reached its optimum operating point.

For the DFE the optimum tap settings can be derived in a similar way. Let \mathbf{x}' denote the combined vector of tap input vector of the FFF and FBF:

$$\mathbf{x}' = [x(k), x(k-1), \dots, x(k-N_f+1), \hat{y}(k-1), \hat{y}(k-2), \dots, \hat{y}(k-N_b)]^T \quad (2.8)$$

and let \mathbf{w}' denote the combined tap coefficient vector, composed of the FFF coefficient vector \mathbf{w}_f and the FBF coefficient vector \mathbf{w}_b :

$$\mathbf{w}' = [\mathbf{w}_f^T \quad \mathbf{w}_b^T]^T = \begin{bmatrix} w_0 \\ w_1 \\ \vdots \\ w_{N_f-1} \\ w_{N_f} \\ w_{N_f+1} \\ \vdots \\ w_{N_f+N_b-1} \end{bmatrix} \quad (2.9)$$

Again it can be shown using the principle of orthogonality that the optimum DFE coefficients are given by [Lo95, Sme97, Sell99b]:

$$\mathbf{w}'_{opt} = \mathbf{R}'_{xx}{}^{-1} \cdot \mathbf{r}'_{xy} \quad (2.10)$$

where: $\mathbf{R}'_{xx}{}^{-1} = (N_f+N_b) \times (N_f+N_b)$ square Hermitian auto-correlation matrix of \mathbf{x}'

\mathbf{r}'_{xy} = cross-correlation vector of the desired data and the DFE tap input

vector \mathbf{x}' of dimension $(N_f+N_b) \times 1$: $\mathbf{r}'_{xy} = E[\mathbf{x}'_k \cdot y^*(k)]$

$y(k)$ = transmitted symbol at time $t = k \cdot T$

[Lo95] realised that the symmetry of \mathbf{R}'_{xx} can be exploited to express it as four submatrices:

$$\mathbf{R}'_{xx} = \begin{bmatrix} \mathbf{\Gamma} & \mathbf{A}^* \\ \mathbf{A}^T & \mathbf{I} \end{bmatrix} \quad (2.11)$$

where: $\mathbf{\Gamma}$ = square matrix of dimension $N_f \times N_f$

\mathbf{A} = cross-correlation matrix between FFF and FBF contents of dimension $N_f \times N_b$

\mathbf{I} = identity matrix of dimension $N_b \times N_b$

Similarly [Lo95] the cross-correlation vector \mathbf{r}'_{xy} can be expressed as two subvectors:

$$\mathbf{r}'_{xy} = \begin{bmatrix} \mathbf{h}^* \\ \mathbf{0} \end{bmatrix} \quad (2.12)$$

where: \mathbf{h} = channel impulse response of length L , i.e. $\mathbf{h} = [h(1), h(2), \dots, h(L)]$ and $L=N_f$ for convenience

$\mathbf{0}$ = matrix of zeros with dimension $N_b \times 1$

Using the special structure of eq. 2.11 the inverse of \mathbf{R}'_{xx} can be written as:

$$\mathbf{R}'_{xx^{-1}} = \begin{bmatrix} [\mathbf{\Gamma} - \mathbf{A}^* \mathbf{A}^T]^{-1} & \mathbf{X} \\ \mathbf{X} & \mathbf{X} \end{bmatrix} \quad (2.13)$$

where: \mathbf{X} represents unspecified matrices of appropriate dimensions

The optimal FFF coefficients only depend on $\mathbf{\Omega}$, where $\mathbf{\Omega} = [\mathbf{\Gamma} - \mathbf{A}^* \mathbf{A}^T]$:

$$\mathbf{w}_f = \mathbf{\Omega}^{-1} \mathbf{r}'_{xy, 1:N_f} \quad (2.14)$$

Once the optimal FFF coefficients have been evaluated it is shown in [Smee97, Sell99b] that the FBF coefficients can be computed as:

$$\mathbf{w}_b = \sum_{i=1}^{N_f} h(k-i) \cdot w_{i-1}, \quad k=1, \dots, N_b \quad (2.15)$$

Eq. 2.15 shows that the optimum FBF coefficients are the convolution of the channel impulse response \mathbf{h} with the FFF coefficients \mathbf{w}_f .

For optimal coefficient settings for the space-time DFE and for the MIMO DFE the interested reader is referred to [Ariya99, Lind99] and [Al-Dha00], respectively.

2.3 Adaptive equalization tuning algorithms

Instead of matrix inversion to calculate the equalizer coefficients, one can iteratively tune the equalizer using adaptive algorithms. Such adaptive equalizers also have the advantage that they can track channel variations. The equalizers studied in this thesis are tuned directly, i.e., with the

data. Another possibility is to tune the equalizer indirectly, which has been explored in [Shuk91, Lo95]. In this case the channel impulse response and the estimate of the noise correlation matrix are necessary. The direct approach is however more robust to channel variations. Widely known tap-update algorithms are the LMS and RLS algorithms, which are reviewed here.

2.3.1 Least mean square algorithm

The LMS algorithm belongs to the family of stochastic gradient algorithms. In essence it is a stochastic version of the well known steepest descent method. The cost function of the LMS algorithm is the MSE criterion:

$$J(n) = E[|e(n)|^2] \quad (2.16)$$

In the LMS algorithm the cost function $J(n)$ is replaced by its instantaneous coarse estimate:

$$\hat{J}(n) = |e(n)|^2 \quad (2.17)$$

The idea behind the LMS algorithm is somewhat similar to the steepest decent method: Arbitrarily initialise the tap coefficients. This corresponds to a point in the bowl shaped hyperdimensional MSE surface. Compute the gradient vector ΔJ . At each iteration update the tap coefficients in the opposite direction corresponding to its gradient component multiplied by a certain step size.

The following treatment of the LMS algorithm is with a LE (see Fig. 2-1) in mind. Hence, the pre-slicer data is given by:

$$z(k) = \mathbf{w}^H(k) \cdot \mathbf{x}(k) \quad (2.18)$$

where: $\mathbf{w}^H(k) = [w_0^*(k), w_1^*(k), \dots, w_{N_f-1}^*(k)]$, i.e. tap coefficient vector at time $t=k \cdot T$

$$\mathbf{x}(k) = [x(k), x(k-1), \dots, x(k-N_f+1)]^T, \text{ i.e. tap input vector at time } t=k \cdot T$$

The error estimate in training mode at time $t = k \cdot T$ is:

$$e(k) = y(k) - z(k) \quad (2.19)$$

In decision directed mode the desired output $y(k)$ is replaced by the estimated output $\hat{y}(k)$.

The gradient of the cost function $\hat{J}(n)$ can be written as:

$$\frac{\partial \hat{J}(k)}{\partial \mathbf{w}} = -2 \cdot e^*(k) \cdot \mathbf{x}(k) \quad (2.20)$$

And hence the recursive tap-update equation is given by:

$$\mathbf{w}(k+1) = \mathbf{w}(k) + \mu \cdot e^*(k) \cdot \mathbf{x}(k) \quad (2.21)$$

where: $\mu = \text{step size}$

Due to its simplicity the LMS algorithm has been applied in many areas, including adaptive equalization, adaptive beamforming, adaptive noise cancellation and adaptive channel estimation.

The LMS algorithm converges in the mean square sense if the step size μ is:

$$0 < \mu < \frac{2}{\lambda_{\max}} \quad (2.22)$$

where: λ_{\max} = largest eigenvalue of the tap input correlation matrix \mathbf{R}_{xx}

The dependency of the step size parameter μ upon the eigenvalue spread of the correlation matrix \mathbf{R}_{xx} is a major drawback of the LMS algorithm. This disadvantage is alleviated in the RLS algorithm, which is treated in the next section. Another price paid by using an adaptive approach is the excess mean square error. The LMS algorithm converges towards the optimum Wiener solution, however it produces a mean square error, which is in excess of the optimum Wiener solution.

The LMS algorithm can also be used for the other equalizer structures by stacking the tap input vector and coefficient vector accordingly. For example in the case of a DFE, the tap input vector is given by eq. 2.8 and the coefficient vector is given by eq. 2.9. The rest of the recursion remains the same.

2.3.2 Recursive least squares algorithm

The main problem of the LMS algorithm is its slow convergence speed. The RLS algorithm is known to be the fastest converging adaptive algorithm and is effectively a special Kalman filter. In contrast to the LMS algorithm, which works on instantaneous estimates, the RLS algorithm works with a time average. The cost function of the RLS algorithm is the exponentially weighted sum of squared errors:

$$J(k) = \sum_{i=0}^k c^{k-i} \cdot |e(i, k)|^2 \quad (2.23)$$

where: c = weighting factor, i.e. $0 < c < 1$

The weighting factor is introduced to avoid the problem of infinite memory and the choice of c makes the RLS algorithm more or less sensitive to recent data. It is common to chose an exponential weighting factor such as that used in eq. 2.23. For the following derivation of the RLS algorithm a LE is assumed. The estimation error is defined as:

$$e(i, k) = y(i) - \mathbf{w}^H(k) \cdot \mathbf{x}(i), \quad i=0, 1, \dots, k \quad (2.24)$$

where: $y(i)$ = desired response at time $t=i \cdot T$

$$\mathbf{w}(k) = [w_0(k), w_1(k), \dots, w_{N_f-1}(k)]^T$$

$$\mathbf{x}(i) = [x_0(i), x_1(i), \dots, x_{N_f-1}(i)]^T$$

The optimum tap weight vector \mathbf{w} for which the cost function of eq. 2.23 attains its minimum is defined by the following normal equations written in matrix form [Hay96]:

$$\mathbf{R}_{ls}(k) \cdot \mathbf{w}(k) = \mathbf{r}_{ls}(k) \quad (2.25)$$

where:
$$\mathbf{R}_{ls}(k) = \sum_{i=0}^k c^{k-i} \cdot \mathbf{x}(i) \cdot \mathbf{x}^H(i) \quad (2.26)$$

$$\mathbf{r}_{ls}(k) = \sum_{i=0}^k c^{k-i} \cdot \mathbf{x}(i) \cdot y^*(i)$$

By isolating the term for $i = k$ in eq. 2.26, one obtains the recursive update equation:

$$\mathbf{R}_{ls}(k) = c \cdot \mathbf{R}_{ls}(k-1) + \mathbf{x}(k) \cdot \mathbf{x}^H(k) \quad (2.27)$$

In a similar fashion a recursion can be derived for the cross-correlation vector:

$$\mathbf{r}_{ls}(k) = c \cdot \mathbf{r}_{ls}(k-1) + \mathbf{x}(k) \cdot y^*(k) \quad (2.28)$$

By applying the matrix inversion lemma to eq. 2.27, one can express the inverse of $\mathbf{R}_{ls}(k)$ as [Hay96]:

$$\mathbf{R}_{ls}^{-1}(k) = c^{-1} \cdot \mathbf{R}_{ls}^{-1}(k-1) - \frac{c^{-2} \cdot \mathbf{R}_{ls}^{-1}(k-1) \cdot \mathbf{x}(k) \cdot \mathbf{x}^H(k) \cdot \mathbf{R}_{ls}^{-1}(k-1)}{1 + c^{-1} \cdot \mathbf{x}^H(k) \cdot \mathbf{R}_{ls}^{-1}(k-1) \cdot \mathbf{x}(k)} \quad (2.29)$$

Setting $\mathbf{P}(k) = \mathbf{R}_{ls}^{-1}(k)$, the Kalman gain vector is defined as:

$$\mathbf{k}(k) = \frac{c^{-1} \cdot \mathbf{P}(k-1) \cdot \mathbf{x}(k)}{1 + c^{-1} \cdot \mathbf{x}^H(k) \cdot \mathbf{P}(k-1) \cdot \mathbf{x}(k)} \quad (2.30)$$

Inserting these definitions in eq. 2.29, it follows:

$$\mathbf{P}(k) = c^{-1} \cdot (\mathbf{P}(k-1) - \mathbf{k}(k) \cdot \mathbf{x}^H(k) \cdot \mathbf{P}(k-1)) \quad (2.31)$$

A similar recursion for the tap weight vector can be found [Hay96]:

$$\mathbf{w}(k) = \mathbf{w}(k-1) + \mathbf{k}(k) \cdot e^*(k) \quad (2.32)$$

With these equations the RLS algorithm can be summarized as follows:

1. compute the equalizer output $\hat{y}(k) = \mathbf{w}^H(k-1) \cdot \mathbf{x}(k)$
2. compute the estimation error $e(k) = y(k) - \hat{y}(k)$
3. compute the Kalman gain vector according to eq. 2.30
4. compute the inverse of correlation matrix according to eq. 2.31
5. update the tap weight vector according to eq. 2.32

In a similar fashion to that mentioned in section 2.3.1, the RLS algorithm can also be applied to the other equalizer architectures through appropriate stacking of the tap weight vector and the tap input vector.

2.4 Complexity reduction techniques

For high-speed wireless communication systems, complexity reduction techniques for the equalization operation have been suggested. Methods can be divided into: a) complexity reduction through modified equalizer architectures, b) complexity reduction at the hardware level and c) complexity reduction via tap-selection.

In [Ariya97b] a *modified DFE architecture* is proposed, where only the FFF needs training and the FBF requires no training and can be realised without multipliers for QPSK. Certain modulation formats such as QPSK allow the FBF to be realised with adders and/or look-up tables. However for large constellations (e.g. 64QAM), the FBF is not multiplication free. In this case the equalization complexity is dominated by the large number of FBF taps (and not the comparatively small number of FFF taps). The modified architecture requires an estimate of the channel and it is shown that the proposed DFE is equivalent to a conventional DFE in the absence of channel estimation errors. The coefficients of the FBF of the proposed DFE can be directly loaded from the channel estimate. With this architecture it is desired to keep the FFF as short as possible and have a long FBF. This is firstly because the FBF does not produce noise enhancement (unlike the FFF), and secondly the FBF can be realised with much less complexity. Further Ariyavisitakul proposes an open loop timing recovery scheme so that the receiver can find optimum symbol timing in order to maximise the output SNR of the equalizer. To *reduce the complexity at the hardware level*, schemes have been proposed which restrict the equalizer coefficients to be a sum of a power-of two [Pir84]. In this way multipliers can be replaced by shift registers and adders. Another method uses a signed power-of-two number representation for the equaliser input data in order to replace all multipliers with barrel shifters and adders [Nix96a, Nix96b]. Additional to this scheme, the delayed least mean square algorithm is suggested for equalizer tap updates. This pipelining technique increases the through put of a DFE equalizer with reasonable hardware cost. However pipelining of the LMS introduces an adaptation delay which for the LMS algorithm can result in stability problems. This effect has been studied by Long [Long89] with the result that by using an appropriately small step size, the convergence speed and the steady-state misadjustment in a stationary environment is only slightly degraded. Thus pipelining trades off complexity with slight performance degradation. Another pipelining technique, which does not suffer from adaptation delay is presented in [Dou98]. A technique, which trades off complexity with through-put is presented in [Bull99]. Here a sequential complex multiplier is proposed, which has only half the through-put of a conventional multiplier, however the complexity (which is directly related to chip area) is only half that of the conventional multiplier.

For sparse multipath channels, *tap selection strategies* pay off by giving significant reductions in computational complexity. Tap selection results in nonuniform tap spacings and this is very

effective in cases where both a long overall span and small intertap spacings are needed. Fevrier [Fev98, Fev99] presents a simple thresholding scheme, based on his equalizer architecture. If the magnitude of a multipath echo is smaller than a certain threshold, the corresponding equalizer tap is set to zero. Ariyavisitakul [Ariya97a] presents a tap allocation technique, which optimises tap-spacing with respect to output SNR at the equalizer. Although being computationally more efficient than the following tap allocation strategies, Ariyavisitakul's method is suboptimal. An exhaustive tree search algorithm for LEs is presented in [Rag93] for the problem of optimising tap positions. An optimal method for tap selection is proposed in [Lee98b]. However this technique requires the solution of a $2N_f+N_b$ set of non-linear equations (N_f =number of feedforward taps, N_b =number of feedback taps) and is therefore far too complex for FBWA applications.

2.5 Multiple antennas at the base station

The highlighted boxes of Fig. 2-6 give an overview of the areas addressed in this research. First as described in section 2.1.1-2.1.2 time-only equalization methods are investigated. However, time-only approaches have very limited capability to suppress CCI [Lo95, Mede99]. The installation of MEAs at the BS offers enhanced system performance, since CCI can be effectively suppressed. Regarding the receiver/transmitter architecture one can distinguish between spatial processing and space-time processing methods. Further space-time processing can be either decoupled or joint.

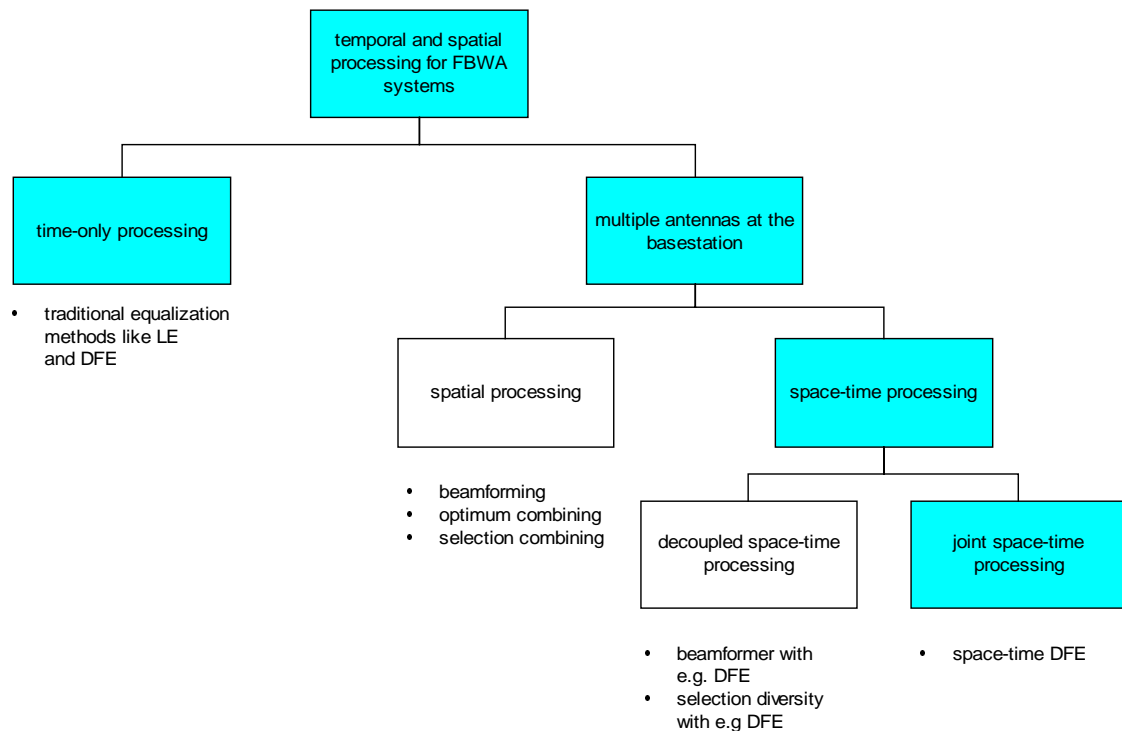


Fig. 2-6: Temporal and spatial processing for FBWA systems

A member of the *spatial processing* category is beamforming. In this context beamforming is narrowband and such a beamformer can be viewed as a spatial equalizer. The broadband beamformer is in essence a space-time linear equalizer [Monz80] and falls in the category of joint space-time processing. A beamformer has only one tap for each antenna input. Although beamforming is effective for narrowband signals, it cannot cope with broadband signals, where the ISI spans several symbol periods.

Beamforming has been applied in many areas including radar, sonar, imaging and communication. One of the first beamformers was the delay-and-sum beamformer reviewed in [Godar97]. Here the amplitude of all weights is the same, but the phase of the beamformer weights differ. A spatial processing approach known as optimum combining has been applied for SDMA in narrowband systems [Wint84, Wint87b] subject to multipath fading. In [Wint84] optimum combining is applied to combat independent flat Rayleigh fading in a digital mobile radio system. Optimum combining can be viewed as an optimum beamformer for narrowband systems with multiple antennas and multipath. One has 3 options with optimum combining: a) to combat fading and enhance the signal quality, b) combat fading and suppress CCI or c) combat fading and detect multiple users in the same time and frequency slot. It has been demonstrated by Winters that optimum combining outperforms maximum ratio combining (MRC) in the case of CCI. One striking result is that optimum combining with one strong interferer and one additional antenna will always perform better than MRC without the interferer. Optimum combining maximises the SNIR. Since maximising the SNIR is equivalent to minimising the MSE, optimum combining can be implemented efficiently in hardware with the LMS algorithm. The RLS algorithm can also be used, but Winters only considers the LMS algorithm in his publications. A description of the LMS and the RLS algorithm applied to beamforming can be found in [Wid67, Monz80, Veen88].

Winters also investigated optimum combining for narrowband in-building mobile systems [Wint87b]. Again SDMA performance was studied for multiple antennas at the BS and single antennas at the remote unit. The BS uses one optimum combiner for each user that makes use of all the signals received by each of the M antennas. The number of antennas determines the number of degrees of freedom. Hence a M element adaptive antenna array using optimum combining can either suppress up to $M-1$ interferers or detect up to M users simultaneously [Wint87b].

The challenge for FBWA is therefore to find low complexity approaches suitable for frequency selective environments, which offer similar advantages to the situation when optimum combining is applied to narrowband systems. Optimum combining has also been studied for frequency selective environments [Ng98b] and the resulting structure is equivalent to a space-time DFE. It falls in the category of joint space-time processing and will be treated later (see section 2.1.3).

Other spatial processing approaches are selection combining and equal gain combining. For equal gain combining all the weights of the spatial processor are set to unity. Selection combining on the other hand selects the antenna with the strongest signal for further processing. Hammerschmidt [Ham99] compares selection combining, optimum combining and single antenna reception at a vehicle. His results show that optimum combining outperforms selection combining. Further, optimum combining without CCI (which has the same performance as maximum ratio combining in this case) also outperforms selection combining. With 3 antennas all the spatial processing methods studied significantly outperform single antenna reception at the vehicle.

Another classification is transmit diversity and receive diversity. With multiple antennas at the BS and a single antenna at the SU, the uplink usually employs receive diversity techniques and the downlink is a candidate for the use of transmit diversity. First, space-time processing in the uplink for FBWA systems with multiple antennas at the BS is reviewed and in the following section, space-time processing in the downlink is addressed.

2.5.1 Space-time processing in the uplink

Decoupled approaches for space-time processing at the mobile are investigated in [Ham00]. The decoupled approach, i.e., selection combining preceding a time-only DFE, is compared with the space-time DFE. The joint space-time optimisation outperforms the decoupled space-time approach.

The space-time DFE is used to suppress CCI in [Ariya99, Ham00]. It is shown that the space-time DFE outperforms single antenna systems in the presence of CCI. Further, if no CCI is present, the space-time DFE significantly enhances the signal quality, which allows for example, much larger cell sizes.

Channel estimation for space-time channels has been explored in [Lind99, Nicol01]. It is seen that reduced rank channel estimation shows an advantage over full-rank ML channel estimation. The time-only domain MLSE has also been extended into a space-time variant by [Ariya99, Lind99]. However, owing to its complexity it has not been considered for the FBWA systems studied in this research.

A theoretical treatment of the finite-length MIMO DFE is presented in [Al-Dha00]. The optimum FFF and FBF coefficients for the delay optimised finite-length MIMO DFE are derived. In a later paper by Komninakis [Kom02] a MIMO DFE in conjunction with a Kalman filter for channel tracking is proposed. The suggested architecture is superior to LMS/RLS MIMO DFEs for time-varying channels. It also describes how the conventional single antenna LMS and RLS algorithms can be extended to the multi-antenna case. However the performance improvement in terms of symbol error rate comes at the cost of increased complexity and it

remains to be seen if the proposed architecture outperforms the MIMO DFE (trained with the LMS or RLS algorithm) in quasi-static channel conditions.

2.5.2 Space-time processing in the downlink

Choi [Choi99a, Choi99b] proposes a transmit diversity scheme for reciprocal channels. It is a form of pre-coding for frequency-selective MIMO channels. The receiver weights of a space-time LE are used for transmission. This separates multiple users under the condition that the channel stays more or less the same during reception and transmission. In time division duplex (TDD), i.e. ping-pong systems, this condition is valid when the channel fading rate is slow and the channel can be seen as quasi static during one reception/transmission interval.

Another interesting transmit diversity scheme is presented in [Alamo98]. This scheme is designed for frequency-flat channels, and hence its applicability to single-carrier FBWA systems in frequency selective channels remains the subject of future work. The encoding is done in space and time (i.e. space-time coding). However, as suggested in this paper, the coding could equivalently be performed in space and frequency through the use of two adjacent carriers. The scheme is presented with two transmit antennas and one receive antenna. Extensions to multiple receive antennas are also discussed. The scheme presented in [Alamo98] however lies in the area of space-time coding. All the results presented in this thesis are achieved without coding. However it is likely that applying coding will give further improvements in system performance (e.g. probability of symbol error), though at the cost of additional complexity. The scheme presented in [Alamo98] has been generalized to an arbitrary number of antennas in [Tar99c].

Chapter 3

Channel Modelling for Fixed Broadband Wireless Access Systems

Most FBWA systems below 10GHz are somewhat similar to mobile cellular systems (such as the GSM cellphone system or the new UMTS (3G) mobile phone systems). Recently a different arrangement known as a mesh architecture has evolved in an attempt to overcome the LOS requirement in some early FBWA systems [MeshN02, Radia02]. However, the main difference between mobile and FBWA systems is that the subscriber units are fixed and not mobile. This is also the reason, why FBWA systems can provide much higher data rates and capacities than mobile systems [Lee98a]. The FBWA propagation environment will now be described and appropriate channel models presented.

3.1 FBWA environments

Fig. 3-1 depicts a typical FBWA environment. Although the transmitter and receiver are fixed, the channel is still time-varying primarily owing to moving scatterers and reflectors in the environment.

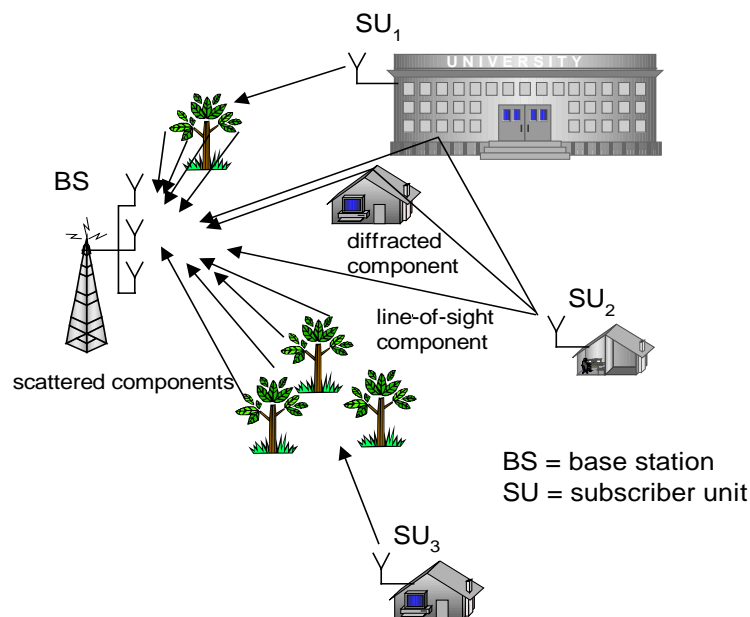


Fig. 3-1: Typical FBWA environment

It turns out that trees are the main source of scattering for FBWA systems. Trees also cause a time-varying propagation environment owing to their movement in the wind and also the foliage variation between seasons. The attenuation factors of the individual paths depend on many factors such as the material or tissue, and its surface structure, for example a wet leaf and a dry leaf will have a different attenuation factor. In [Kim99] it has been shown that foliage combined with rain has a significant impact on the attenuation. These factors all contribute to a changing FBWA propagation environment.

Typically at a receiver a number of rays arrive within one delay bin (i.e. cluster), which is not resolvable by the receiver (owing to its limited bandwidth). In general a number of such clusters give rise to delay spread. If the symbol duration is shorter than the delays spread, ISI results. ISI can be severe in FBWA systems, since the symbol duration gets shorter with increasing data rates. Hence the channel experienced by FBWA systems is usually frequency-selective at typical data-rates.

If the channel consists of only diffuse non-resolvable multipath components (also known as flat fading), the Rayleigh probability density function (pdf) provides a good model for describing the statistics of the amplitude variations of the received signal [Pro95]. Young discovered from measurements made in New York in 1952, that the amplitude variations follow a Rayleigh pdf [Young52]:

Rayleigh pdf:

$$f_{Ray}(x) = \frac{1}{2 \cdot \sigma^2} \cdot \exp\left\{-\frac{x}{2 \cdot \sigma^2}\right\}, x \geq 0 \quad (3.1)$$

where: σ^2 is the variance

If a strong deterministic line-of-sight path or a strong specular path exists the Rician pdf is usually employed to model the small-scale fading. The Rician pdf is given by [Pro95]:

Rician pdf:

$$f_{Rice}(x) = \frac{x}{\sigma^2} \cdot \exp\left\{-\frac{x^2 + s^2}{2 \cdot \sigma^2}\right\} \cdot I_0\left(\frac{x \cdot s}{\sigma^2}\right), x \geq 0 \quad (3.2)$$

where: I_0 is the 0th-order modified Bessel function of the first kind
 s^2 is the noncentrality parameter

The ratio between the deterministic component and the diffuse component is known as the Rician K-factor:

$$K = \frac{P_{LOS}}{P_{diff}} \quad (3.3)$$

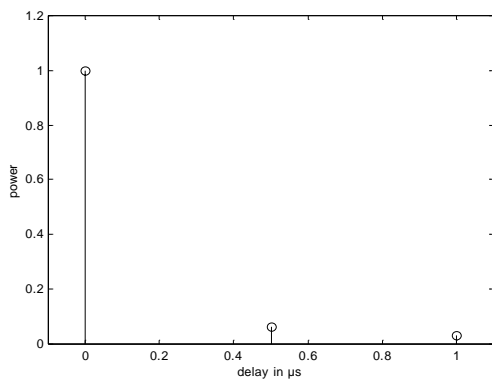
where: P_{LOS} is the power of the deterministic (e.g. line-of-sight) component

P_{diff} is the power of the random diffuse component

So for example a K-factor of zero represents a Rayleigh channel, while a K-factor greater than zero represents a Rician channel.

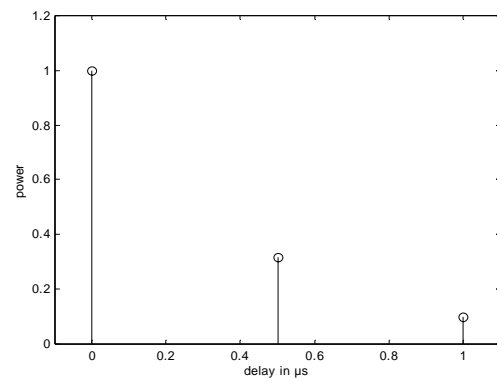
3.2 Channel modelling for single antenna FBWA systems

The channel profiles for the single antenna FBWA systems investigated in this research are the Stanford University SUI channel models [Erceg01]. From the 6 channel models published, SUI-2 and SUI-3 for omni directional antennas at the SU are chosen. SUI-2 represents a typical LOS link, whereas SUI-3 represents a typical NLOS link.



	tap1	tap2	tap3
delay in μs	0	0.5	1
power in dB	0	-12	-15
K-Factor	10	0	0
Doppler in Hz	0.4	0.4	0.4

Fig. 3-2: SUI-2 channel model



	tap1	tap2	tap3
delay in μs	0	0.5	1
power in dB	0	-5	-10
K-Factor	0	0	0
Doppler in Hz	0.4	0.4	0.4

Fig. 3-3: SUI-3 channel model

A total of 6 different radio channel models for MMDS FBWA systems in 3 terrain categories have been defined:

- terrain type A: hilly terrain with moderate-to-heavy tree density
- terrain type B: intermediate path loss conditions are captured in this terrain
- terrain type C: flat terrain with light tree density

SUI-2 represents a worse case link for terrain type C (flat terrain with light tree density). SUI-1 and SUI-2 are Rician channels, whereas the other channels, i.e., SUI-3 to SUI-6 are Rayleigh channels. SUI-3 is a typical channel model for terrain type B. These two power delay profiles are used exclusively throughout the research. The Rayleigh channels are more hostile and exhibit a greater root mean square delay spread (D_{RMS}). The D_{RMS} is defined as:

$$D_{RMS} = \sqrt{\frac{\sum_k (\tau_k - \tau_m) \cdot a_k^2}{\sum_k a_k^2}} \quad (3.4)$$

where: a_k^2 = amplitude of path k
 τ_k = delay of path k
 τ_m = mean excess delay

The mean excess delay is defined as:

$$\tau_m = \frac{\sum_k \tau_k \cdot a_k^2}{\sum_k a_k^2} \quad (3.5)$$

SUI-2 has a D_{RMS} of 0.2 μs and SUI-3 a D_{RMS} of 0.3 μs . D_{RMS} is generally used as an indicator for the level of ISI induced by the radio channel. Strong echoes following the main path have a significant influence on the D_{RMS} , whereas small echoes have little influence.

3.3 Channel modelling for space-time processing in the uplink

The modelling approach to be described in section 3.3.1 for spatial channels has been used extensively in the field of space-time coding, e.g. [Tar99a, Tar99b]. Similarly most earlier theoretical work on capacity assumes frequency flat and ideal diversity channels [Fosch98, Wint87a]. This model is also representative for mobile communication scenarios where the mobile is surrounded by local scatterers. However for the uplink this model is too idealistic. The subsequent channel modelling approaches of sections 3.3.2 and 3.3.3 give more realistic channels for the uplink. The performance of space-time algorithms depends strongly on the envelope fading correlation and values greater than 0.5 [Salz94] have a significant effect on the performance. In order to study BS space-time algorithms for realistic FBWA environments more accurate channel models are necessary. A good overview of spatial channel models for antenna array communication systems is given in [Ert98] including the spatial modelling techniques to be presented in sections 3.3.2 and 3.3.3.

3.3.1 Ideal diversity channel

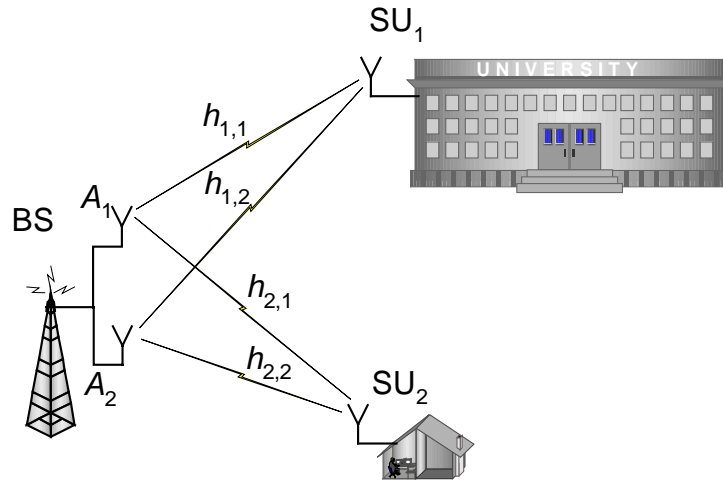


Fig. 3-4: FBWA system with BS equipped with dual antenna array

An ideal frequency selective diversity channel is modelled with independent identically distributed (i.i.d.) random vectors. Each i.i.d random vector $h_{u,m}$ (where the index $u=1 \dots U$ and $m=1 \dots M$, where U is the number of users and M is the number of antennas at the BS) corresponds to one channel realization between a certain SU-BS antenna pair. Hence the zero-lag cross-correlation between these channels is zero, or in other words the envelope correlation coefficient ρ is zero. For narrowband systems, the ideal frequency-flat diversity channel is similarly modelled with an i.i.d. random variable, which corresponds to the path gain and phase between a certain SU-BS antenna pair. The channel power delay profile used in this research for FBWA systems in ideal diversity conditions is the same as that given in section 3.2. The number of channel taps (i.e. length of vector $h_{u,m}$) is 3 for all the SUI models.

3.3.2 Statistical channel models

3.3.2.1 'One-ring' spatial model

The one-ring model was first introduced by Lee [Lee73]. The scatterers are placed on a ring around the mobile, hence the name. This model is suitable for modelling FBWA channels at the BS. It has been used with slight modification in many other papers [Ada86, And91, Par91, Turk91]. Parsons and his collaborators derived a closed-form expression for the cross-correlation ρ using a trigonometric approximation in [Ada86]. This work was extended for 3D space (i.e. modelling the elevation) in [Par91, Turk91]. In [Par91] the mobile is considered whereas in the companion paper [Turk91] the BS is covered. In the 3D extension, the scatterers are now placed on a cylinder. The derivation of ρ in Parsons work is also

applicable to the GWSSUS channel model to be presented in the next section. The only difference is that Parsons used $N(\varphi_0, \varphi_{sp}^2)$ (i.e. a Gaussian pdf with mean φ_0), whereas $N(0, \varphi_{sp}^2)$ (i.e. a Gaussian pdf with zero mean) is used in the GWSSUS model. However both lead to the same result. Further when the elevation is considered, Parsons and his colleagues [Par91, Turk91] used the following pdf (eq. 3.6), whereas in my model to be detailed later a Gaussian pdf will be employed:

$$p(\theta) = \begin{cases} \frac{\pi}{4 \cdot |\theta_m|} \cdot \cos\left(\frac{\pi}{2} \frac{\theta}{\theta_m}\right) & |\theta| \leq |\theta_m| \leq \frac{\pi}{2} \\ 0 & \text{elsewhere} \end{cases} \quad (3.6)$$

Fuhl [Fuhl98] extended Lee's original model [Lee73] to take into account local scatterers at the BS and also LOS components. However, the fading cross-correlation was only analysed for the local scatterer model (i.e. no LOS component and the scatterers are assumed to be located close to the mobile).

All the work on the one-ring model except [Abdi02] only considers the Rayleigh case for deriving the fading cross-correlation. However LOS and specular components (i.e. Rician fading) have a strong influence on the fading cross-correlation.

3.3.2.2 Gaussian wide sense stationary uncorrelated scatterer model

The GWSSUS statistical channel model, which was originally proposed by Zetterberg [Zet97] is to be used in this research to model the uplink of a FBWA system. This model is a two-dimensional extension to the well-known COST channel models [Far97, COST89, Ham00]. In contrast to the one-ring spatial model previously presented in section 3.3.2.1, the GWSSUS model does not make any assumptions about the location of the scatterers. Only the DOA of the multipath rays is modelled and this is effectively what the receiver sees.

Further in [Ham00] the GWSSUS modelling approach is also used for the evaluation of antenna arrays at the mobile. Since this model is used in the subsequent chapters of this thesis for the evaluation of space-time processing in the uplink it will now be described in detail. Further, the original model from Zetterberg is extended to model Rician fading. For Rician fading a closed-form expression for the fading cross-correlation coefficient ρ is derived by combining results from Asztely [Aszt96] and Abid [Abdi02]. Further it is proposed to extend the use of the GWSSUS modelling approach to model spatial SUI channels. Previously the GWSSUS model has only been used in the context of cellular mobile radio environments.

Modelling the steering vector in 3D space

The modelling of the steering vector for a BS antenna array in 3D space will now be described. Fig. 3-5 shows the GWSSUS channel model with 3 clusters and a uniform linear array (ULA) antenna with 4 elements.

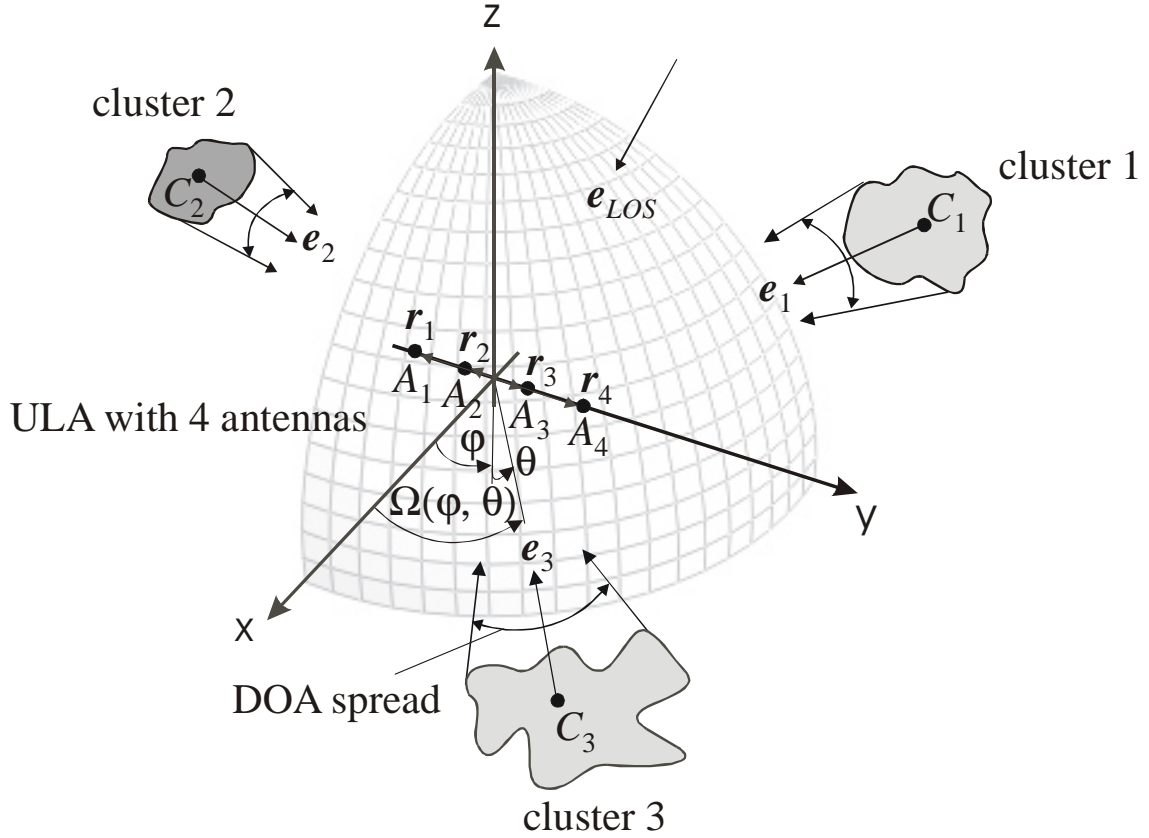


Fig. 3-5: GWSSUS channel model

where: φ = azimuth, i.e. an angle in the x-y-plane
 θ = elevation, i.e. an angle in the y-z-plane

A unit vector e pointing towards the origin of the coordinate system with azimuth φ and elevation θ is defined as:

$$e'(\varphi, \theta) = \begin{bmatrix} \cos \varphi \\ \sin \varphi \\ \sin \theta \end{bmatrix} \quad (3.7)$$

where: $e(\varphi, \theta) = -\frac{1}{|e'(\varphi, \theta)|} \cdot e'(\varphi, \theta)$.

Let e_{diff} be the unit vector of the diffuse component and e_{LOS} be the unit vector of the LOS component.

\mathbf{r} are position vectors from the origin to the antenna element A . The steering vectors \mathbf{a}_{diff} and \mathbf{a}_{LOS} correspond to the diffuse and the LOS component, respectively and are defined as follows:

$$\mathbf{a}_{diff}^l(\boldsymbol{\Omega}_{diff}^l) = \begin{bmatrix} e^{-j\frac{2\pi}{\lambda} \mathbf{e}_{diff}^l(\boldsymbol{\Omega}_{diff}^l) \bullet \mathbf{r}_1} \\ e^{-j\frac{2\pi}{\lambda} \mathbf{e}_{diff}^l(\boldsymbol{\Omega}_{diff}^l) \bullet \mathbf{r}_2} \\ \vdots \\ e^{-j\frac{2\pi}{\lambda} \mathbf{e}_{diff}^l(\boldsymbol{\Omega}_{diff}^l) \bullet \mathbf{r}_M} \end{bmatrix} = \begin{bmatrix} a_{diff,1}^l(\boldsymbol{\Omega}_{diff}^l) \\ a_{diff,2}^l(\boldsymbol{\Omega}_{diff}^l) \\ \vdots \\ a_{diff,M}^l(\boldsymbol{\Omega}_{diff}^l) \end{bmatrix} \quad (3.8)$$

$$\mathbf{a}_{LOS}(\boldsymbol{\Omega}) = \begin{bmatrix} e^{-j\frac{2\pi}{\lambda} \mathbf{e}_{LOS} \bullet \mathbf{r}_1} \\ e^{-j\frac{2\pi}{\lambda} \mathbf{e}_{LOS} \bullet \mathbf{r}_2} \\ \vdots \\ e^{-j\frac{2\pi}{\lambda} \mathbf{e}_{LOS} \bullet \mathbf{r}_M} \end{bmatrix} \quad (3.9)$$

$$a_{diff,m}^l(\boldsymbol{\Omega}_{diff}^l) = e^{-j\frac{2\pi}{\lambda} \mathbf{e}_{diff}^l(\boldsymbol{\Omega}_{diff}^l) \bullet \mathbf{r}_m}, \quad a_{LOS,m}(\boldsymbol{\Omega}_{LOS}) = e^{-j\frac{2\pi}{\lambda} \mathbf{e}_{LOS}(\boldsymbol{\Omega}_{LOS}) \bullet \mathbf{r}_m} \quad (3.10)$$

where: $m = \text{antenna index}, m=1 \dots M$

$l = \text{scatterer index}; l=1 \dots N_{scat}$

$N_{scat} = \text{number of scatterers, here } N_{scat}=50$

Defining the steering vectors in terms of position vector \mathbf{r} and unit vector \mathbf{e} , allows the array geometry to be specified within the channel model so that the modelling is not restricted to any particular antenna array geometry.

The channel tap vector $\mathbf{h}_{u,c}$ for a certain user u is modelled in terms of the steering vectors for a certain cluster c as follows:

$$\mathbf{h}_{u,c} = A_{LOS} \cdot e^{j\phi_{LOS}} \cdot \mathbf{a}_{LOS}(\boldsymbol{\Omega}_{LOS}) + \frac{A_{diff}}{\sqrt{N_{scat}}} \sum_{l=1}^{N_{scat}} b_{diff}^l \cdot e^{j\phi_{diff}^l} \cdot \mathbf{a}_{diff}^l(\boldsymbol{\Omega}_{diff}^l) \quad (3.11)$$

$$\mathbf{h}_{u,c} = \begin{bmatrix} h_{u,1,c} \\ h_{u,m,c} \\ \vdots \\ h_{u,M,c} \end{bmatrix}; \quad \mathbf{h}_{u,c} = \mathbf{h}_{u,c}^{LOS} + \mathbf{h}_{u,c}^{diff}$$

where: $u = \text{user index}, u=1 \dots U$

$m = \text{antenna index}, m=1 \dots M$

$c = \text{cluster index or equivalently delay index}; c=1 \dots C$

$l = \text{scatterer index}; l=1 \dots N_{scat}$

$N_{scat} = \text{number of scatterers, here } N_{scat}=50$

$U = \text{number of users}$

$M = \text{number of antenna elements}$

$C = \text{number of clusters}$

A_{LOS} = amplitude of the LOS component

A_{diff} = amplitude of the diffuse component

b_{diff}^l = attenuation factor for scatterer l

ϕ_{diff}^l = phase of the diffuse component

ϕ_{LOS} = phase of the LOS component

As seen from eq. 3.11 the channel tap vector $\mathbf{h}_{u,c}$ is composed of a LOS component and a diffuse component. Note the attenuation factor of the LOS component is incorporated in A_{LOS} . The K-Factor is defined in terms of A_{diff} and A_{LOS} :

$$K = \frac{A_{LOS}^2}{A_{diff}^2} \quad (3.12)$$

and

$$A_{LOS} = \sqrt{\frac{1}{1 + \frac{1}{K}} \cdot P_{tap}}, \quad A_{diff} = \sqrt{\frac{1}{1 + K} \cdot P_{tap}} \quad (3.13)$$

where: P_{tap} is the channel tap power specified by the SUI power delay profile

Modelling the frequency-selective spatial channel with a 2D FIR filter

The frequency selective spatial channel between a certain SU and a BS equipped with a MEA can be modelled with a 2D FIR filter as shown in Fig. 3-6.

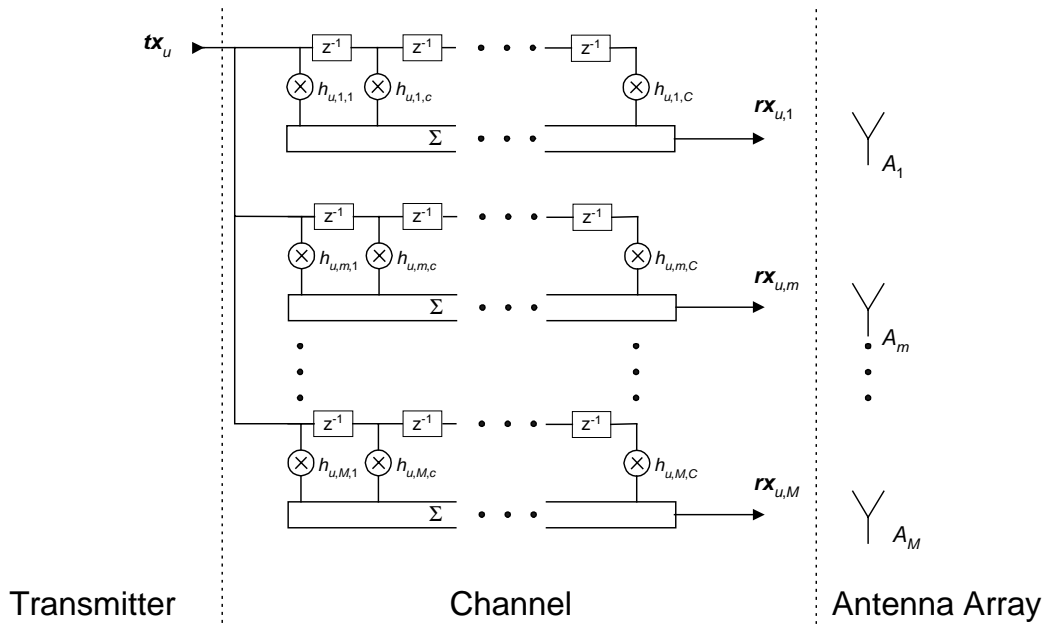


Fig. 3-6: Modelling the frequency-selective channel with a 2D FIR filter structure

This is just a simple extension of the well-known tapped delay line model of frequency-selective channels [Pro95, chapter 14].

Closed-form expression for the envelope cross-correlation ρ for horizontal wave propagation

The spatial cross-correlation ρ between two antenna channels h_p and h_q is defined as:

$$\rho(t) = \frac{1}{\sqrt{P_p \cdot P_q}} E[h_p(t) \cdot h_q^*(t)] \quad (3.14)$$

$$P_p = E[|h_p(t)|^2] \text{ and } P_q = E[|h_q(t)|^2]$$

where: p and q are BS antenna indices, i.e. $p=1 \dots M$ and $q=1 \dots M$ and $p \neq q$

M is number of antennas at the BS.

The channels h_p and h_q are scalars. This is because the fading cross-correlation ρ is usually defined for a narrowband (i.e. frequency-flat) channel [Abdi02, Aszt96, Ham99, Ham00, Salz94, Ulya01]. Consequently for this analysis, the GWSSUS spatial channel model has only one cluster.

According to Abdi, eq. 3.14 is composed of a LOS component and a diffuse component:

$$\rho(t) = \rho_{LOS}(t) + \rho_{diff}(t)$$

$$\text{where: } \rho_{LOS_{p,q}} = \frac{K}{K+1} \cdot a_{LOS,p} \cdot a_{LOS,q}^*$$

$$\rho_{diff_{p,q}} = \frac{1}{K+1} \cdot E[a_{diff,p} \cdot a_{diff,q}^*]$$

$$\rho_{LOS_{p,q}} = \frac{K}{K+1} \cdot \exp\left\{j \cdot \frac{2\pi}{\lambda} \cdot \mathbf{e}_{LOS} \cdot (\mathbf{r}_q - \mathbf{r}_p)\right\}. \quad (3.15)$$

Assuming the azimuth φ and elevation θ are i.i.d. random variables, the expectation of $\rho_{diff_{p,q}}$

is:

$$\rho_{diff_{p,q}} = \frac{1}{K+1} \cdot \int_{-\infty}^{+\infty} \int_{-\infty}^{+\infty} \exp\left\{j \cdot \frac{2\pi}{\lambda} \cdot \mathbf{e}_{diff} \cdot (\mathbf{r}_q - \mathbf{r}_p)\right\} \cdot f_\varphi \cdot f_\theta \cdot d\varphi \cdot d\theta \quad (3.16)$$

where: f_φ = pdf of azimuth

f_θ = pdf of elevation.

In the following two sections a closed-form expression for the fading-cross correlation for a ULA is derived. The subsequent analysis is based on horizontal wave propagation, i.e., the elevation is set to zero. Further, the BS and SU are fixed and the Doppler effect is neglected, since the Doppler variations are slow compared to the burst duration for FBWA systems. It is assumed that the antenna array consists of omni-directional elements. The azimuth φ is a Gaussian distributed random variable with mean φ_0 and standard deviation φ_{sp} , i.e. $\varphi \sim N(\varphi_0, \varphi_{sp}^2)$.

Fading cross-correlation of the LOS component

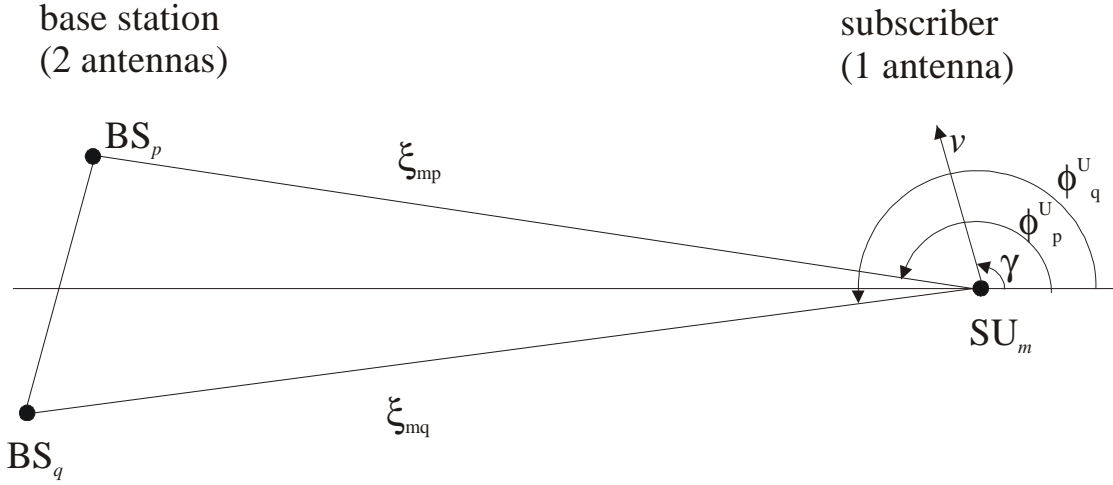


Fig. 3-7: SIMO channel modelling according to Abdi [Abdi02]

Fig. 3-7 shows the propagation model of Abdi [Abdi02] applied to the situation where the subscriber unit has only one antenna (i.e., a single input multiple output (SIMO) channel). Further assuming horizontal wave propagation (i.e. $\theta=0$), the results from Abdi for the cross-correlation of the LOS component simplify to:

$$\rho_{mp,mq}^{LOS}(\tau, t) = \sqrt{\frac{K_{mp} \cdot K_{mq}}{(K_{mp} + 1) \cdot (K_{mq} + 1)}} \cdot \exp \left\{ \begin{array}{l} -\frac{j \cdot 2\pi}{\lambda} [\xi_{mp} - \xi_{mq}] - j \cdot 2\pi \cdot f_D [\cos(\phi_q^U - \gamma)] \cdot \tau \\ + j \cdot 2\pi \cdot f_D [\cos(\phi_p^U - \gamma) - \cos(\phi_q^U - \gamma)] \cdot t \end{array} \right\} \quad (3.17)$$

In Fig. 3-7 v and γ represent the velocity and the direction of the motion of the user, respectively. Hence assuming a fixed subscriber position and neglecting the Doppler ($v=0, f_D=0$) eq. 3.17 simplifies to:

$$\rho_{mp,mq}^{LOS} = \sqrt{\frac{K_{mp} \cdot K_{mq}}{(K_{mp} + 1) \cdot (K_{mq} + 1)}} \cdot \exp \left\{ -\frac{j \cdot 2\pi}{\lambda} [\xi_{mp} - \xi_{mq}] \right\} \quad (3.18)$$

Where the exponential term accounts for the phase difference between antenna BS_p and BS_q . This expression can also be expressed in a form that depends only on the azimuth ϕ_{LOS} by assuming planar wave propagation and that the scatterers are located in the far field as shown in Fig. 3-8.

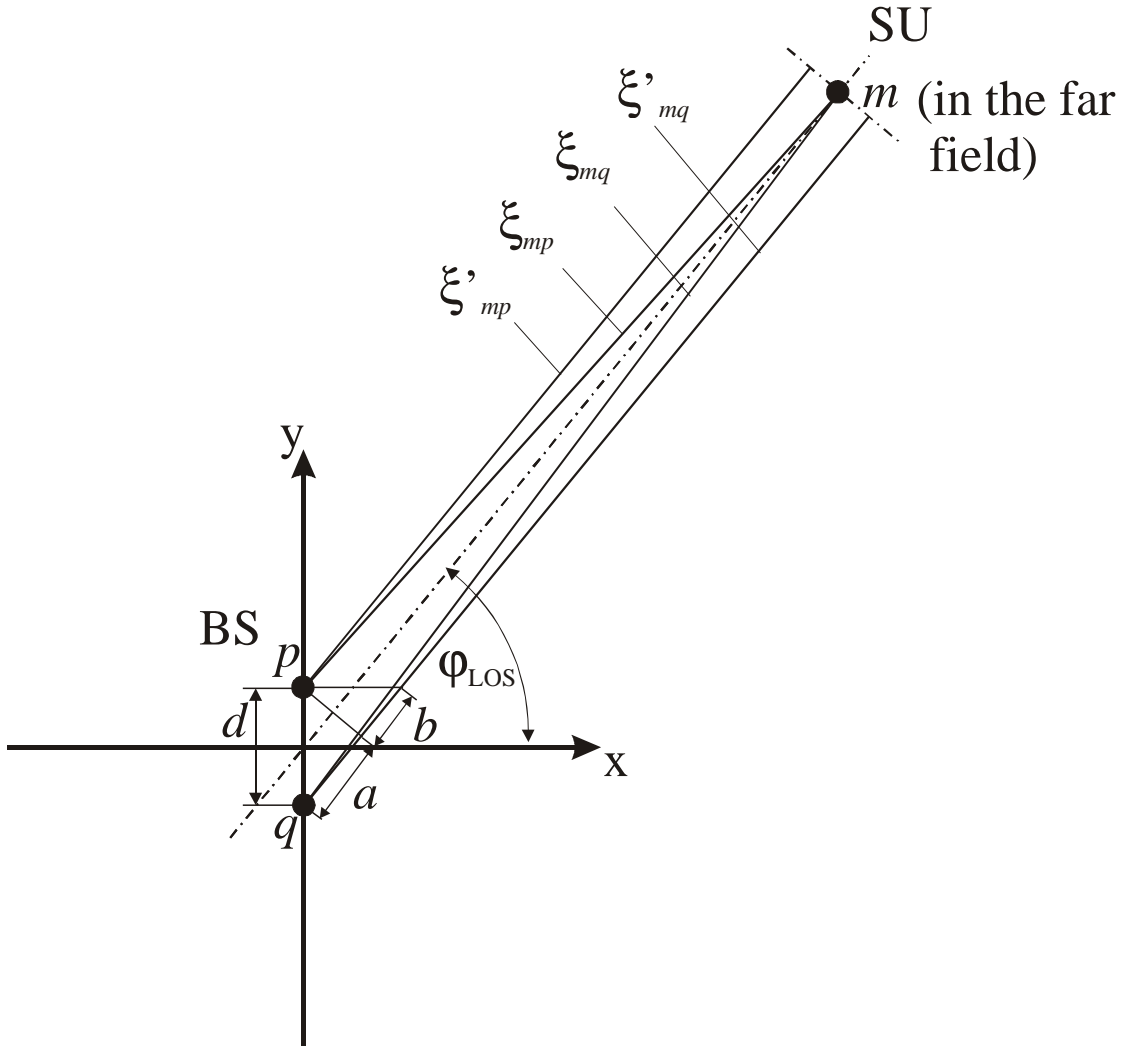


Fig. 3-8: LOS paths when SU is located in the far field

When the SU is in the far field the following approximation can be applied:

$$\xi_{mp} - \xi_{mq} \approx \xi'_{mp} - \xi'_{mq}, \text{ consequently}$$

$$I : a = \xi'_{mq} - \xi'_{mp}$$

$$II : d = r \cdot \cos(90^\circ - \varphi_{LOS}) = r \cdot \sin(\varphi_{LOS})$$

$$III : d^2 = r \cdot a$$

$$IV : r = a + b$$

$$\text{Substituting III in II gives: } d = \frac{d^2}{a} \cdot \sin(\varphi_{LOS}) \Leftrightarrow a = d \cdot \sin(\varphi_{LOS})$$

$$\text{And in I gives: } \xi'_{mp} - \xi'_{mq} = -d \cdot \sin(\varphi_{LOS})$$

Hence:

$$\rho_{LOS} = \sqrt{\frac{K_{mp} \cdot K_{mq}}{(K_{mp} + 1) \cdot (K_{mq} + 1)}} \cdot \exp \left\{ j \cdot 2 \cdot \pi \cdot (p - q) \cdot \frac{d}{\lambda} \cdot \sin(\varphi_{LOS}) \right\} \quad (3.19)$$

where: p = BS antenna index, e.g. for dual antennas BS $p=1..2$

q = BS antenna index, e.g. for dual antennas BS $q=1..2$

$m = \text{SU antenna index, e.g., } m=1 \text{ for SIMO channels}$

Letting the K-Factor for each spatial channel be the same, i.e. $K_{mp}=K_{mq}=K$ gives:

$$\rho_{LOS} = \frac{K}{K+1} \cdot \exp\left\{j \cdot 2 \cdot \pi (p-q) \cdot \frac{d}{\lambda} \cdot \sin(\varphi_{LOS})\right\} \quad (3.20)$$

fading cross-correlation of the diffuse component

The correlation coefficient of the diffuse component ρ_{diff} is derived by Asztely in [Aszt96] and this result can be combined with the correlation coefficient of the LOS component [Abdi02] to obtain the overall correlation coefficient:

$$\rho = \rho_{LOS} + \rho_{diff} \quad (3.21)$$

The separation between the antenna elements p and q is $d \cdot (q-p)$, hence for Rician fading the cross-correlation of the diffuse component is a scaled version of the one Asztely derived. For Rayleigh fading the formula in [Aszt96] can be utilized directly.

$$\varphi_i \sim N(0, \varphi_{sp}^2)$$

$$\begin{aligned} \rho_{diff} &= \sqrt{\frac{1}{(K_{mp}+1) \cdot (K_{mq}+1)}} \cdot E\left[\exp\left\{j \cdot 2 \cdot \pi (p-q) \cdot \frac{d}{\lambda} \cdot \sin(\varphi_0 + \varphi_i)\right\}\right] \\ \rho_{diff} &= \sqrt{\frac{1}{(K_{mp}+1) \cdot (K_{mq}+1)}} \cdot \int_{-\infty}^{\infty} \exp\left\{j \cdot 2 \cdot \pi (p-q) \cdot \frac{d}{\lambda} \cdot \sin(\varphi_0 + \varphi_i)\right\} \cdot \\ &\quad \frac{1}{\sqrt{2\pi} \cdot \varphi_{sp}} \cdot \exp\left\{-\frac{\varphi_i^2}{2 \cdot \varphi_{sp}^2}\right\} d\varphi_i \end{aligned} \quad (3.22)$$

where: $\varphi_0 = \text{mean azimuth}$

$\varphi_{sp} = \text{azimuth spread or DOA spread}$

$\varphi_i = \text{normal distributed azimuth with standard deviation } \varphi_{sp} \text{ and zero mean}$

The derivation of a closed-form expression for ρ_{diff} is possible through the following trigonometric approximation [Aszt96] (valid for small φ_i):

$$\sin(\varphi_0 + \varphi_i) = \sin(\varphi_0) \cdot \cos(\varphi_i) + \cos(\varphi_0) \cdot \sin(\varphi_i) \text{ and } \cos(\varphi_i) = 1, \sin(\varphi_i) = \varphi_i$$

$$\sin(\varphi_0 + \varphi_i) \approx \sin(\varphi_0) + \varphi_i \cdot \cos(\varphi_0)$$

The whole derivation is somewhat lengthy and can be found in Appendix A. Here only the main results are presented. Hence the spatial cross-correlation between the fading of the diffuse component is:

$$\begin{aligned} \rho_{diff} &\approx \sqrt{\frac{1}{(K_{mp}+1) \cdot (K_{mq}+1)}} \cdot \exp\left\{j \cdot 2\pi \cdot (p-q) \frac{d}{\lambda} \cdot \sin(\varphi_0)\right\} \\ &\quad \exp\left\{-\frac{1}{2} \left(2\pi \cdot (p-q) \frac{d}{\lambda} \cdot \cos(\varphi_0) \cdot \varphi_{sp}\right)^2\right\} \end{aligned} \quad (3.23)$$

Further setting $K_{mp}=K_{mq}=K$ (i.e., the K-factor for each SU-BS antenna channel is the same) gives:

$$\rho_{diff} = \frac{1}{K+1} \cdot \int_{-\infty}^{\infty} \exp\left\{j \cdot 2 \cdot \pi (p-q) \cdot \frac{d}{\lambda} \cdot \sin(\varphi_0 + \varphi_i)\right\} \cdot \frac{1}{\sqrt{2\pi} \cdot \varphi_{sp}} \cdot \exp\left\{-\frac{\varphi_i^2}{2 \cdot \varphi_{sp}^2}\right\} d\varphi_i \quad (3.24)$$

And applying the trigonometric approximation from before:

$$\rho_{diff} \approx \frac{1}{K+1} \cdot \exp\left\{j \cdot 2\pi \cdot (p-q) \frac{d}{\lambda} \cdot \sin(\varphi_0)\right\} \cdot \exp\left\{-\frac{1}{2} \left(2\pi \cdot (p-q) \frac{d}{\lambda} \cdot \cos(\varphi_0) \cdot \varphi_{sp}\right)^2\right\} \quad (3.25)$$

Again assuming that the K-factor of each SU-BS antenna channel is the same and applying the trigonometric approximation for both the LOS and the diffuse component, the cross-correlation ρ according to eq. 3.21 is:

$$\rho \approx \frac{K}{K+1} \cdot \exp\left\{j \cdot 2 \cdot \pi (p-q) \cdot \frac{d}{\lambda} \cdot \sin(\varphi_{LOS})\right\} + \frac{1}{K+1} \cdot \exp\left\{j \cdot 2\pi \cdot (p-q) \frac{d}{\lambda} \cdot \sin(\varphi_0)\right\} \cdot \exp\left\{-\frac{1}{2} \left(2\pi \cdot (p-q) \frac{d}{\lambda} \cdot \cos(\varphi_0) \cdot \varphi_{sp}\right)^2\right\}, \quad (3.26)$$

where p and q are antenna indices, thus the fading cross-correlation between antenna 1 and antenna 2 is:

$$\rho = \rho_{LOS} + \rho_{diff} \approx \frac{K}{K+1} \cdot \exp\left\{-j \cdot 2 \cdot \pi \cdot \frac{d}{\lambda} \cdot \sin(\varphi_{LOS})\right\} + \frac{1}{K+1} \cdot \exp\left\{-j \cdot 2\pi \cdot \frac{d}{\lambda} \cdot \sin(\varphi_0)\right\} \cdot \exp\left\{-\frac{1}{2} \left(2\pi \cdot \frac{d}{\lambda} \cdot \cos(\varphi_0) \cdot \varphi_{sp}\right)^2\right\}$$

Closed-form expression for the fading cross-correlation ρ for 3D wave propagation

In this section a closed-form expression for the fading cross-correlation ρ is presented which also takes the elevation θ into consideration. Based on [Far97] the steering vector for a ULA can be expressed as a function of the azimuth and the elevation. Hence ρ_{LOS} and ρ_{diff} for the situation where $K=K_{mp}=K_{mq}$ are:

$$\rho_{LOS} = \frac{K}{K+1} \cdot \exp\left\{j \cdot 2\pi \cdot (p-q) \cdot \frac{d}{\lambda} \cdot \sin(\varphi_0) \cdot \cos(\theta_0)\right\} \quad (3.27)$$

where: $\varphi_i \sim N(0, \varphi_{sp}^2)$

$$\theta_i \sim N(0, \theta_{sp}^2)$$

and, $\rho_{diff} = \frac{1}{K+1} \cdot E\left[\exp\left\{j \cdot 2 \cdot \pi (p-q) \cdot \frac{d}{\lambda} \cdot \sin(\varphi_0 + \varphi) \cdot \cos(\theta_0 + \theta)\right\}\right]$

$$\rho_{diff} = \frac{1}{K+1} \cdot \int_{-\infty}^{\infty} \int_{-\infty}^{\infty} \exp\left\{j \cdot 2 \cdot \pi \cdot (p-q) \cdot \frac{d}{\lambda} \cdot \sin(\varphi_0 + \varphi_i) \cdot \cos(\theta_0 + \theta_i)\right\} \cdot \frac{1}{\sqrt{2\pi} \cdot \varphi_{sp}} \cdot \exp\left\{-\frac{\varphi_i^2}{2 \cdot \varphi_{sp}^2}\right\} \cdot \frac{1}{\sqrt{2\pi} \cdot \theta_{sp}} \cdot \exp\left\{-\frac{\theta_i^2}{2 \cdot \theta_{sp}^2}\right\} d\varphi_i d\theta_i. \quad (3.28)$$

After some lengthy mathematical derivation (see Appendix A: A.3) this equation can be transformed into eq. 3.29 using the following trigonometric approximation (valid for small azimuth φ_i and small elevation θ_i):

$$\sin(\varphi_0 + \varphi_i) = \sin(\varphi_0) \cdot \cos(\varphi_i) + \cos(\varphi_0) \cdot \sin(\varphi_i) \approx \sin(\varphi_0) + \varphi_i \cdot \cos(\varphi_0)$$

$$\cos(\theta_0 + \theta_i) = \cos(\theta_0) \cdot \cos(\theta_i) - \sin(\theta_0) \cdot \sin(\theta_i) \approx \cos(\theta_0) - \theta_i \cdot \sin(\theta_0)$$

$$\rho_{diff} \approx \frac{1}{K+1} \cdot \exp\left\{j \cdot 2\pi \cdot (p-q) \cdot \frac{d}{\lambda} \cdot \sin(\varphi_0) \cdot \cos(\theta_0)\right\} \cdot \exp\left\{-\frac{1}{2} \cdot \left[2\pi \cdot (p-q) \cdot \frac{d}{\lambda} \cdot \varphi_{sp}\right]^2 \cdot \cos^2(\varphi_0) \cdot \cos^2(\theta_0)\right\} \cdot \exp\left\{\frac{1}{2} \cdot \frac{\theta_{sp}^2 \cdot a'^2}{b'}\right\} \cdot \sqrt{\frac{1}{b'}} \quad (3.29)$$

where: $a' = 2 \cdot \cos^2(\varphi_0) \cdot \cos(\theta_0) \cdot \sin(\theta_0) + j \cdot 2\pi \cdot (p-q) \cdot \frac{d}{\lambda} \cdot \sin(\varphi_0) \cdot \cos(\theta_0)$

$$b' = 1 + \frac{1}{2} \cdot \left[2\pi \cdot (p-q) \cdot \frac{d}{\lambda} \cdot \varphi_{sp}\right]^2 \cdot \cos^2(\varphi_0) \cdot \sin^2(\theta_0) \cdot 2 \cdot \theta_{sp}^2$$

3.3.2.3 Gaussian angle of arrival model

The Gaussian angle of arrival (GAA) model is a special case of the GWSSUS model. In the GAA model it is assumed that the power of a certain cluster, and the distribution of this power, with respect to the azimuth is Gaussian with a certain mean and standard deviation [Zet97]. The derivations in the previous section deal exclusively with the GAA case.

3.3.2.4 Model parameters and assumptions for simulating a FBWA uplink

For this simulation model the attenuation factors for all scatterers are set to unity, i.e., $b_{diff}^l = 1$ in eq. 3.11. However each scatterer has a random phase $\phi_{diff}^l \sim U(0,1)$. The same modelling approach was used in [Khat01]. Schulze proposes a similar model for Monte-Carlo simulation of the radio channel for single antenna systems in [Schulz89]. Again the attenuation factor for each path is set to unity, but the phase is a random variable. However the angular domain is not modelled. Setting the attenuation factors to unity for modelling purpose is also the approach in [Par91, Turk91].

It follows from the central limit theorem that the magnitude of the diffuse channel tap vector components $\mathbf{h}_{u,c}^{diff}$ in eq. 3.11 and explicitly shown in eq. 3.30 approaches a Rayleigh pdf for $N_{scat} \rightarrow \infty$.

$$\mathbf{h}_{u,c}^{diff} = \frac{A_{diff}}{\sqrt{N_{scat}}} \sum_{l=1}^{N_{scat}} b_{diff}^l \cdot e^{j\phi_{diff}^l} \cdot \mathbf{a}_{diff}^l(\boldsymbol{\Omega}_{diff}^l) = \begin{bmatrix} h_{u,1,c}^{diff} \\ h_{u,m,c}^{diff} \\ \vdots \\ h_{u,M,c}^{diff} \end{bmatrix} \quad (3.30)$$

The physical reasoning behind this modelling is that we assume that each cluster is composed of a number of rays of approximately the same attenuation. One can imagine that a group of scattered rays of similar power could emerge from for example a tree and arrive within the same delay bin (i.e. cluster). The GWSSUS model used in this research [Zet97] uses $N_{scat}=50$ and this closely resembles a Rayleigh pdf. It is also possible to let b_{diff}^l be a random variable with e.g., a Rayleigh pdf and $b_{diff}^l \in \mathfrak{R}$ [Sal87]. Again with the central limit theorem it can be shown that the vector components $\{h_{u,1,c}, h_{u,m,c}, \dots, h_{u,M,c}\}$ tend to a zero-mean complex Gaussian random variable for $N_{scat} \rightarrow \infty$ and hence the magnitude of the vector components follow a Rayleigh distribution. Such a stochastic process is called a Gaussian wide sense stationary uncorrelated scattering process. The addition of $\mathbf{h}_{u,c}^{LOS}$ in eq. 3.11 for $K>0$ generates a Rice magnitude.

As mentioned before it is assumed that the azimuth φ and elevation θ are independent Gaussian random variables with a certain mean and variance, denoted as:

$$\varphi \sim N(\varphi_0, \varphi_{sp}^2)$$

$$\theta \sim N(\theta_0, \theta_{sp}^2)$$

Further it is assumed that all the scatterers are in the far field. This is justified if the dimension of the antenna array is much smaller than the distance from the scatterer to the BS. Hence planar wave propagation is assumed. Also the narrowband array assumption is utilized. This means, that the baseband signal can be regarded as constant over the time it takes the electromagnetic wave to travel through the antenna array. Or in other words, this means that the array size is assumed to be small compared to the distance covered at the speed of light during one symbol period.

It is assumed that the FBWA system under consideration in this research uses short bursts for communication. The radio channel is generally characterised by a time-varying channel impulse response. However, it is reasonable to regard the channel as constant over the duration of one burst for FBWA, since the burst duration is very small compared to the temporal variations of the channel (i.e. Doppler fading rate is very slow for FBWA channels [Erceg01]). This means a quasi-static analysis approach is taken in this research. However the channel changes randomly from one burst to another.

In accordance with the SUI channel models [Erceg01] the arrival time of the clusters is fixed. With the exception of the previous derivations of the fading cross-correlation ρ , the channel is regarded as frequency-selective.

3.3.2.5 Numerical examples of ρ

Fig. 3-9 shows the absolute value of the fading cross-correlation using the closed-form expression of eq. 3.26 for different antenna spacings and different azimuth spreads. The elevation is not modelled here and hence only horizontal wave propagation is considered. The mean azimuth angle as defined in Fig. 3-5 is 60° for the LOS component and 30° for the diffuse component. A K-factor of 10 according to the SUI-2 model is used [Erceg01].

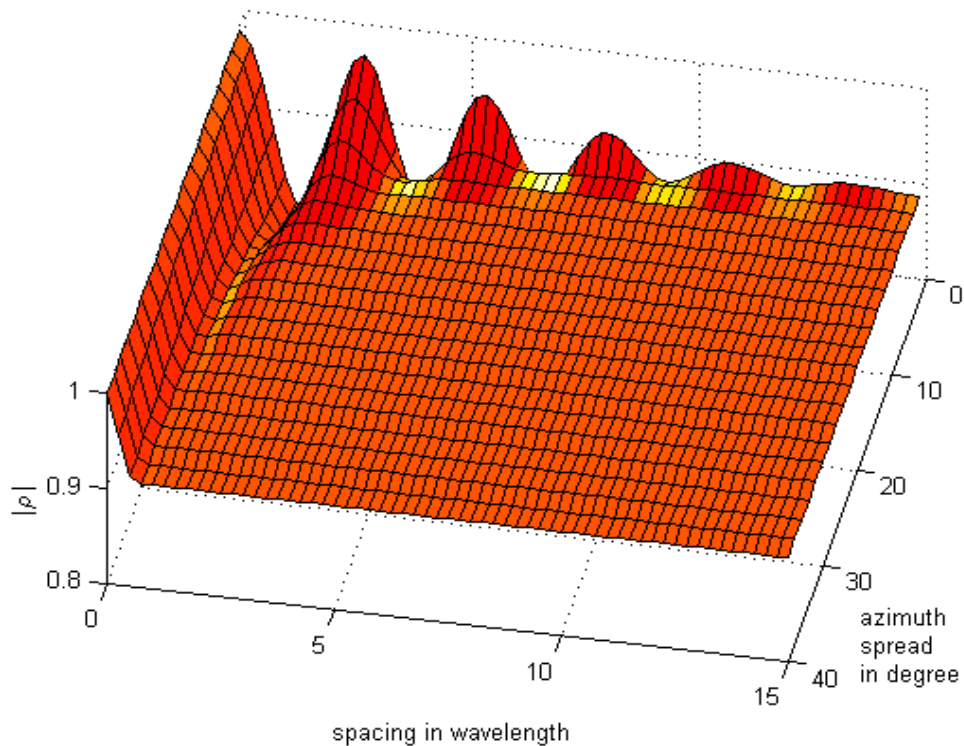


Fig. 3-9: Fading cross-correlation ρ for a mean DOA of 30° for the diffuse component and a mean DOA of 60° for the LOS component with a K-factor of 10

It is interesting to see that even at an azimuth spread of 40° and an antenna separation of 15 wavelengths, the fading cross-correlation is still 0.91. This holds true as long as the narrowband array assumption is valid. The deterministic LOS component has a great effect on the cross-correlation coefficient. This also agrees with the observation, that if a LOS component is present without any diffuse component, the fading cross-correlation will be unity [Salz94].

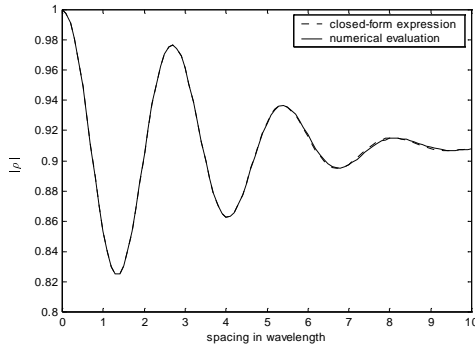


Fig. 3-10: Closed-form expression for ρ and numerical evaluation for a DOA spread of 3° for scenario of Fig. 3-9

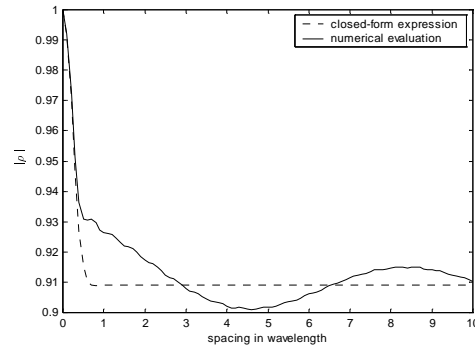


Fig. 3-11: Closed-form expression for ρ and numerical evaluation for a DOA spread of 40° for scenario of Fig. 3-9 (max. error = 2.2%)

A comparison of the closed-form expression with the numerical evaluation for two values of DOA spread performed using Mathematica² is shown in Fig. 3-10 and Fig. 3-11. The maximum error stays within 2.2% for these scenarios.

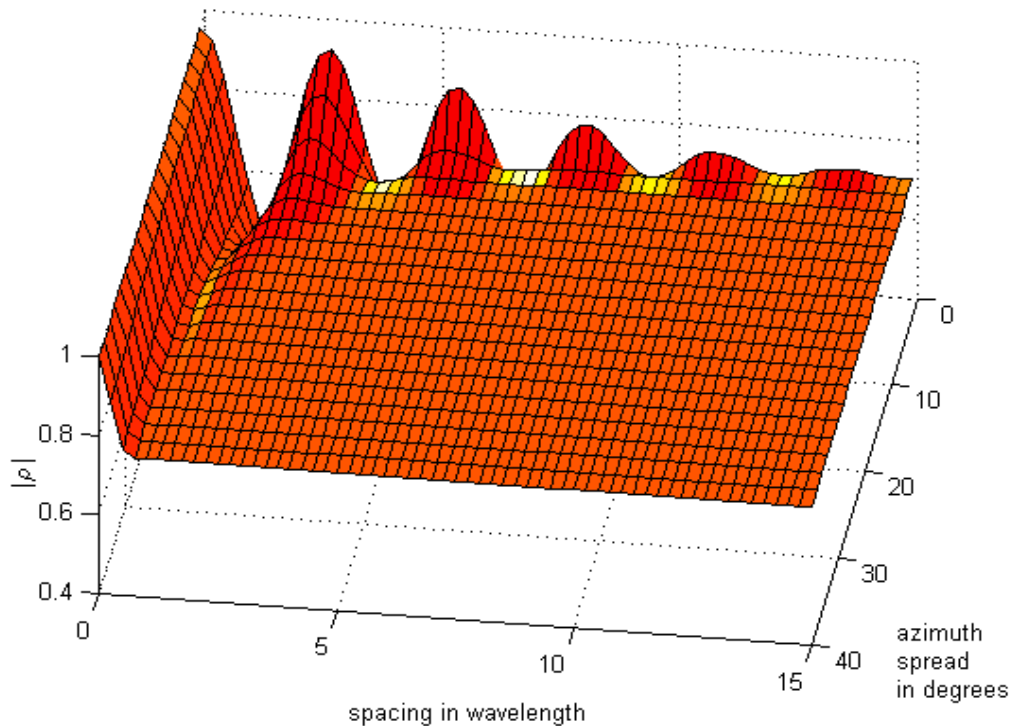


Fig. 3-12: Fading cross-correlation ρ for a mean DOA of 30° for the diffuse component and a mean DOA of 60° for the LOS component with a K -factor of 3

² Mathematica is an integrated environment for technical computing from Wolfram Research, Inc.

In order to show the impact of the K-Factor, the fading cross-correlation ρ is evaluated for the same settings as for Fig. 3-9, but now with a K-Factor of only 3. This reduces ρ to 0.75 for large antenna separations and large DOA spreads. In essence the LOS component introduces a mean component in $|\rho|$, whereas the diffuse component causes the fluctuations.

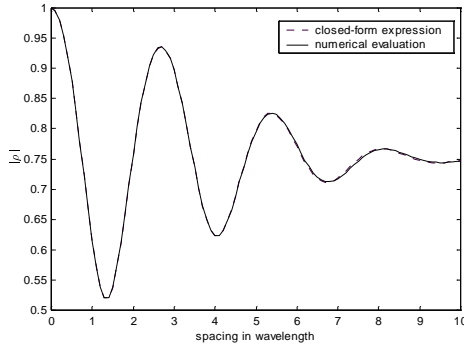


Fig. 3-13: Closed-form expression for ρ and numerical evaluation for a DOA spread of 3° for scenario of Fig. 3-12

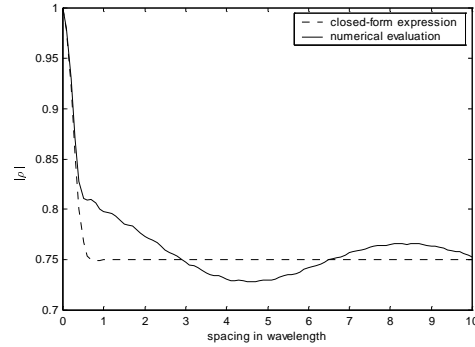


Fig. 3-14: Closed-form expression for ρ and numerical evaluation for a DOA spread of 40° for scenario of Fig. 3-12 (max. error = 8%)

Fig. 3-13 and Fig. 3-14 compare the results obtained using the closed-form expression of eq. 3.26 with the results obtained with the numerical evaluation of eq. 3.21 and eq. 3.22. It is seen that the maximum error is about 8%.

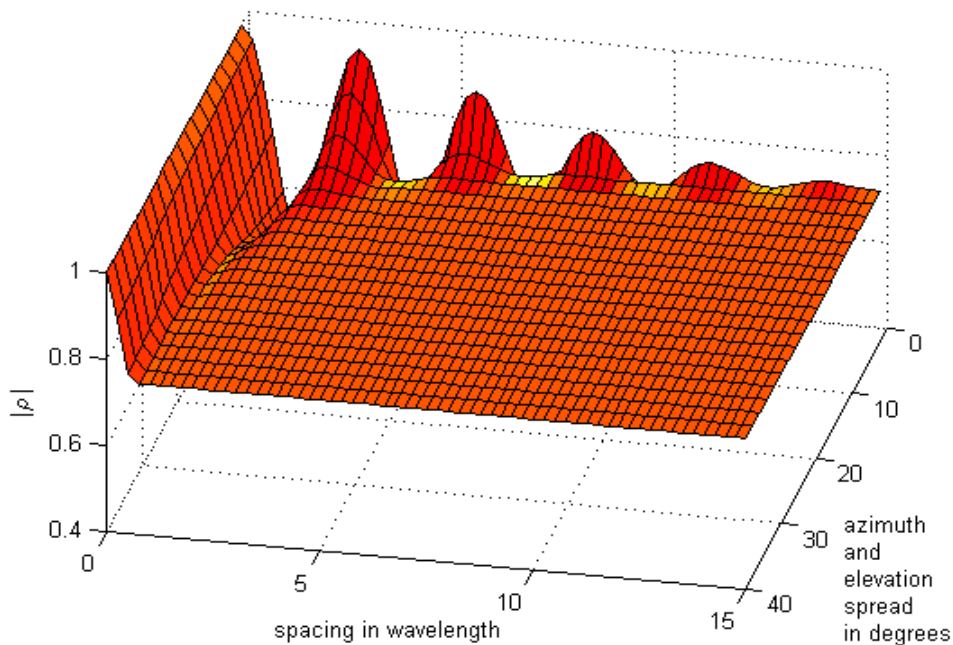


Fig. 3-15: Fading cross-correlation ρ for a mean DOA of 30° in azimuth for the diffuse component and a mean DOA of 60° in azimuth for the LOS component with a K-factor of 3, the mean DOA in elevation for both components is 10°

Finally, elevation is modelled as well. The same scenario as before is assumed except this time a mean elevation of 10° for both the LOS component and the diffuse component is assumed. Here the closed-form expression evaluates in a few seconds, whereas the numerical evaluation takes a number of hours in Mathematica.

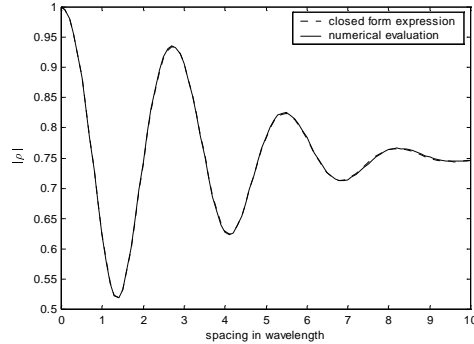


Fig. 3-16: Closed-form expression for ρ and numerical evaluation for a DOA spread of 3° for scenario of Fig. 3-15

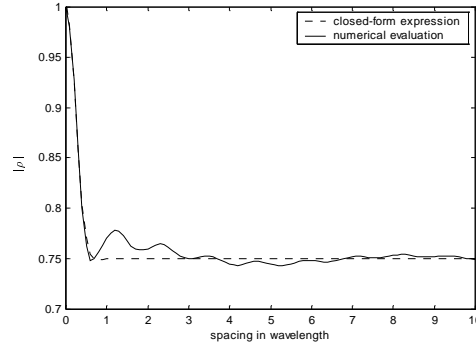


Fig. 3-17: Closed-form expression for ρ and numerical evaluation for a DOA spread of 40° for scenario of Fig. 3-15 (max. error = 4%)

The maximum error observed in Fig. 3-16 and Fig. 3-17 is 4%. Again the closed-form results agree closely with the numerical evaluations.

3.3.3 Ray tracing simulation

Ray tracing is the most accurate simulation based method for a particular environment, but also the most computationally expensive. A ray tracing simulation is mainly used for predicting signal strength in a geographic area and is subsequently used to determine suitable BS placement [Ver02a, Ver02b, Erceg97, Wright98]. Ray tracing uses maps, usually in a digital format, to predict the propagation in a certain wireless environment and is therefore a deterministic channel modelling approach. Ray tracing tools are capable of generating the channel impulse response for a specified environment [Ver02a, Ver02b, Fort95, Sei94].

In [Ver02a, Ver02b] ray tracing is used for automatic BS placement. Unfortunately, diffraction and scattering are not modelled, but these two propagation mechanisms are significant for FBWA channels [Cros00, Erceg99, Erceg01]. In [Tame98] foliage (e.g. trees and hedges) is taken into account in the ray tracing model and is shown to have a significant impact on model accuracy when compared to measurements in rural and urban environments.

As well as being used to predict signal strength and coverage for BS placement the WiSE toolkit also enables realistic capacity simulations to be performed [Chuah00, Ling01].

Despite the strength of ray tracing for optimising BS location, ray tracing is not usually used for simulating the small scale fading effects pertinent for assessing equalization and space-time processing algorithms. These algorithms are usually tested over a variety of channel conditions

and therefore statistical channel models (e.g. such as those in section 3.3.2) are the preferred choice. Another reason is the very high computational complexity of ray tracing compared to statistical channel models. For example the ray tracing tool of Verstak [Ver02a, Ver02b] runs in parallel on a 200 node Beowulf cluster of Linux workstations.

3.4 Conclusions

Channel modelling approaches appropriate for the uplink of FBWA systems have been presented. The original GWSSUS channel model from Zetterberg [Zet97] is modified to accommodate Rician fading and FBWA channels. The combination of previous single antenna measurement results for FBWA environments [Erceg01] with the GWSSUS channel model has resulted in a statistical channel model for FBWA systems.

Via a trigonometric approximation a closed-form expression for the fading cross-correlation ρ for multiple BS antennas has been derived. This approximation holds when the DOA spread is small, which is usually the case for the macrocells typical for a FBWA network. The closed-form expressions presented for Rician channels using the GWSSUS channel model has not been previously derived. This expression permits the fading cross-correlation ρ to be quickly evaluated for both 2D (horizontal) and 3D (both horizontal and vertical) wave propagation.

Realistic assumptions for simulating the FBWA uplink are summarized in section 3.3.2.4. Numerical examples are given in section 3.3.2.5 for ρ in selected environments. The derived closed-form expressions are compared with numerical evaluations performed using Mathematica. It is seen that the closed-form expressions are accurate if the DOA spread is low, which is a reasonable assumption for reception at a BS where the antenna is placed above the heights of the roof tops.

Chapter 4

Equalization Requirement Study for Single Antenna MMDS FBWA Systems

4.1 Introduction

In order to be competitive, FBWA systems must offer similar data rates to their wireline counterparts. At high data rates, the ISI induced by the dispersive channel becomes a severe problem. The delay spreads associated with such channels can be detrimental when high data rates are considered. The key building block in combating ISI is the equalizer. The higher the data rate, the more complex the equalizer. Dependent upon terrain and land use, the propagation characteristics of FBWA channels can vary from Rician through to Rayleigh (ie, from LOS to NLOS operation). In order to represent these quite different propagation characteristics two channel models are used, namely SUI-2 (i.e. Rician channel) and SUI-3 (i.e. Rayleigh channel) ([Erceg01] and also see Chapter 3, section 3.2). In this study the trade-off between equalizer complexity and performance for FBWA systems is investigated.

Standardization of FBWA systems is currently carried out by the IEEE 802.16 Working Group on Broadband Wireless Access Standards [IEEE802]. It shows that neither single-carrier nor multi-carrier systems are ideal for all operating frequency ranges. Sometimes multi-carrier systems show an advantage and in other situations single-carrier systems prove better. Further, choices regarding time-domain or frequency-domain equalization, the type of equalizer and the tap-update algorithm widens the design space. Factors such as LOS and/or NLOS conditions, the frequency band, as well as the required data rate determines which approach is the most suitable one.

This chapter examines time-domain equalization for single-carrier single-antenna MMDS FBWA systems. A linear equalizer with least mean square updating (LMSLE), a LMSDFE, a decision feedback equalizer with recursive least square updating (RLSDFE) and a LSLDFE are considered. In the literature, the LSLDFE equalizer has not previously been considered for MMDS FBWA systems. It is shown here that the LSLDFE is actually a good choice for MMDS systems. First the algorithms studied are presented in section 4.2. Then the simulation parameters and the assumptions made are discussed in section 4.3. The performance of the different equalizers is measured in terms of their convergence time, P_s and complexity. These performance measures are presented in section 4.4 and 4.5. Finally in section 4.6, conclusions

are drawn upon which time-domain equalizer is the most suitable for single carrier FBWA systems.

4.2 Algorithms studied

The LMS and RLS algorithms used in this simulation are based on [Hay96] and the LSL algorithm is based on [Ling85]. A similar study of these algorithms is also presented in [Naray96], but not explicitly for FBWA systems. Also an equalization requirement study is presented in [Dane96], but only for the LMS algorithms and a DFE arrangement for indoor wireless environments. The stepsize of the LMS algorithm is 0.01 and the weighting factor for the RLS and LSL is 0.99. The maintap (or equivalently the decision delay) for both algorithms is set to be equalizer tap 6 when using the 8 FF tap, 7 FB tap DFE architecture, denoted as DFE(8,7). For the DFE(16,12) architecture, the maintap is set to be equalizer tap 11. The LE has either 15 taps or 28 taps depending which channel (SUI-2 or SUI-3, respectively) is to be equalized. The Rayleigh channel SUI-3 is more hostile than the Rician channel SUI-2 ([Erceg01] and see also Chapter 3, section 3.2) and demands longer equalizer structures in order to achieve satisfactory performance.

The LSL algorithm belongs to the family of fast RLS algorithms. These are RLS algorithms with a linearly increasing complexity with the number of equalizer taps. Further background on the LMS, RLS and LSL algorithm can be found in Chapter 2 and [Ling85, Lee97].

4.3 Simulation model and simulation parameters

The simulation model used in this study is shown in Fig. 4-1. The figure depicts a single-carrier FBWA system with time domain equalization. The advantage of such a system design is that powerful equalization architectures and tap update algorithms exists. Further, a cost effective system design is possible because components such as the power amplifier do not have to be highly linear and therefore expensive. However the biggest disadvantage of a time domain approach is its complexity for channels with severe multipath delay. To overcome this problem the complexity is reduced via the use of a fast RLS algorithm, namely the LSLDFE. Another observation, which favours the use of time domain equalization is that only a very few FBWA channels exhibit very severe multipath [Port00]. Porter reports in his measurements that for omnidirectional antennas at the SU, only 4% of the measured channels had a $D_{RMS} > 1\mu\text{s}$ for LOS conditions and 10% had a $D_{RMS} > 1\mu\text{s}$ for NLOS conditions. When a directional antenna is employed at the SU, no single channel observation had a $D_{RMS} > 40\text{ns}$ for LOS conditions and only 5% had a $D_{RMS} > 1\mu\text{s}$ for NLOS conditions.

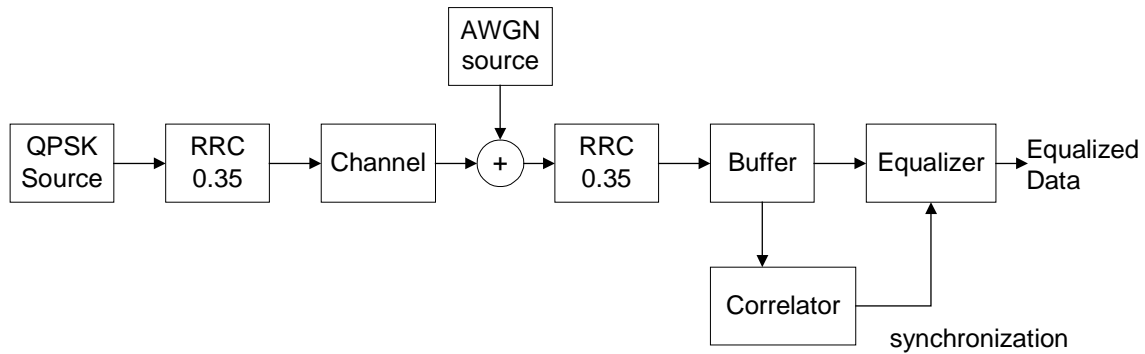


Fig. 4-1: Simulation model

Other possible approaches include the application of an orthogonal frequency division multiplexing (OFDM) system or a single carrier system with frequency domain equalization. Both alternatives have their advantages and drawbacks:

An OFDM system has the big advantage, that it can mitigate the delay spread problem. On the other hand, an OFDM system is potentially more costly than a time domain approach, since it requires highly linear power amplifiers. Further its sensitivity to frequency offsets requires an accurate automatic frequency control. Additionally the cyclic symbol extensions required to ‘absorb’ delay spread reduce efficiency.

Single carrier frequency domain equalization is less sensitive to transmitter non-linearities and to phase noise than OFDM and is a promising approach for severe multipath channels ([Erceg01]: e.g. SUI5, SUI6). Unfortunately, a DFE is not straightforward to implement in the frequency domain, and hence linear equalizers in the frequency domain are common. Unfortunately, the linear equalizer yields very poor error rate performance on channels that have spectral nulls [Ling85].

The time-domain system studied in this thesis uses QPSK modulation with a symbol rate of 5 MS/s, giving a gross data rate of 10Mb/s. The two root raised cosine filters at the transmitter and at the receiver have a roll-off factor of 0.35, use 20 samples per symbol and are truncated to a total length of 200 samples. A 5MS/s rate is compatible with the 6MHz channel bandwidth specified by the federal communications commission (FCC) for the MMDS band [UBS01, Beny00]. Hence to achieve higher data rates high order modulation schemes such as 16 QAM or 64 QAM will be required. Further assumptions are that burst mode digital communication is used and that the channel stays constant during the reception of each burst.

4.4 Performance

The performance is measured in terms of convergence speed and probability of symbol error. The convergence plots are evaluated at a SNR of 20dB at the equalizer input. The equalizers are trained for either 700 or 1200 symbols, for the SUI-2 channel or the SUI-3 channel,

respectively. A large number of training symbols is chosen in order to make sure that the equalizers are fully converged. The payload is set to 10000 symbols and 200 symbols are reserved for synchronization. The convergence plots are the result of averaging a total of 500 channel realizations and the probability of symbol error results are evaluated using a total of 250 packets. It is advantageous to have an equalizer as short (i.e., as few taps) as possible, since the longer the FF-filter, the higher the noise enhancement. The equalizer architectures are chosen based on a number of convergence test runs with various equalizer lengths and then the shortest equalizer architecture is selected based on the MMSE. By conducting a number of convergence simulations with various FF and FB-filter lengths it has been determined that a minimum equalizer length of 15 taps is required for the SUI-2 channel and that a minimum equalizer length of 28 taps is required for the SUI-3 channel.

First, the results for the SUI-2 channel model (i.e., Rician channel) are presented followed by the results for the SUI-3 channel (i.e., Rayleigh channel).

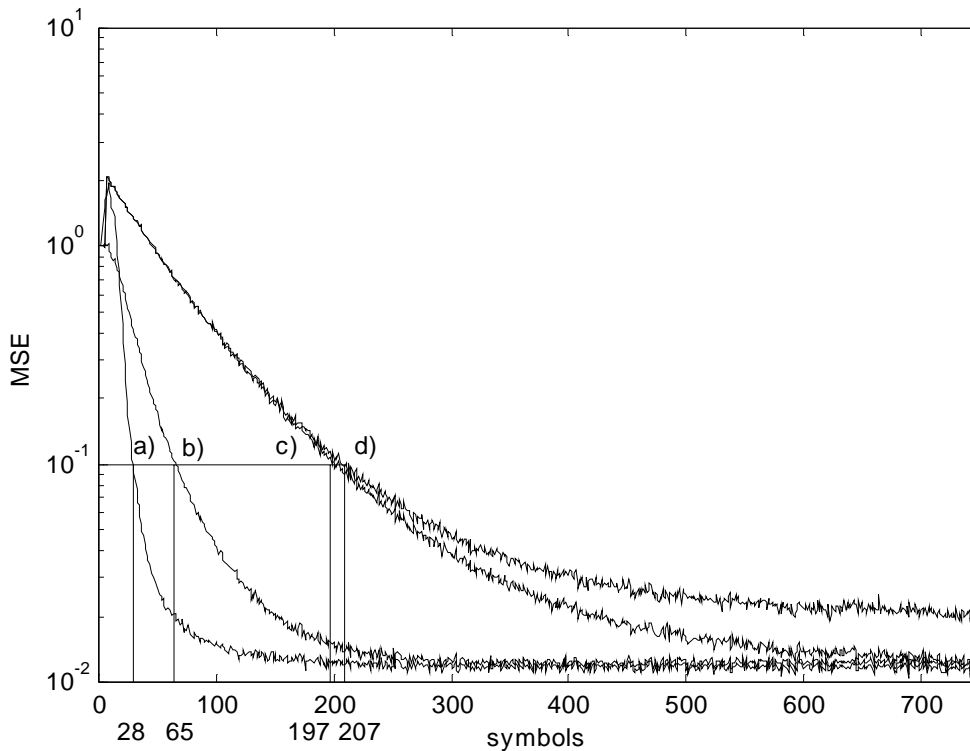


Fig. 4-2: Convergence rate for channel SUI-2:

a) RLSDFE, b) LSLDFE c) LMSDFE and d) LMSLE

The convergence plots of Fig. 4-2 show that the RLSDFE is the fastest converging equalizer, followed by the LSLDFE, the LMSDFE and then by the LMSLE. For example in order to achieve a MSE of 10^{-1} the RLSDFE needs 28 symbols, the LSLDFE needs 65 symbols, the LMSDFE needs 197 symbols and finally the LMSLE needs 207 symbols. The LMS algorithm is seen to converge very slowly for the SUI-2 channel. Further the results indicate that the LMSLE

shows poor performance and is therefore not suitable for MMDS systems. Additionally the LMSLE converges to a higher MSE and hence will show a worse P_s compared to the other equalizers.

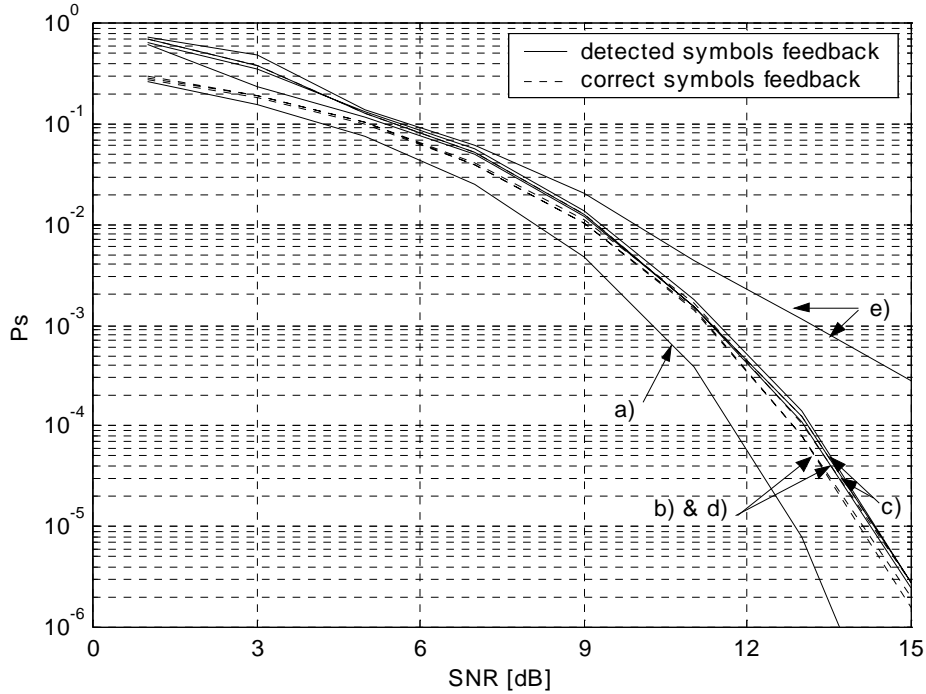


Fig. 4-3: Probability of symbol error for channel SUI-2:

a) matched filter bound for AWGN channel, b) RLSDFE,
c) LSLDFE, d) LMSDFE and e) LMSLE

Fig. 4-3 gives P_s as a function of SNR with the SUI-2 channel. Curve a) shows the theoretical performance of QPSK without ISI according to [Gib97]:

$$P_s \approx \operatorname{erfc} \left(\sqrt{SNR} \cdot \sin \left(\frac{\pi}{4} \right) \right) \quad (4.1)$$

where: P_s = probability of symbol error

erfc = complementary error function

SNR = signal to noise ratio

It is seen that all the DFE arrangements (RLSDFE, LSLDFE and LMSDFE) have a similar P_s . Hence the main advantage of using the LSL and the RLS compared to the LMS algorithm is the increased convergence speed, since the P_s performance of all the equalizers is more or less the same. Comparing the simulated results with the theoretical P_s of QPSK in the absence of ISI [Gib97], one sees that the DFEs come very close to this 'best case' performance. The LE exhibits a poor P_s and hence is not powerful enough for MMDS FBWA systems. The dashed lines show the performance if the correct symbols are fed back in the FBF. Comparing this

performance with that achieved when the detected symbols are fed back it is seen that the effect of error propagation in the DFE is insignificant for the SUI-2 channel.

Next the equalizer performance the SUI-3 channel (Rayleigh) is investigated. The convergence plots of Fig. 4-4 show the same trend as for the Rician SUI-2 channel. However, it is seen that all the equalizers need slightly longer to converge in response to the more hostile channel conditions. For example in order to achieve a MSE of 10^{-1} the RLSDFE needs 52 symbols, the LSLDFE needs 77 symbols, the LMSDFE needs 267 symbols and the LMSLE needs 370 symbols. The SUI-3 channel is much more of a problem for the LE than the SUI-2 channel, i.e., the MMSE for the LE is very high. Also the MMSE of all equalizers is slightly higher than for the SUI-2 channel. Consequently the P_s performance for the SUI-3 conditions will also be worse than for SUI-2.

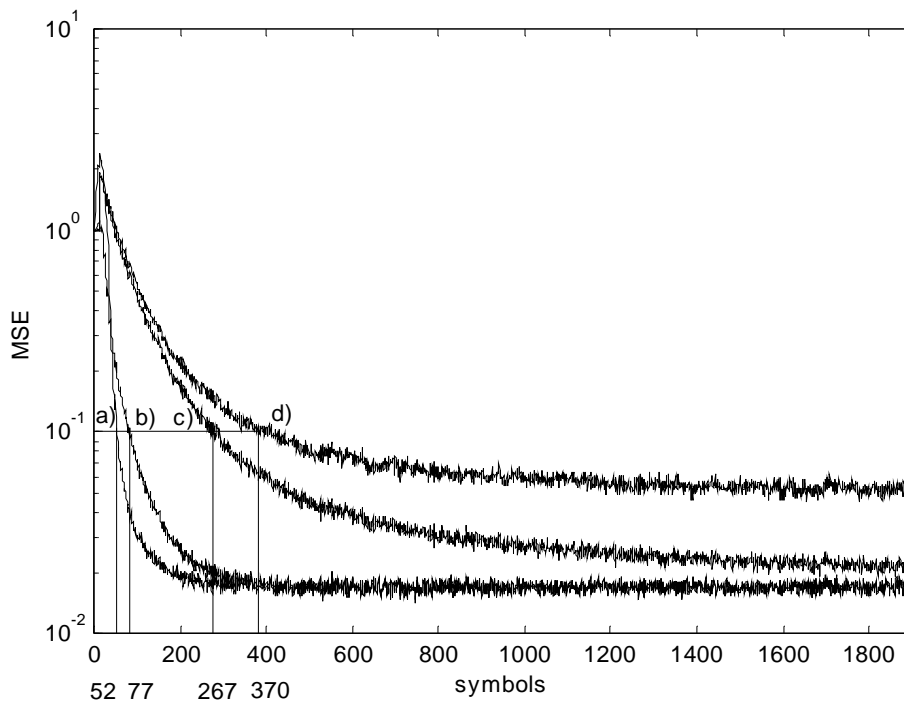


Fig. 4-4: Convergence rate for channel SUI-3:

a) RLSDFE, b) LSLDFE c) LMSDFE and d) LMSLE

Fig. 4-5 shows the P_s of the investigated equalizers for the SUI-3 channel. Again, curve a) shows the theoretical performance of QPSK without ISI according to eq. 4.1. The P_s of the DFEs is now further away from the theoretical bound. This is because the SUI-3 channel is more hostile and has stronger multipath components resulting in more severe ISI. As before it can be observed that all the DFE arrangements show a similar P_s performance. However, the LMSLE is not powerful enough for the SUI-3 channel and fails to deliver adequate performance. Again the dashed lines show the performance if the symbols fed back are correct and the solid lines show the performance in decision directed mode (i.e., the detected symbols

are fed back). Comparing the performance when the correct symbols are fed back with that when the detected symbols are fed back it is seen that the effect of error propagation in the DFE is more evident, certainly more so than for the SUI-2 channel.

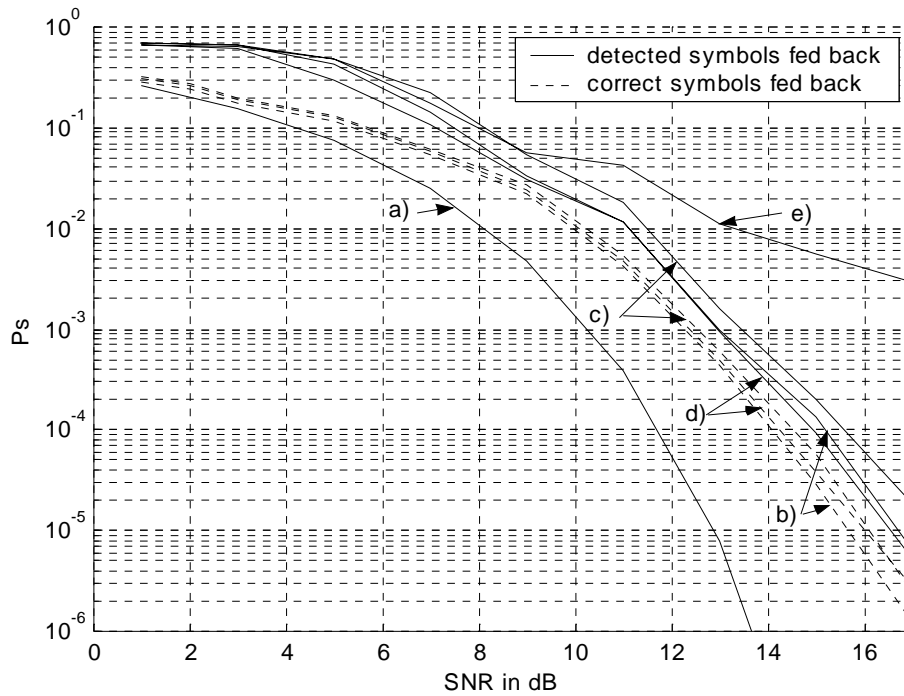


Fig. 4-5: Probability of symbol error for channel SUI-3:

a) matched filter bound for AWGN channel, b) RLSDFE,
c) LSLDFE, d) LMSDFE and e) LMSLE

Although the P_s of the LMSDFE is similar to the other DFEs, this will not be the case for a system with a short training sequence length (see Fig. 4-2 and Fig. 4-4). In this case the LMSDFE will not be fully converged, when switched to the decision directed mode. Here convergence speed is emphasized with regard to P_s , because for FBWA systems bandwidth is a scarce resource and fast converging algorithms are therefore essential particularly in the uplink.

4.5 Complexity

In this section the computational complexity of the LMS, RLS and LSL tap-update algorithms is discussed. In FBWA systems complexity is a crucial issue and therefore low complexity algorithms with good performance are vital. The complexity curves are shown in Fig. 4-6. In these curves it is assumed that for the LSLDFE the FB filter length is equal to the FF filter length. The quoted numbers on the curves are the complexity when using the equalizer architectures of the previous simulations.

Hence from Fig. 4-6 and Table 4-1 the complexity for equalizers with a total of 15 taps in the SUI-2 channel is 630 operations per output for the RLS, 378 operations per output for the LSL and 31 operations per output for the LMS algorithms. The equalizers appropriate for the SUI-3 channel (i.e., with a total of 28 taps) have a complexity of 2086 operations per output for the RLS, 717 operations per output for the LSL and 57 operations per output for the LMS algorithms.

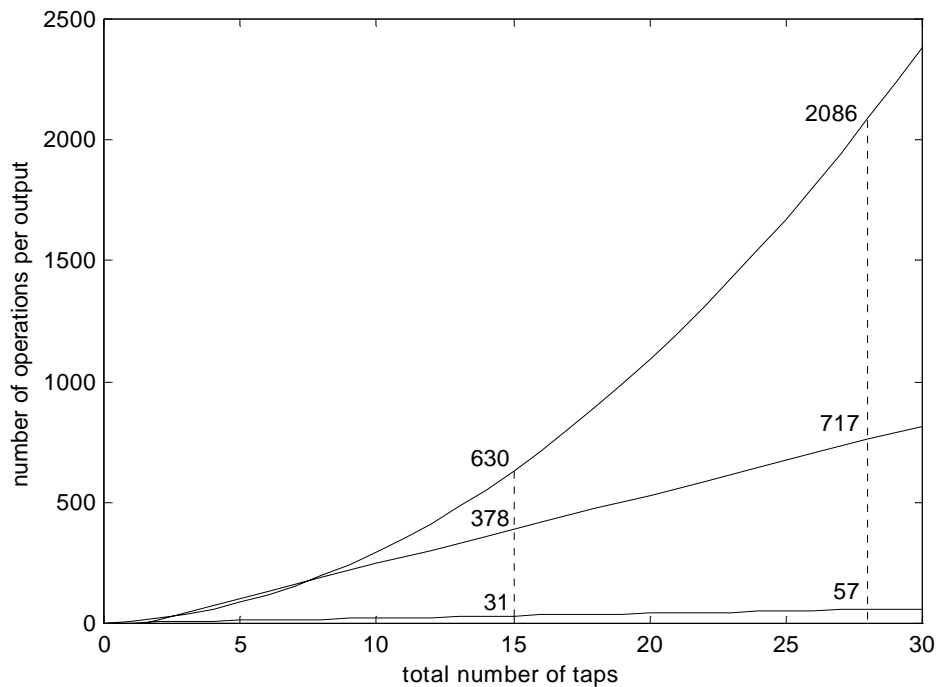


Fig. 4-6: Complexity: a) LMS, b) LSL and c) standard RLS (for equations see Table 4-1)

Algorithm	Operations (Total)	Divisions
LMS	$2 \cdot N_{\text{taps}} + 1$	0
RLS	$2.5 \cdot N_{\text{taps}}^2 + 4.5 \cdot N_{\text{taps}}$	2
LSL	$18 \cdot \text{FF} + 39 \cdot \text{FB} - 39$	$2 \cdot \text{FF}$

Table 4-1: Arithmetic operations per sample [Ling85]

The complexity of the LSL is about half that of the RLS for the SUI-2 channel and for the SUI-3 channel the complexity of the LSL is nearly 3 times lower than RLS. Thus for MMDS systems it is clear that an RLS algorithm with a linearly increasing complexity (e.g. LSL) offers the best performance/complexity trade-off. In this case LSL offers similar performance to RLS, but with greatly reduced complexity.

The complexity of the LMS is very low for both channels considered. However, despite the advantage of the low computational complexity, the LMS algorithm does not offer an acceptable convergence rate as seen in Fig. 4-2 and in Fig. 4-4.

The SUI-2 and SUI-3 channels represent typical FBWA propagation environments. However, occasionally one may experience much more severe ISI conditions, such as those represented by the SUI-5 and SUI-6 channel models. Time-domain equalization will become very complex for these channels and further complexity reduction techniques maybe necessary. Specifically: Complexity reduction may be achieved at the hardware level [Nix96b, Bull99**Error! Reference source not found.**], through tap-selective equalization [Ariya97a], through a special equalizer architecture [Ariya97b] where no training is needed for the FB-filter or via other fast start-up techniques [Sell99a, Sell99b].

4.6 Conclusions

The lattice equalizer (LSLDFE) has not been considered previously for use in FBWA systems. It is seen that for the MMDS system the lattice equalizer offers an excellent complexity-performance trade-off. Although the LMSDFE offers similar P_s performance, its convergence speed is much slower. Comparing the LSLDFE with the RLSDFE, the LSLDFE has a superior complexity versus performance trade-off. It is also seen that the LE is not powerful enough for the studied FBWA channels and it shows especially poor performance in the case of the SUI-3 channel.

High order modulation schemes such as 16 and 64 QAM as well as higher data rates will be the next step. However, to achieve low error rates at acceptable SNRs it is likely that multiple antennas will be necessary. Multiple antennas at the BS are the subject of the remainder of this thesis and specifically the subject of single-user detection utilising multiple antennas is addressed in Chapter 6, section 6.3.1.

Chapter 5

Cross-Correlation Channel Estimation for Multi-Antenna Fixed Broadband Wireless Access Base Stations

5.1 Introduction

Installing multiple antennas at the BS enables SDMA in the uplink for FBWA systems. Many space-time equalization algorithms require a good estimate of the channel impulse response. Additionally, a good estimate of the channel impulse response is vital for successive interference cancellation, a technique, which will be described later in chapter 6. A low complexity solution for channel estimation for application to multi-user detection using a BS with multiple antennas is therefore sought.

Single-user cross-correlation channel estimation is a standard technique for obtaining a good estimate of the channel impulse response [Benv84, Lo93, Sell99b]. Unfortunately, the standard cross-correlation channel estimation for a single-user system cannot be directly applied to multi-user SDMA/TDMA FBWA systems using multiple antenna arrays. This chapter describes an extension of the single-user cross-correlation channel estimation technique to multi-user systems. The proposed cross-correlation method is compared with full-rank maximum likelihood (FR-ML) channel estimation [Nicol01] and it is seen to achieve the same performance as the FR-ML method, but with reduced complexity.

Table 5-1 shows various system configurations, categorized by the number of transmit and receive antennas. For single-user SISO channels the original correlator based method can be used directly [Benv84, Sell99b]. However, when multiple SUs operate in the same time and frequency slot in SIMO channels, the proposed cross-correlation channel estimation method is necessary. For the other two types of channels the proposed techniques offers a computational efficient solution compared to FR-ML approaches when employing multi-user or single-user detection.

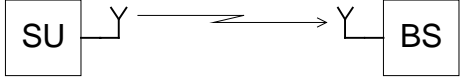
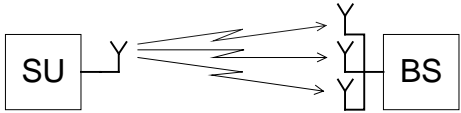
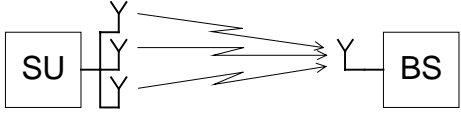
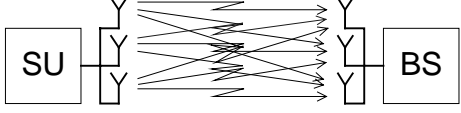
system configurations	channel
	SISO (single input single output)
	SIMO (single input multiple output)
	MISO (multiple input single output)
	MIMO (multiple input multiple output)

Table 5-1: various channels for different system configurations

Channel estimation for SIMO SDMA systems has concentrated on maximum likelihood channel estimation [Lind99]. A similar approach to the one presented in this section has been suggested for CDMA/TDMA systems [Stein94], however, m-sequences were used for sequence construction, compared with the optimum complex sounding sequences in the proposed scheme. Further the proposed method is derived based on the cross-correlation properties of such sequences. The authors of [Stein94] on the other hand propose a computationally efficient implementation of the maximum likelihood channel estimation technique. It is interesting to note that although Steiner's method and the proposed method have a very similar structure, the proposed technique begins from a cross-correlation channel estimation standpoint whereas [Stein94] begins from a maximum-likelihood channel estimation standpoint. The only difference in the structure is that Steiner's method uses cyclic correlators compared to the conventional correlators used in the proposed scheme.

5.2 Single-user cross-correlation channel estimation

A common technique for estimating the channel impulse response of a linear time-invariant system, is to transmit a known pilot (or sounding) sequence with good correlation properties. Cross-correlating the received samples $x(k)$ with the known sounding (or correlation) sequence [Benv84, Sell99b] yields a good estimate of the impulse response of the radio channel. Digital sequences with good autocorrelation properties (e.g. pseudo-random sequences) can be used for correlation-based channel estimation. The received symbol samples are:

$$x(k) = \sum_{i=0}^L p(k-i) \cdot h(i) + n(k) \quad (5.1)$$

where: $h(i)$ = channel impulse response sample

$n(k)$ = AWGN sample

L = length of channel impulse response

$p(k)$ = pilot symbol, and i.e. $\mathbf{p} = [p_1, p_2, \dots, p_k, \dots, p_{3 \cdot N}]^T = [\mathbf{s}, \mathbf{s}, \mathbf{s}]^T$

\mathbf{s} = sounding sequence, i.e. $\mathbf{s} = [s_1, s_2, \dots, s_N]^T$

N = length of sounding sequence \mathbf{s}

The pilot \mathbf{p} in this case is the sounding sequence \mathbf{s} repeated 3 times. This extension of the sounding sequence \mathbf{s} is to ensure that there is no degradation due to edge effects or in other words to ensure periodic correlation properties. The correlator output is given by:

$$R_{s,x}(i+1) = \sum_{n=1}^N s(n) \cdot x^*(n+i), \quad i = 0, \dots, 2 \cdot N \quad (5.2)$$

The conjugate of $R_{s,x}$ scaled by N provides the estimate of the channel impulse response:

$$\hat{h}(i) = \frac{1}{N} \cdot R_{s,x}^*(i+N), \quad i = 1, \dots, N \quad (5.3)$$

This method has been developed for single antenna systems [Benv84, Sell99b], e.g. systems where one user is detected at a particular time. Also in these references a pseudo-random noise sequence is used as the correlation sequence. Although pseudo-random noise sequences give acceptable channel estimates, the accuracy of the estimate can be greatly increased by the use of optimum sounding sequences [Ng98a].

The main advantage of the cross-correlation method is its simplicity. Therefore it is a good candidate for channel estimation in FBWA systems. Unfortunately, the approach cannot be directly applied to multi-antenna SDMA systems, because without careful design of the pilot sequence one ends up with a superposition of all the individual user channels. This chapter presents the extension of the cross-correlation channel estimation method to multi-antenna SDMA systems.

5.3 Multi-user cross-correlation channel estimation

5.3.1 System

The proposed multi-user cross-correlation channel estimation process is designed with the following system in mind. Each subscriber unit, say, SU_u is equipped with one antenna and transmits the pilot sequence \mathbf{p}_u , where $u = 1 \dots U$. The BS is equipped with M antennas. Hence there are U SIMO channels, one for each user. At each antenna of the BS, signals due to U

channel impulse responses plus AWGN are superimposed, e.g. on antenna 1: $h_{1,1}+h_{2,1}+\dots+h_{U,1}+N_1$. Fig. 5-1 shows the SDMA/TDMA system model.

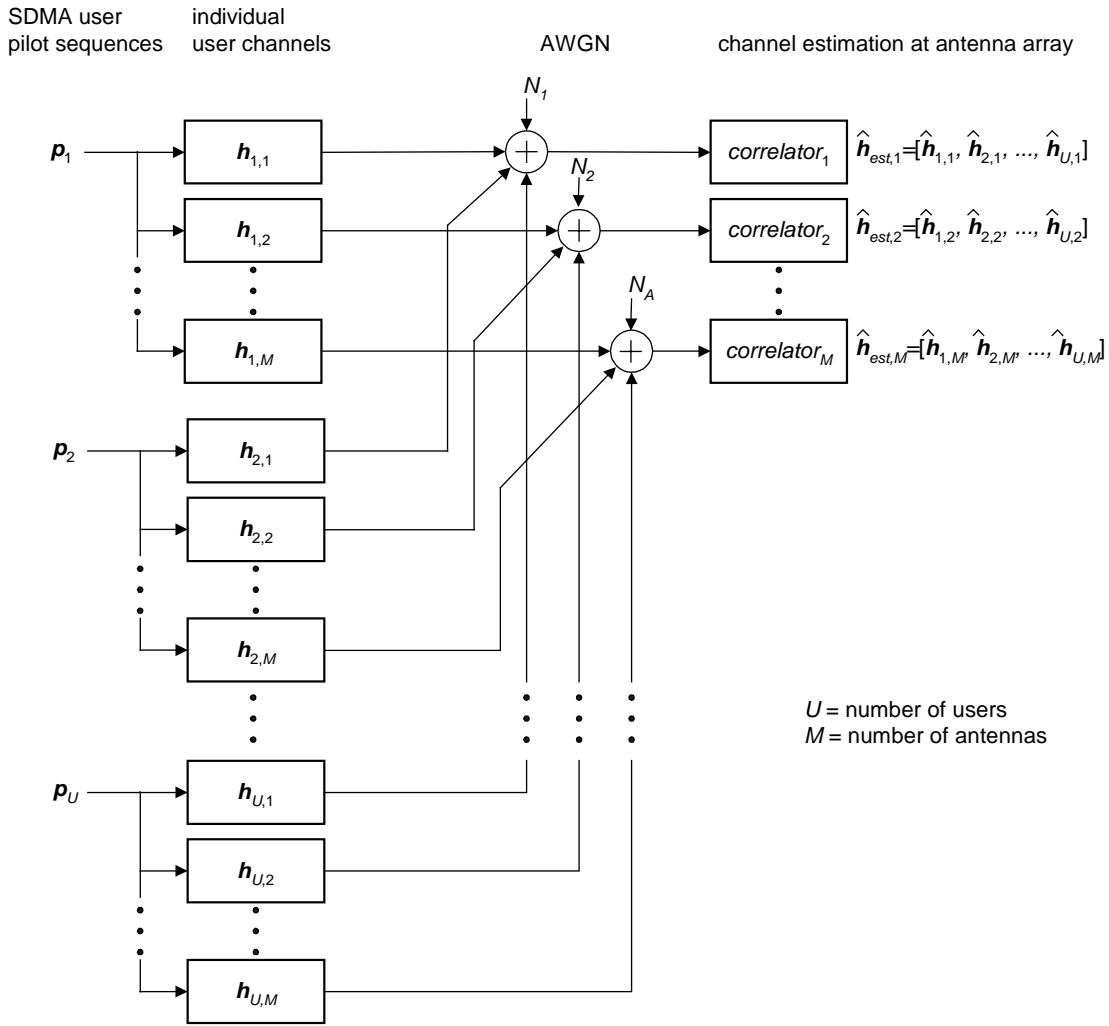


Fig. 5-1: SDMA/TDMA system model

It is assumed that the system is synchronized, i.e., the individual user signals arrive at the same time at the BS. For an example system with four SDMA users per TDMA time slot frame synchronization is achieved through the frame structure shown in Fig. 5-2.

	synchronization	channel estimation	training	data
$user_1$	$s_1(9:16) s_1 s_1(1:8)$	$s_1 s_1 s_1$	t_1	d_1
$user_2$	0 0 0	$s_2 s_2 s_2$	t_2	d_2
$user_3$	0 0 0	$s_3 s_3 s_3$	t_3	d_3
$user_4$	0 0 0	$s_4 s_4 s_4$	t_4	d_4

Fig. 5-2: SDMA packet

During the synchronization period, only one user, namely $user_1$ is allowed to transmit. Note that the synchronization field of $user_1$ is a modified version of sequence s_1 . It can be seen that sequence s_1 is cyclically extended, i.e. $[s_1(9:16) s_1 s_1(1:8)]$ Fig. 5-3 shows the correlator output

on antenna 1 (correlator₁ output). First the correlator output produces the frame synchronization pulse. After an interval of 2.5 times the length of s_1 , known as the mothersequence the channel estimate appears. The correlator output between the synchronization pulse and the channel estimate contains inaccurate channel estimates due to aperiodic cross-correlation.

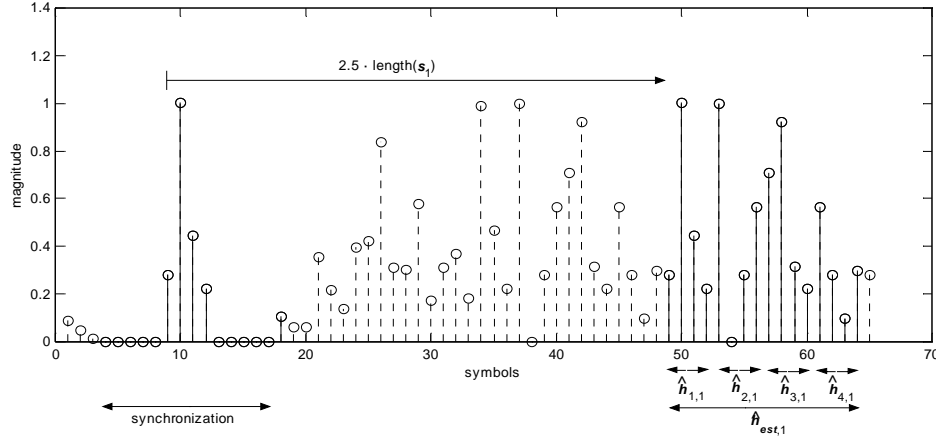


Fig. 5-3: Correlator output on antenna 1

5.3.2 Cross-correlation method

During the channel estimation procedure, each SU_u transmits its pilot sequence \mathbf{p}_u at the same time slot and at the same frequency. Each pilot sequence \mathbf{p}_u consists of the assigned sequence \mathbf{s}_u repeated three times, i.e.

$$\mathbf{p}_u = \{\mathbf{s}_u \mathbf{s}_u \mathbf{s}_u\}. \quad (5.4)$$

This is done to assure periodic correlation properties. User $user_1$ is assigned the mothersequence s_1 and all the other users are assigned cyclically shifted versions of the mothersequence. Following channel estimation further symbols are reserved for equalizer training. Finally the actual data symbols for each user are transmitted in parallel as shown in Fig. 5-2. After each SU_u transmits its pilot sequences \mathbf{p}_u , the pilot sequences \mathbf{p}_u are convolved with the individual channel realizations that exist between each BS receive antenna m and each user u . Following the addition of AWGN the received pilot sequence on antenna m can be represented as:

$$\mathbf{p}_{rx,m} = \sum_{u=1}^U \mathbf{p}_u * \mathbf{h}_{u,m} + N_m, \quad m = 1 \dots M \quad (5.5)$$

where: \mathbf{p}_u = transmitted pilot sequence of SU_u
 $\mathbf{h}_{u,m}$ = channel impulse response between user u and antenna m
 N_m = AWGN at antenna m
 * denotes convolution.

For each antenna processing channel there is one correlator, namely correlator _{m} estimating U user channels. Each correlator is loaded with the mothersequence s_1 . Hence each correlator m

cross-correlates the conjugate of the received pilot sequence $\mathbf{p}_{rx,m}$ with s_1 . This gives the cross-correlation $R_{s_1, \mathbf{p}_{rx,m}}$:

$$R_{s_1, \mathbf{p}_{rx,m}}(i+1) = \sum_{n=1}^N s_1(n) \cdot \mathbf{p}_{rx,m}^*(n+i), \quad i = 0 \dots 2 \cdot N \quad (5.6)$$

The conjugate of $R_{s_1, \mathbf{p}_{rx,m}}$ scaled by the sequence length N gives the desired cross-correlation channel estimate $\hat{\mathbf{h}}_{est,m}$:

$$\hat{\mathbf{h}}_{est,m}(i) = \frac{1}{N} \cdot R_{s_1, \mathbf{p}_{rx,m}}^*(i+N), \quad i = 1 \dots N \quad (5.7)$$

The channel estimate $\hat{\mathbf{h}}_{est,m}$ obtained on each antenna contains the individual channel estimates $\hat{\mathbf{h}}_{u,m}$ of all the U users:

$$\hat{\mathbf{h}}_{est,m} = [\hat{\mathbf{h}}_{1,m}, \hat{\mathbf{h}}_{2,m}, \dots, \hat{\mathbf{h}}_{U,m}] \quad (5.8)$$

In the following section the design of the sequence set S , composed of s_1, s_2, \dots, s_U is outlined.

5.3.3 Definitions

In the following discussions periodic auto-correlation and periodic cross-correlation is assumed.

The sequence set S is defined as:

$$S = \begin{Bmatrix} s_{1,1} & s_{1,2} & \dots & s_{1,N} \\ s_{2,1} & s_{2,2} & \dots & s_{2,N} \\ \vdots & \vdots & \ddots & \vdots \\ s_{U,1} & s_{U,2} & \dots & s_{U,N} \end{Bmatrix}, \quad (5.9)$$

where the individual sequences for each user u are given by:

$$s_u = [s_{u,1}, s_{u,2}, \dots, s_{u,N}] \quad (5.10)$$

Given a sequence set S of size $U \{s_u(n)\}$, $u = 1 \dots U$, each individual sequence having length N , the definition of the periodic auto-correlation function (ACF , $r=s$) and the periodic cross-correlation function (CCF , $r \neq s$) is given by [Sue94]:

$$R_{r,s}(\tau) = \sum_{n=1}^N s_r(n) \cdot s_s^*(n+\tau) \quad (5.11)$$

where: $s_r(n)$ = individual symbol of sequence s_r at sequence index n

$r, s = 1, 2, \dots, U$, i.e. the number of SDMA users

$n = 1, 2, \dots, N$, i.e. the sequence index

Note, in eq. 5.11 the addition $n+\tau$ is performed modulo N . A sequence set is said to be orthogonal if the set has the following property:

$$R_{r,s}(\tau) = \begin{cases} N & \text{for } \tau = 0, r = s \\ 0 & \text{for } \tau = 0, r \neq s \end{cases} \quad (5.12)$$

Walsh sequences are examples of such sequences. Further a sequence set is said to be Z -orthogonal or is a zero cross-correlation zone (ZCZ) sequence set if the set S has the following property:

$$R_{r,s}(\tau) = \begin{cases} N & \text{for } \tau = 0, r = s \\ 0 & \text{for } \tau = 0, r \neq s \\ 0 & \text{for } 0 < |\tau| < Z \end{cases} \quad (5.13)$$

Where Z is defined to be equal to the minimum value of the Z -zone of the ACF or the CCF (whichever is the lower value):

$$Z = \min(Z_{ACF}, Z_{CCF}) \quad (5.14)$$

Further s_1 , the first sequence in the set S is called the mothersequence. Finally, an optimum sounding sequence is defined as:

$$R_{r,s}(\tau) = \begin{cases} N & \text{for } \tau = 0, r = s \\ 0 & \text{for } 0 < |\tau| < N, r = s \end{cases} \quad (5.15)$$

The impulsive ACF of eq. 5.15 of an optimum sounding sequence is illustrated in Fig. 5-4. Such a sequence is optimal with respect to cross-correlation channel estimation. The sequences proposed by Ng [Ng98a] have this property.

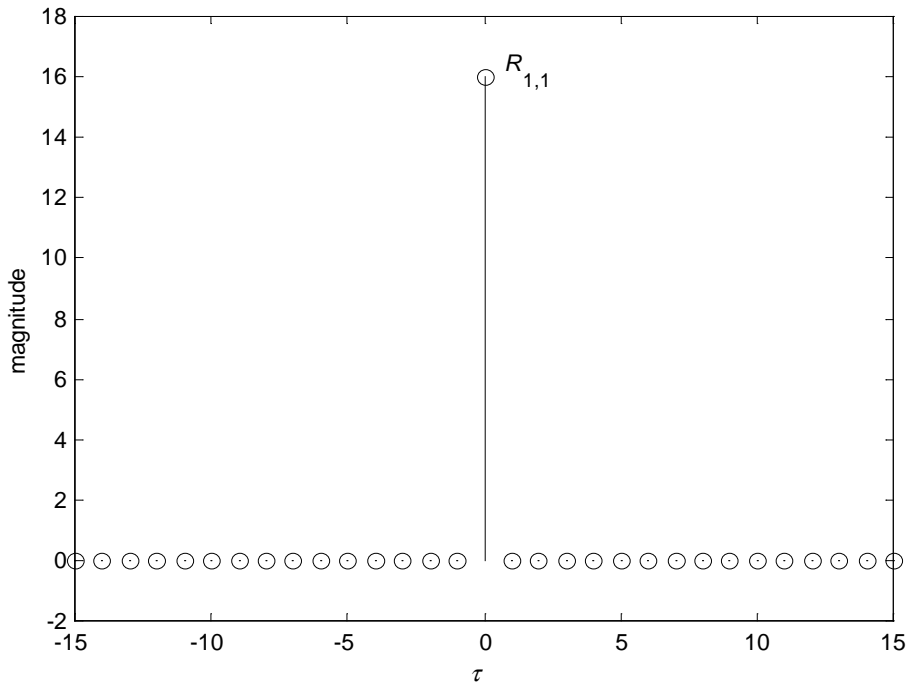


Fig. 5-4: Autocorrelation of optimum sounding sequence of length $N=16$

Fig. 5-5 illustrates the optimal sounding sequence $s_1=[3302120331001001]$. Here, the symbols are defined as:

$$0 = +\sqrt{0.5} + \sqrt{0.5}i$$

$$1 = -\sqrt{0.5} + \sqrt{0.5}i$$

$$2 = -\sqrt{0.5} - \sqrt{0.5}i$$

$$3 = +\sqrt{0.5} - \sqrt{0.5}i$$

The sequences proposed by Ng [Ng98a] belong to the family of poly-phase sequences. Additionally these complex sequences have constant magnitude. The properties of these sequences will be used in the next section to construct the sequence set for the proposed cross-correlation channel estimation method.

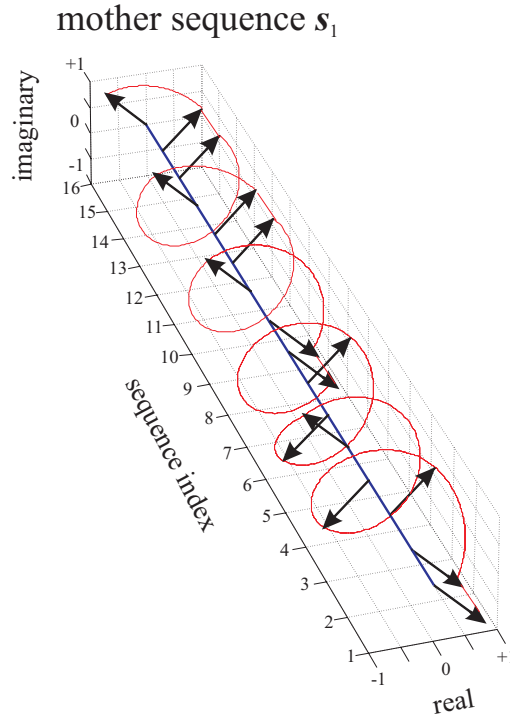


Fig. 5-5: Mothersequence s_1

5.3.4 ZCZ sequence set construction

The authors of [Ng98a] propose the use of constant magnitude optimal complex sequences for channel sounding. The method proposed here is based on these sequences, since the mothersequence s_1 in the set is derived using the method of construction in [Ng98a]. These sequences have some very interesting properties which can be exploited for cross-correlation channel estimation of multiple users. First these sequences have the desirable impulsive characteristic of eq. 5.15. Also via the shift property of the periodic *ACF* (of period N), every cyclically shifted version of such a sequence is also an optimal sounding sequence:

$$R_{r,s}(\tau) = \sum_{n=1}^N s_r(n) \cdot s_s^*(n+\tau) = \sum_{n=1-cSft}^{N-cSft} s_r(n) \cdot s_s^*(n+\tau), \quad r = s \quad (5.16)$$

In eq. 5.16 $cSft$ denotes the cyclic shift value. Note, a cyclic shift of the mothersequence is the same as changing the limits of the sum in eq. 5.16. Further all *CCFs* of the mothersequence with

cyclically shifted versions have only one correlation peak occurring at $\tau = cSft$ with a height of magnitude N and zero values elsewhere. A positive value for $cSft$ denotes a cyclic shift to the right and a negative value of $cSft$ denotes a cyclic shift to the left. This is illustrated in Fig. 5-6 for a sequence set S of size $U=4$ with sequences of length of $N=16$. Each individual sequence in the set is cyclically shifted by 4 to the right compared to the previous sequence in the set.

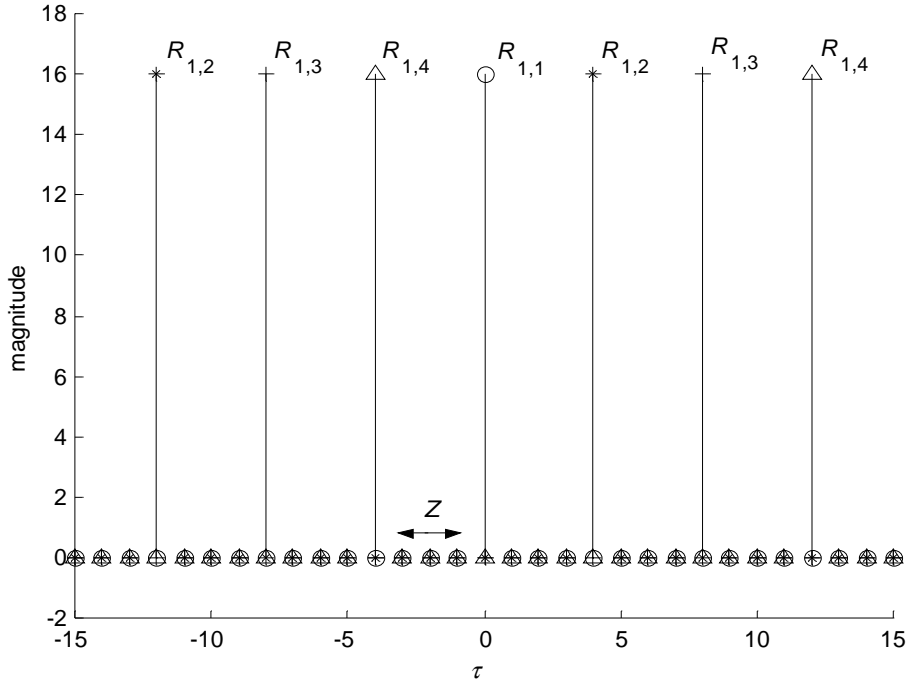


Fig. 5-6: Correlation functions of a sequence set of size 4

The correlation property of Fig. 5-6 is an essential property and having found such a mothersequence the following recursion is applied, which calculates the relative cyclic shift values among the sequences in such a way that the Z -zone is maximised. The Z -zone specifies the maximum channel dispersion, which can be handled by the estimation process. The following recursion generates three arrays, namely the cyclic shift value array $cSft(i)$, the user array $users(i)$ and the Z -zone array $Z(i)$:

$$i=2, \quad cSft(1)=N, \quad users(1)=1, \quad Z(1)=N-1$$

$$\text{while } cSft(i) > 1$$

$$cSft(i) = \left\lfloor \frac{cSft(i-1)}{2} \right\rfloor$$

$$users(i) = \left\lfloor \frac{N}{cSft(i)} \right\rfloor$$

$$Z(i) = cSft(i) - 1$$

$$i = i + 1$$

end

The array users(i) gives the number of SDMA/TDMA users with a maximum channel dispersion of $Z+1$, which can be supported by having a relative cyclic shift amongst all sequences in the set S equal to $cSft(i)$ resulting in a Z -zone length of $Z(i)$. The recursion is best explained with an example, e.g. running the recursion for a mothersequence s_1 of length $N=16$ gives:

$$\begin{aligned} cSft(i) &= [16 \quad 8 \quad 4 \quad 2 \quad 1] \\ Z(i) &= [15 \quad 7 \quad 3 \quad 1 \quad 0] \\ users(i) &= [1 \quad 2 \quad 4 \quad 8 \quad 16] \end{aligned}$$

Looking at the array elements with index 3, this means 4 users can be supported by cyclically shifting every sequence with respect to the previous sequence in the set S by 4 to the right. This results in a Z -zone of 3 for this set S . This is the example shown in Fig. 5-6 and it can be seen that all the $CCFs$ have only one peak of height N . It is essential that this condition is fulfilled, otherwise the channel estimate will have different scaling factors. The magnitude of the $CCFs$ are bounded by [Sar80]:

$$|CCF_{x,y}| \leq \sqrt{ACF_x(0) \cdot ACF_y(0)} \quad (5.17)$$

This means that the maximum height of the CCF is N with two constant magnitude complex sequences [Ng98a] with length N . Further, the sum of the squared magnitude values of the CCF between two complex valued sequences have an upper and a lower bound [Sar80] specified by:

$$\sum_{\tau=0}^{N-1} |CCF_{x,y}(\tau)|^2 \leq ACF_x(0) \cdot ACF_y(0) + \sqrt{\left(\sum_{\tau=1}^{N-1} |ACF_x(\tau)|^2\right)} \cdot \sqrt{\left(\sum_{\tau=1}^{N-1} |ACF_y(\tau)|^2\right)} \quad (5.18)$$

lower bound:

$$\sum_{\tau=0}^{N-1} |CCF_{x,y}(\tau)|^2 \geq ACF_x(0) \cdot ACF_y(0) - \sqrt{\left(\sum_{\tau=1}^{N-1} |ACF_x(\tau)|^2\right)} \cdot \sqrt{\left(\sum_{\tau=1}^{N-1} |ACF_y(\tau)|^2\right)} \quad (5.19)$$

When using the optimum sounding sequences of Ng [Ng98a] the upper and lower bound reduces to eq. 5.20, since the terms in the square roots are zero and therefore the upper bound and the lower bound are equal:

$$\sum_{\tau=0}^{N-1} |CCF_{x,y}(\tau)|^2 = ACF_x(0) \cdot ACF_y(0) \quad (5.20)$$

Further, eq. 5.20 states that if the CCF has only one peak and is zero elsewhere, then for sequences x and y the magnitude of this peak is equal to the square root of the product of the auto-correlations at time lag 0. This is equal to N in this case.

In short the proposed method can be summarized as follow:

1. Generate an optimum mothersequence and construct sequence set S via cyclically shifting the mothersequence s_1
2. Assign each user u their pilot sequence p_u

3. Load each correlator with the mothersequence s_1
4. The correlator outputs give the cross-correlation channel estimate for all the SDMA/TDMA users

5.4 FR-ML channel estimation

For comparison, the FR-ML channel estimation method of [Nicol01] is implemented. First the Toeplitz matrix $\mathbf{X}^{(u)}$ of dimension $W \times N$ composed of the u -th transmitted sounding sequence is introduced. W is the length of the channel impulse response and N is the sequence length. The matrix \mathbf{X} is obtained by stacking all the Toeplitz matrices of all individual users u :

$$\mathbf{X} = \begin{bmatrix} \mathbf{X}^{(1)} \\ \mathbf{X}^{(2)} \\ \vdots \\ \mathbf{X}^{(U)} \end{bmatrix} \quad (5.21)$$

The individual channel impulse responses $\mathbf{h}_{u,m}$ (see Fig. 5-1) between SU_u and the BS antenna array can be described by the $M \times W$ space-time channel matrix $\mathbf{H}^{(u)}$:

$$\mathbf{H}^{(u)} = [\mathbf{h}_{u,1}, \mathbf{h}_{u,2}, \dots, \mathbf{h}_{u,M}]^T \quad (5.22)$$

All the channel impulse responses of all the users are represented by \mathbf{H} , which is obtained by stacking the individual space-time channel matrices $\mathbf{H}^{(u)}$:

$$\mathbf{H} = [\mathbf{H}^{(1)}, \mathbf{H}^{(2)}, \dots, \mathbf{H}^{(U)}] \quad (5.23)$$

In this way, the received symbols \mathbf{Y} can be conveniently expressed in matrix notation:

$$\mathbf{Y} = \mathbf{H} \cdot \mathbf{X} + \mathbf{N} \quad (5.24)$$

where: \mathbf{N} = AWGN matrix of dimension $M \times N$

The FR-ML channel estimate is then computed as follows [Nicol01]:

$$\hat{\mathbf{H}}_{FR-ML} = \hat{\mathbf{R}}_{yx} \cdot \hat{\mathbf{R}}_{xx}^{-1} \quad (5.25)$$

where: $\hat{\mathbf{R}}_{yx} = \mathbf{Y} \cdot \mathbf{X}^H / N$

$$\hat{\mathbf{R}}_{xx} = \mathbf{X} \cdot \mathbf{X}^H / N$$

5.5 Performance

To study the performance of the proposed method, a mothersequence s_1 of length $N=16$ is utilized. The channel taps are symbol spaced and all the channel impulse responses are four taps long. The sequence set S is of size $U=4$ and contains sequences s_u . The following sequences s_u are used:

$$S = \begin{bmatrix} s_1 \\ s_2 \\ s_3 \\ s_4 \end{bmatrix} = \begin{bmatrix} 3302120331001001 \\ 1001330212033100 \\ 3100100133021203 \\ 1203310010013302 \end{bmatrix}$$

where: $0 = +\sqrt{0.5} + \sqrt{0.5}j$
 $1 = -\sqrt{0.5} + \sqrt{0.5}j$
 $2 = -\sqrt{0.5} - \sqrt{0.5}j$
 $3 = +\sqrt{0.5} - \sqrt{0.5}j$

The numerical example uses the following Rayleigh channels:

$$\mathbf{H}^{(1)} = \begin{bmatrix} 0.28e^{0.785j} & 1.00e^{0.100j} & 0.45e^{-0.463j} & 0.22e^{-1.107j} \\ 0.41e^{0.245j} & 0.45e^{2.034j} & 0.14e^{-0.785j} & 0.51e^{2.944j} \\ 0.71e^{0.142j} & 0.10e^{3.142j} & 0.50e^{1.571j} & 0.14e^{0.785j} \\ 0.71e^{-1.713j} & 1.00e^{0.000j} & 0.14e^{2.356j} & 0.36e^{0.588j} \end{bmatrix}, \mathbf{H}^{(2)} = \begin{bmatrix} 1.00e^{0.000j} & 0.00e^{0.000j} & 0.28e^{0.785j} & 0.57e^{-0.785j} \\ 0.32e^{2.820j} & 0.28e^{0.785j} & 0.51e^{1.768j} & 0.10e^{1.571j} \\ 0.70e^{0.000j} & 0.30e^{0.000j} & 0.14e^{0.785j} & 0.20e^{0.000j} \\ 0.58e^{2.601j} & 0.78e^{2.447j} & 0.14e^{-2.356j} & 0.224e^{-2.034j} \end{bmatrix}$$

$$\mathbf{H}^{(3)} = \begin{bmatrix} 0.71e^{-0.142j} & 0.92e^{-0.219j} & 0.32e^{1.249j} & 0.22e^{1.107j} \\ 0.45e^{2.034j} & 0.60e^{1.571j} & 0.14e^{-0.785j} & 0.32e^{-1.249j} \\ 1.00e^{1.571j} & 0.71e^{1.429j} & 0.20e^{0.000j} & 0.10e^{1.571j} \\ 0.10e^{0.000j} & 0.51e^{0.197j} & 0.60e^{0.000j} & 0.14e^{-0.785j} \end{bmatrix}, \mathbf{H}^{(4)} = \begin{bmatrix} 0.57e^{-0.785j} & 0.28e^{0.785j} & 0.10e^{-1.571j} & 0.30e^{-1.571j} \\ 0.28e^{-2.356j} & 0.71e^{-1.713j} & 0.10e^{1.571j} & 0.14e^{-0.785j} \\ 1.00e^{0.000j} & 0.50e^{0.000j} & 0.30e^{0.000j} & 0.10e^{0.000j} \\ 0.14e^{-2.356j} & 0.42e^{-2.356j} & 0.71e^{-2.356j} & 0.28e^{-2.356j} \end{bmatrix}$$

The error between the estimated channel $\hat{\mathbf{H}}$ and the known channel \mathbf{H} is defined as

$$\Delta\mathbf{H} = \mathbf{H} - \hat{\mathbf{H}}. \text{ The MSE is defined as } MSE = E\left[\frac{1}{U \cdot W \cdot M} \|\Delta\mathbf{H}\|^2\right].$$

The following two figures show the cross-correlation channel estimate on antenna 1. Fig. 5-7 shows the performance of the cross-correlation channel estimation if no AWGN is present. It is seen that the method gives ideal channel estimates in this case. This shows that the sequence design is optimum and no additional error is introduced due to non-optimum sounding sequences (e.g. pseudo noise sequences).

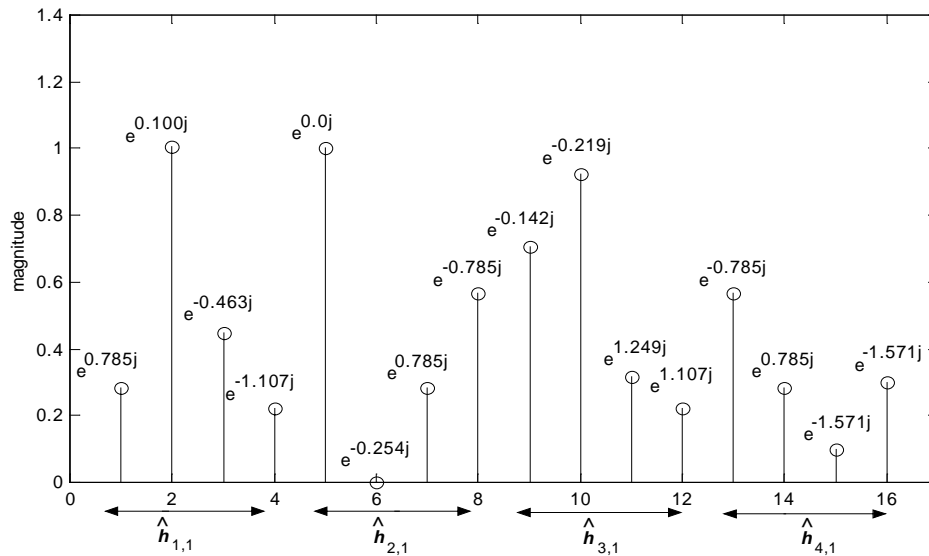


Fig. 5-7: Channel estimate of antenna 1 $\hat{h}_{est,1}$ without AWGN

If noise is present the channel estimates degrade. Fig. 5-8 shows the same example with a SNR of 20dB. Therefore the accuracy of the channel estimate is only affected by the presence of AWGN.

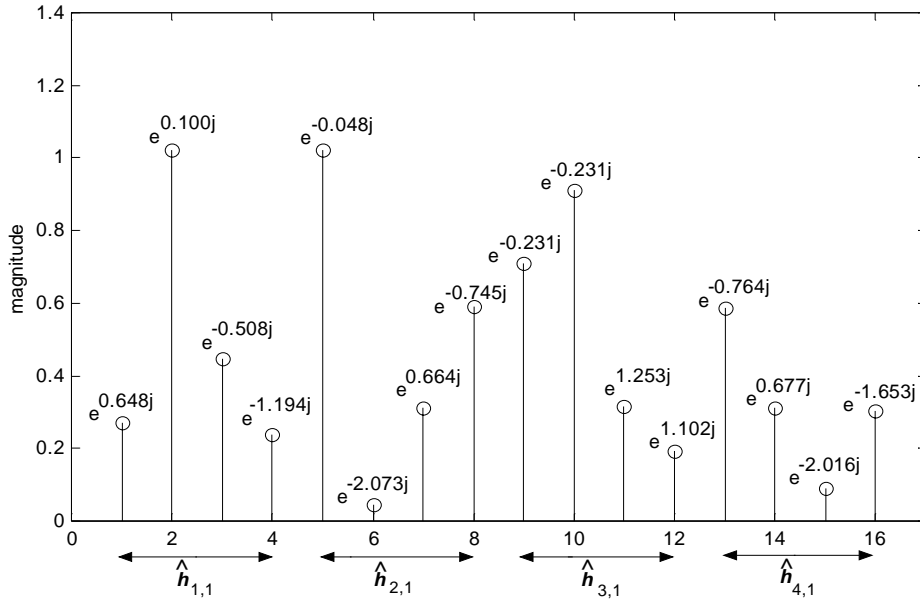


Fig. 5-8: Channel estimate of antenna 1 $\hat{h}_{est,1}$ with a SNR of 20dB

Fig. 5-9 compares the proposed cross-correlation channel estimation with the FR-ML channel estimate made according to eq. 5.25. The MSE of the channel estimate at various SNRs is computed with 100 channel realizations at each SNR. As expected the MSE decreases as the SNR is increased. Both methods give the same performance.

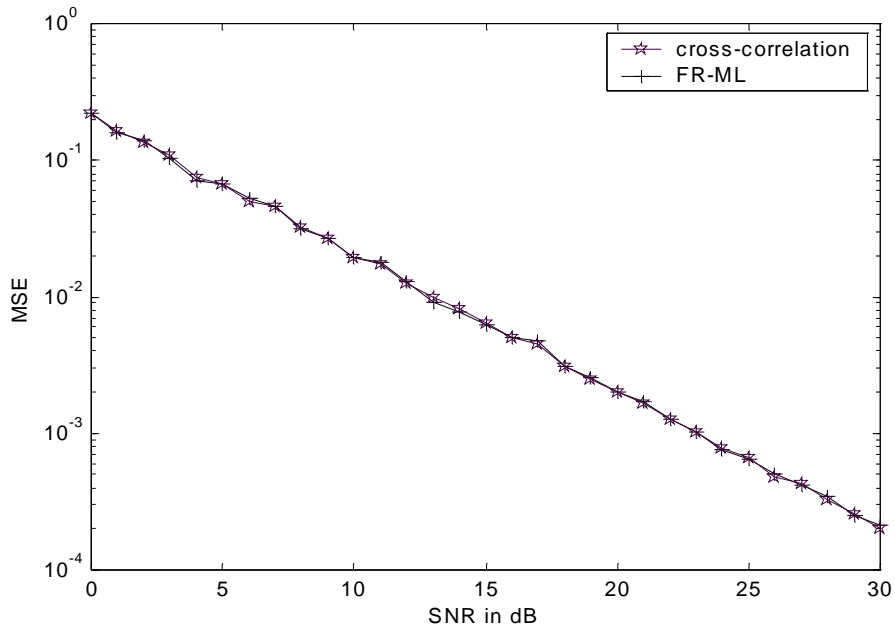


Fig. 5-9: MSE vs. SNR

5.6 Conclusions

It has been shown how the optimum sounding sequence proposed in [Ng98a] can be extended to a ZCZ sequence set, which is optimal for cross-correlation channel estimation for SIMO systems. Once an optimum complex sounding sequence with constant magnitude is found (i.e. the sequences from [Ng98a]) a ZCZ sequence set is simply constructed by cyclic shifting of this sequence. The proposed sequence set has the advantage compared to other ZCZ sequence sets that multiple SDMA channels can be estimated using only one correlator loaded with the mothersequence s_1 . The application of the proposed ZCZ sequence set for cross-correlation channel estimation in a SDMA/TDMA FBWA system shows that highly accurate channel estimates can be obtained with this method. This method has the same performance as a FR-ML channel estimate, but with reduced computational complexity.

Note, quasi-static channel conditions are assumed throughout this chapter. With time-varying channel conditions the channel estimation process will be more complicated. The proposed cross-correlation channel estimation approach may not lead to very good results in this case and enhancements may be necessary. For time-varying channels more elaborate methods are proposed in [Fech94] and references therein.

Chapter 6

Space-Time Processing in the Uplink for Fixed Broadband Wireless Access

6.1 Introduction

In this chapter the cross-correlation channel estimation method proposed in the previous chapter is applied to a complete system. The channel estimation method is used for frame synchronization, for estimating the power of the individual SDMA user signals and for reconstructing the interference caused by individual SDMA users at the antenna input.

The idea behind SDMA is to form as many independent channels (usually up to M , where M is the number of antennas) as possible for the transmission of radio signals at the same time and at the same frequency. This enhances system capacity by enabling the transmission of M users in parallel.

SDMA is implemented in the proposed system by the installation of MEAs at the BS. The SUs still have only a single antenna. The cost, power consumption and also the antenna size are still a concern at the SU, and so shifting the processing power toward the BS is a good approach for FBWA systems. Hence, every uplink, i.e. SU-BS link is a SIMO channel (see Chapter 5, Section 5.1).

The use of MEAs at the BS of a single carrier TDMA FBWA system is considered in this chapter. The uplink in this system is investigated and a novel receive diversity system is proposed. Space-time processing offers an interesting solution to enhance the wireless link quality, to suppress CCI and to enable SDMA.

The proposed system combines conventional space-time DFEs with SIC. The performance of the proposed system is investigated via numerous Monte-Carlo simulations and is compared to that of a conventional MIMO DFE. It is shown via the simulations that the proposed system offers an improvement in the P_s for a two-user system (i.e. two users per frequency channel and time slot) compared to a space-time DFE without SIC. Also the proposed system shows an advantage compared to a standard MIMO DFE in terms of the P_s .

For training the space-time DFE either the LMS or RLS algorithm is used. The LMS algorithm shows good performance only when single-user detection is performed. However, for multi-user detection the RLS algorithm is used to ensure fast convergence.

First the proposed system and similar systems proposed in the literature are described in section 6.2. Next the system model and SIC are discussed in section 6.2.1 and section 6.2.2, respectively. In section 6.2.3 the signal ordering technique used in the suggested approach is discussed. The performance of the proposed system is presented in section 6.3. Prior to the consideration of multi-user detection, the performance of single-user detection with a standard space-time DFEs is presented. The system performance for a multi-user SDMA/TDMA FBWA system is presented for the following situations: a) when conventional space-time DFEs are employed, b) when the proposed system (i.e. a combination of space-time DFEs with SIC) is employed and c) when a conventional MIMO DFE is employed. Finally conclusions are drawn in section 6.4.

6.2 Proposed SDMA/TDMA FBWA system

Fig. 6-1 shows the block diagram for a 2 SDMA user system. First cross-correlation channel estimation as proposed in Chapter 5 is performed. Based on their received power, the individual user signals are ordered. This process will be explained in more detail in section 6.2.3. First the strongest user (i.e. user 1) is detected using a space-time DFE. After the strongest user's symbol sequence is detected, the SIC stage estimates the interference contribution of the strongest user with the aid of the cross-correlation channel estimate. The estimate of the interference contribution from the strongest user is subtracted from the antenna input to form the input to the second detection stage, where the next strongest user is detected. Although investigations have been restricted to a two-user system, this process can be repeated to detect more than two users. This detection procedure is known as SIC [Verdu98], and will be described in more detail in section 6.2.2.

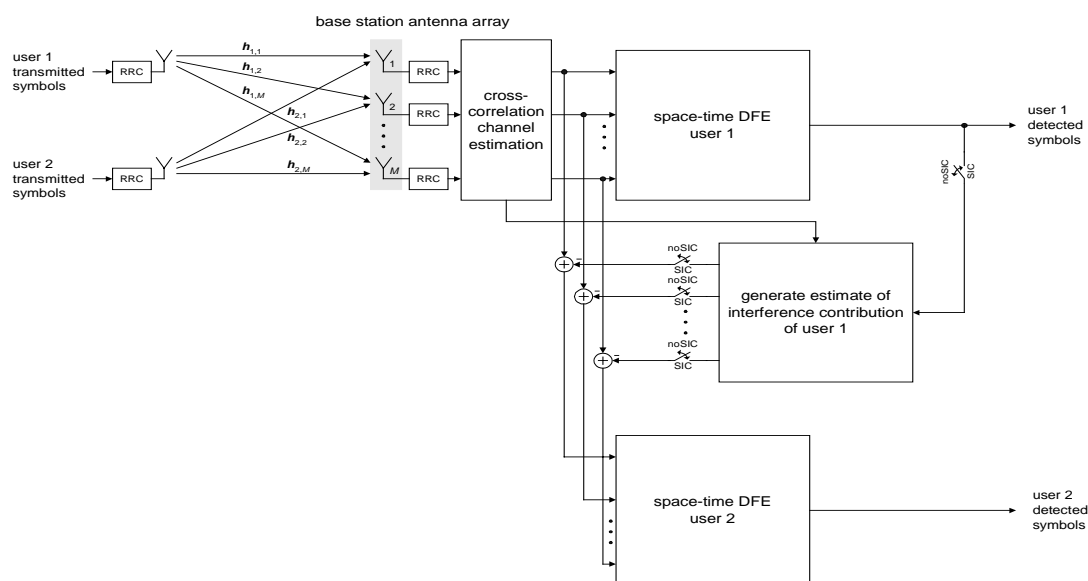


Fig. 6-1: Proposed SDMA/TDMA FBWA system for 2 SDMA users

A well known space-time system which uses SIC is known as the Bell Laboratories Layered Space-Time (BLAST) wireless communication architecture [Fosch96, Fosch99, Gold99, Woln98]. BLAST is a very bandwidth-efficient approach to wireless communication. A user signal stream is divided into a number of sub-streams, which are transmitted in parallel by an antenna array. The effective transmission rate is increased roughly in proportion to the number of transmitter antennas. Subsequently a receive antenna array detects these sub-streams. The original diagonal layered BLAST (D-BLAST) from Foschini [Fosch96] requires advanced coding techniques (known as space-time coding). Although D-BLAST has communication efficiency advantages compared to the less complex vertical layered BLAST (V-BLAST) [Fosch99, Gold99, Woln98], it is too complex for practical implementation at the moment. Also with diagonal layering some overhead is introduced at the start and at the end of the transmitted burst [Fosch99].

The V-BLAST wireless communication architecture [Fosch99, Gold99, Woln98] is a less complex version of D-BLAST. Hence, V-BLAST is more appropriate for FBWA. However, both systems are narrowband, i.e., they use a spatial equalizer (known as a beamformer) for receiver processing. For V-BLAST, no inter-substream coding or coding of any kind is required, although conventional coding can be employed for the individual substreams [Woln98]. The simulation results in [Gold99] show clearly that the use of SIC in the V-BLAST algorithm greatly improves the block error rate. Boubaker [Bou02] presents an interesting performance study of V-BLAST over frequency selective channels. Frequency selective channels cause ISI and it is seen that ISI significantly degrades the performance of V-BLAST, particularly in the case where high-level modulation schemes are used. The delay spread of the channel is a critical parameter and when it exceeds a certain threshold the system performance is severely degraded. A very similar architecture to the one presented in this chapter has been published in [Loza00]. The system of Lozano [Loza00] is an extension of the narrowband V-BLAST to wideband applications. In essence the spatial equalizer from the narrowband V-BLAST system is replaced by a space-time DFE. It is shown that narrowband V-BLAST suffers severe performance degradation in the presence of ISI. The wideband V-BLAST system proposed by Lozano clearly outperforms the original narrowband V-BLAST system [Fosch99, Gold99, Woln98] in frequency selective fading. The signal ordering in [Loza00] is performed in the MMSE sense (i.e. equivalent to signal ordering based on the output SNR), whereas signal ordering based on the input receive power is proposed for this scheme. This approach is less complex and it will be shown to offer a useful performance complexity trade-off compared with the approach in [Loza00]. Also the equalizer coefficients of Lozano's receiver are obtained through the Wiener-Hopf solution, whereas here the use of adaptive training algorithms such as the LMS and RLS algorithm is proposed. The effect of error propagation through the successive stages is mentioned in [Loza00], however its effects are not investigated in detail. Lozano also assumes

ideal channel estimation. However the work to be presented here the performance is given for both ideal channel estimates and realistic noisy channel estimates, obtained via the scheme presented in Chapter 5. Another subtle difference is that every substream in this approach stems from a different user and multi-user detection is performed, whereas in the BLAST systems, single-user detection is performed (i.e. every substream stems from the same user). The user terminals and the BS are equipped with a MEA array in [Loza00], whereas in my approach only the BS is equipped with a MEA array and all the user terminals use a single antenna. Having only single antennas at the user terminals keeps their costs low.

Another space-time system, which utilizes SIC has been proposed by Vandenameele [Vande00]. This combined OFDM/SDMA approach uses multiple single-antenna user terminals and an antenna array with A elements at the BS, which not only gives a multiplicative capacity advantage but also permits inexpensive user terminals. The antenna arrangements used in [Vande00] is the same as in my proposal. OFDM employing a cyclic prefix provides an elegant technique to combat the frequency selective channels found in FBWA systems. In essence the frequency selective channel is transformed into a set of frequency flat channels, and equalization is reduced to a set of parallel single-tap multiplications. Vandemeele's scheme [Vande00] is studied for an indoor wireless LAN scenario, however it could also be applied to FBWA, i.e. it provides an interesting system approach for FBWA which employs OFDM and multiple antennas at the BS. The system proposed in this chapter however gives a single-carrier approach for the FBWA application, which also uses a MEA array at the BS. The preliminary IEEE802.16 standard for the 2-11 GHz bands currently specifies 3 FBWA system approaches [Ekl02]:

1. WirelessMAN-SC2
2. WirelessMAN-OFDM
3. WirelessMAN-OFDMA

The first is a single-carrier approach, whereas the other two are OFDM approaches. In the WirelessMAN-OFDM approach, multiple access is provided by TDMA, whereas in the WirelessMAN-OFDMA approach, multiple access is provided by addressing a subset of the multiple carriers to individual receivers [Ekl02].

6.2.1 System model

In the proposed scenario, U SUs transmit simultaneously over their respective frequency selective channels to a BS equipped with an antenna array. The BS receive antenna array sees the SU signals transmitted in parallel in the same time slot and at the same frequency superimposed over each other. The received symbols \mathbf{X} can be expressed in matrix notation:

$$\mathbf{X} = \mathbf{N} + \sum_{u=1}^U \mathbf{X}_u = \mathbf{N} + \mathbf{H} \cdot \mathbf{S} \quad (6.1)$$

where: \mathbf{N} is a $M \times L$ AWGN matrix

\mathbf{H} is the $M \times (U \cdot C)$ channel impulse matrix incorporating RRC filtering

\mathbf{S} is the $(U \cdot C) \times L$ matrix of transmitted user symbols

\mathbf{X}_u denotes the part of the signal due to user u

L is the total number of transmitted symbols

C is the total number of channel taps (i.e. clusters)

U is the total number of users, i.e. $u = 1 \dots U$

M is the total number of antennas at the BS, i.e. $m = 1 \dots M$

and:

$$\mathbf{H} = \begin{bmatrix} \mathbf{h}_{1,1}^T & \dots & \mathbf{h}_{U,1}^T \\ \vdots & \ddots & \vdots \\ \mathbf{h}_{1,M}^T & \dots & \mathbf{h}_{U,M}^T \end{bmatrix}, \mathbf{h}_{u,m}^T = (h_{u,m,1} \dots h_{u,m,C}) \quad (6.2)$$

$$\mathbf{S} = \begin{bmatrix} \mathbf{S}_1 \\ \vdots \\ \mathbf{S}_U \end{bmatrix}, \mathbf{S}_u = \begin{bmatrix} s_{u,1} & \dots & s_{u,C} & \dots & s_{u,L} \\ \vdots & \ddots & \vdots & & \vdots \\ 0 & \dots & s_{u,1} & \dots & s_{u,L-C+1} \end{bmatrix} \quad (6.3)$$

Using this notation, the channel impulse response matrix \mathbf{H} is composed of the following individual user channel impulse response submatrices \mathbf{H}_u :

$$\mathbf{H} = [\mathbf{H}_1 \quad \dots \quad \mathbf{H}_U], \mathbf{H}_u = \begin{bmatrix} h_{u,1,1} & \dots & h_{u,1,C} \\ \vdots & \ddots & \vdots \\ h_{u,M,1} & \dots & h_{u,M,C} \end{bmatrix} \quad (6.4)$$

Where $\mathbf{h}_{u,m}^T$ in eq. 6.2 represents a channel impulse response of length C between SU u and BS antenna m . Parameter C specifies the maximum length of all the individual channel impulse responses.

6.2.2 Successive interference cancellation

The idea behind SIC is that when the decisions about an SDMA user symbol sequence have been made, this detected symbol sequence can be used to recreate the interference contribution of this user. This estimate of the interference contribution is subtracted from the original received waveform. Supposing that no decision errors are made the interference produced by the previously detected user will be cancelled. Once the subtraction has taken place, the detection is performed again with one fewer user (i.e. it is assumed at this stage that the resulting signal is free from the interference caused by the previous user). Obviously detection errors affect the performance of the SIC scheme and the effect of error propagation through the SIC stages is investigated further in 6.3.2.2.

The first stage in the process utilizes the correlator-based channel estimation method to obtain, timing synchronization, user channel estimates $\tilde{\mathbf{H}}_u$ and an estimate of the users signal power. Based on the estimated signal power of the users and without loss of generality, the users in the proposed SDMA system are ordered from user 1 to user U in such a way that the strongest is labelled user 1 and the weakest is labelled user U . The detection process starts first by detecting the strongest signal (i.e. user 1). Then the effect of the strongest user $\tilde{\mathbf{X}}_1$ on the antenna array input \mathbf{X} is estimated via the following operation:

$$\tilde{\mathbf{X}}_1 = \tilde{\mathbf{H}}_1 \cdot \mathbf{Y}_1, \mathbf{Y}_1 = \begin{bmatrix} y_{1,1} & \cdots & y_{1,C} & \cdots & y_{1,L} \\ \vdots & \ddots & \vdots & & \vdots \\ 0 & \cdots & y_{1,1} & \cdots & y_{1,L-C+1} \end{bmatrix} \quad (6.5)$$

where: $\tilde{\mathbf{H}}_1$ is the channel estimate for user 1 obtained from the correlator

$\mathbf{y}_1 = (y_{1,1} \dots y_{1,L})$ are the symbol decisions for user 1

$\tilde{\mathbf{X}}_1$ is then subtracted from \mathbf{X} to form the input to the second stage, where user 2 is detected. This process is repeated until the weakest user is detected. In this way the interference contributions of all the stronger users are cancelled before the weaker user is detected.

6.2.3 Signal ordering

As previously advocated, a common approach is to detect the individual users in the order of decreasing receive power [Verdu98]. This form of signal ordering is quite common in CDMA systems [Yoon93, Verdu98] and it is also used in the combined OFDM/SDMA approach of Vandenameele [Vande00]. The SIC process implemented in such a way cancels out more and more of the strongest interfering signals.

However, the input receive power is not necessarily the best metric to use in all scenarios. For example in V-BLAST systems, the signals are ordered based on the output SNR in the maximin sense [Woln98, Fosch99, Gold99]. In other words, the signal ordering in V-BLAST is based on the post-detection SNR, i.e. maximization of the worst (minimum) post detection SNR.

Briefly the iterative detection procedure proposed in the suggested scheme is to:

1. Order the received user signals based on their individual receive power P_{in} (i.e. P_{in} of user 1 $>$ P_{in} of user 2 $>$... $>$ P_{in} of user n)
2. Detect strongest user first (i.e. user 1)
3. Estimate the interference contribution from strongest user (using the cross-correlation channel estimate)
4. Cancel the interference contribution from the strongest user (i.e. user 1)
5. Repeat points 2 to 4 until all the users are detected

6.3 Simulation Results

In all the simulations QPSK modulation with a symbol rate of 5MS/s is assumed yielding a gross data rate of 10Mb/s. RRC filtering is performed at the SU and in each receiver chain (i.e. antenna) of the BS with a roll-off factor of 0.35. The RRC filters are truncated to 200 samples and have 20 samples per symbol. These system parameters are appropriate for the MMDS band. In order to study realistic system performance the GWSSUS channel model of Chapter 3, section 3.3.2.2 is used. The power delay profile for each cluster is specified using the SUI-2 and the SUI-3 channel models [Erceg01]. The number of scatterers N_{scat} for each cluster is set to 50. Burst mode transmission is assumed and the channel is assumed static during one burst. Table 6-1 gives the GWSSUS channel model angular parameters used for single-user detection and for user 1 when multi-user detection is being investigated.

power delay profile	SUI-2			
cluster	e_{LOS}	e_1	e_2	e_3
mean azimuth φ_0	60°	30°	80°	40°
azimuth spread φ_{sp}	0°	3°	3°	3°
power delay profile	SUI-3			
cluster	e_{LOS}	e_1	e_2	e_3
mean azimuth φ_0	60°	30°	80°	40°
azimuth spread φ_{sp}	0°	40°	40°	40°

Table 6-1: GWSSUS model parameters for user 1

Table 6-2 gives the GWSSUS channel model angular parameters for user 2:

power delay profile	SUI-2			
cluster	e_{LOS}	e_1	e_2	e_3
mean azimuth φ_0	40°	80°	20°	80°
azimuth spread φ_{sp}	0°	3°	3°	3°
power delay profile	SUI-3			
cluster	e_{LOS}	e_1	e_2	e_3
mean azimuth φ_0	40°	80°	20°	80°
azimuth spread φ_{sp}	0°	40°	40°	40°

Table 6-2: GWSSUS model parameters for user 2

Further, horizontal wave propagation is assumed (i.e. elevation $\theta = 0^\circ$) and the antenna array configuration at the BS is a ULA. Additionally the system is synchronous, so all the individual user signals arrive at the BS at the same time.

6.3.1 Single-user detection

6.3.1.1 Convergence investigation

First, the performance of a space-time DFE trained with the LMS algorithm for single-user detection is studied. A ULA with an element spacing of 0.5λ is assumed. Note that for the MMDS band the wavelength λ is approximately 0.12m. The DOA spread is set to 3° or 40° , depending whether delay power profile of SUI-2 or SUI-3 is used. The other settings are given in Table 6-1. The small DOA spread together with the SUI-2 Rician channel characteristics is representative of a good LOS link. The larger DOA spread together with the SUI-3 power delay profile models a typical NLOS FBWA link. For the SUI-2 channel, the space-time DFE has 8 symbol spaced FF vector taps and 7 symbol spaced FB taps, denoted as space-time DFE (8,7). The maintap is set to FF vector tap 6. Note that one FF vector tap has M components, where M is the number of antennas in the BS MEA array. The SNR at the input to the antenna array is set to 20dB where the SNR is defined as the average SNR at each antenna. Fig. 6-2 gives the convergence curves for this system for various numbers of antennas.

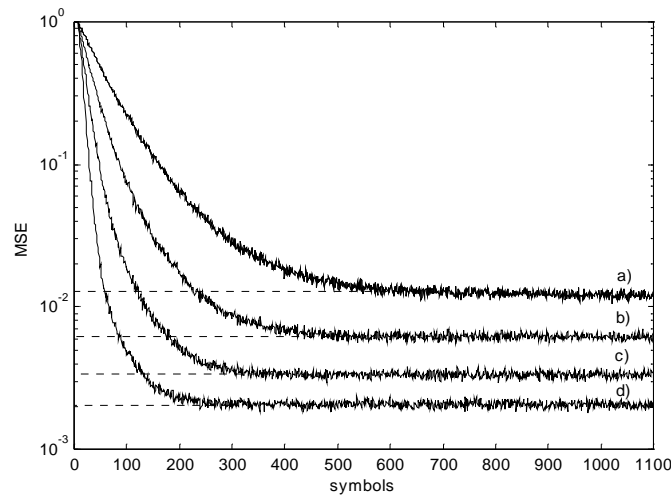


Fig. 6-2: Convergence curves for space-time DFE (8,7), ULA(0.5λ spacing), DOA spread 3° for SUI-2 channel with: a) 1 antenna, b) 2 antennas, c) 4 antennas and d) 8 antennas

It is interesting to see that as the number of antennas increases the convergence rate is improved, though at the cost of increased complexity. The MSE is also greatly improved when employing more antennas.

For the SUI-3 channel, two space-time DFE architectures are used: a) the one used in the previous SUI-2 channel and b) a space-time DFE with 15 symbol spaced FF vector taps and 10 symbol spaced FB taps, denoted as space-time DFE (15,10). The maintap for this longer space-time DFE is set to FF vector tap 10. Again, the SNR at the input to the antenna array is set to 20dB. Fig. 6-3 and Fig. 6-4 give the convergence plots for systems a) and b), respectively.

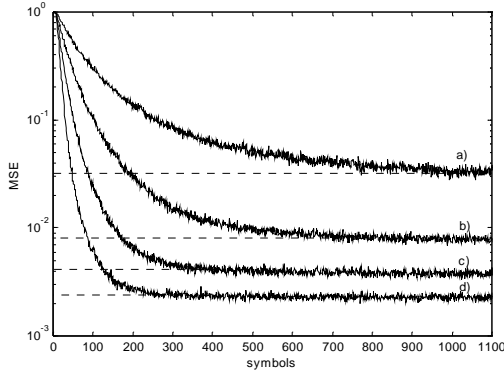


Fig. 6-3: Convergence rate for SUI-3 using space-time DFE(8,7), ULA(0.5λ spacing), DOA spread 40° : a) 1 antenna, b) 2 antennas, c) 4 antennas and d) 8 antennas

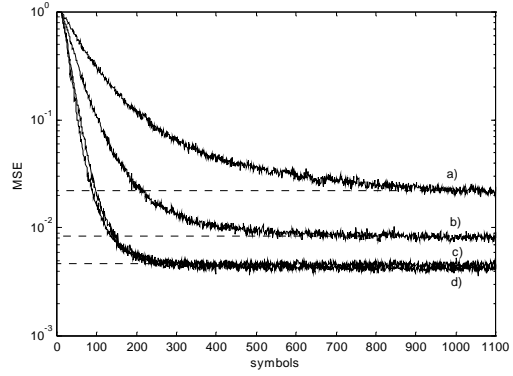


Fig. 6-4: Convergence rate for SUI-3 using space-time DFE(15,10), ULA(0.5λ spacing), DOA spread 40° : a) 1 antenna, b) 2 antennas, c) 4 antennas and d) 8 antennas

It is seen that the longer space-time DFE architecture is more effective for a small number of antennas, however for 4 or 8 antennas, the longer DFE has a higher noise enhancement and hence the MMSE for of 8 antennas is no better than achieved for 4 antennas. For the shorter space-time DFE architecture the MMSE improves as the number of antennas increases. In this case noise enhancement is not so detrimental as for the longer DFE. Note, in the case of 8 antennas, the longer space-time DFE has 7 additional vector taps (making a total of 56 additional taps) in its FF section.

6.3.1.2 Probability of symbol error

Fig. 6-5 shows the P_s as a function of SNR for different numbers of antennas for the space-time DFE (8,7) in the SUI-2 channel. The following parameters are chosen to train the space-time DFE as a function of the number of antennas:

- a) 1 antenna: training sequence length = 1000 symbols
- b) 2 antenna: training sequence length = 800 symbols
- c) 4 antenna: training sequence length = 400 symbols
- d) 8 antenna: training sequence length = 300 symbols

The payload of each burst is set to 4000 data symbols and in addition 200 symbols are reserved for synchronization and correlation operations. It can be seen that P_s can be greatly improved for a single user system by the use of a MEA at the BS.

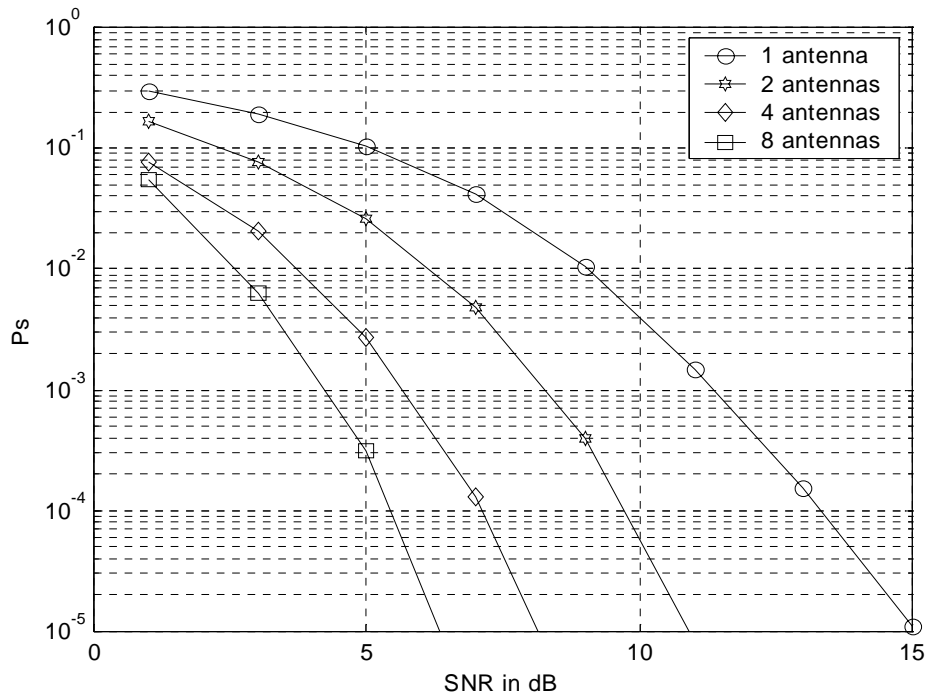


Fig. 6-5: P_s for SUI-2 channel

Fig. 6-6 shows that P_s is a function of the input SNR for various numbers of antennas using either the space-time DFE (8,7) or the space-time DFE (15,10) in the SUI-3 channel. The other parameters are the same as for the SUI-2 simulation. Clearly the shorter space-time DFE is not powerful enough for either the 1 or 2 antennas situation. In both cases the short space-time DFE has an irreducible P_s floor. Making the space-time DFE longer resolves this problem and for 1 or 2 antennas noise enhancement is not an issue. However, for 4 or 8 antennas the longer space-time DFE does not perform as well as the shorter space-time DFE. In this case the noise enhancement in the FF section is detrimental when the number of antennas is 4 or more. In the 1 or 2 antennas situation the shorter space-time DFE cannot cope with certain bad non-minimum phase channels. Such channels have for example the main cursor at tap position 3, and some pre-cursor echoes. Statistically however, these channels seldom occur with the SUI-3 power delay profile. The longer space-time DFE can however equalize even these troublesome SUI-3 channel realizations as seen in Fig. 6-6. On the other hand, with 4 or 8 antennas the shorter space-time DFE is more appropriate owing to less noise enhancement in the FF section compared with the longer equalizer.

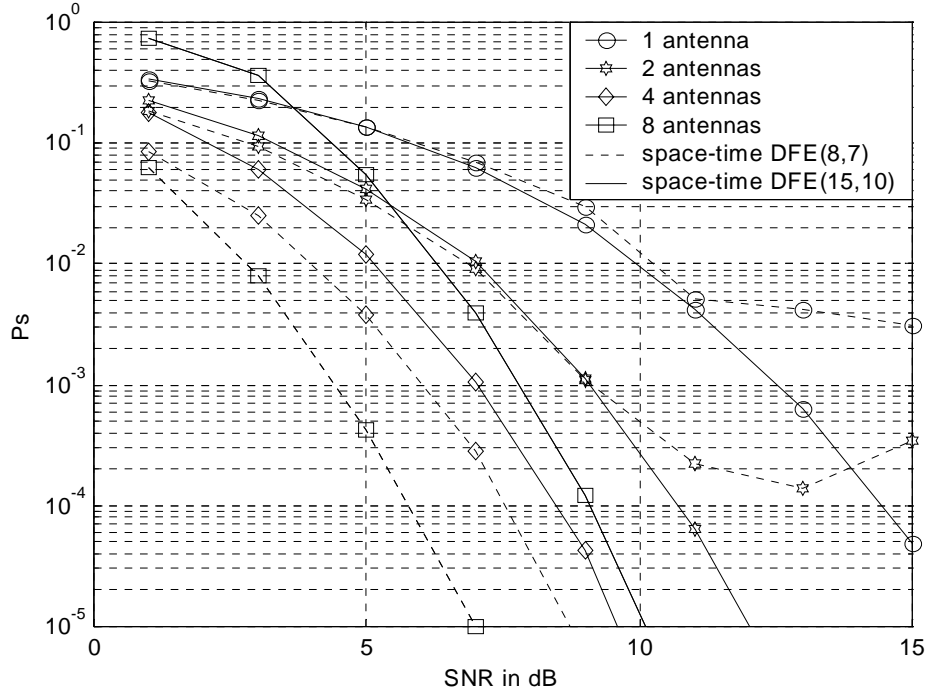


Fig. 6-6: P_s for SUI-3 channel

Fig. 6-5 and Fig. 6-6 show that the link quality can be greatly improved through the use of multiple antennas at the BS. MEA arrays open the door for the use of high-order modulation schemes (e.g. 64-QAM or 256-QAM), where otherwise the SNR necessary to achieve low P_s with only a single-antenna would be too high.

6.3.2 Multi-user detection

Multi-user detection using SDMA will now be investigated. Signals from multiple users are transmitted at the same frequency and in the same time slot. At the BS the SDMA/TDMA receiver separates the individual users. It is assumed that a MAC protocol divides the available bandwidth into SDMA/TDMA slots. U -users are assigned to each SDMA/TDMA slot, which results in an U -fold bandwidth reuse. The performance of the proposed SDMA/TDMA system is shown for 2 users and 2 detection scenarios. The first approach detects the 2 users in parallel using two space-time DFEs and the second approach detects the 2 users successively using two space-time DFEs and employing SIC.

6.3.2.1 Convergence investigation

The SNR for a 2-user system with no CCI is defined here as follows:

$$\text{SNR} = \frac{P_{\text{user}_1}}{P_{\text{noise}}} \quad (6.6)$$

where: P_{user_1} = average power of the user 1 signal on each antenna

P_{noise} = average noise power on each antenna

The SIR for a 2-user system with no CCI is:

$$SIR = \frac{P_{user_1}}{P_{user_2}} \quad (6.7)$$

where: P_{user_2} = average power of the user 2 signal on each antenna

The signal to noise plus interference ratio (SNIR) for a two user system with no CCI is defined as:

$$SNIR = \frac{P_{user_1}}{P_{user_2} + P_{noise}} \quad (6.8)$$

In the sequel SNR strictly means the SNR for user 1. The SNR of user 2 is actually the SNR of user 1 divided by the SIR given in eq. 6.7. Thus, if for example the SNR of user 1 is 20dB and the SIR is 5dB, the SNR of user 2 is actually 15dB. Further for these settings the SNIR is 4.86dB.

Fig. 6-7 shows the convergence plot for a 2-user system for various scenarios using space-time DFEs (15,10) and the SUI-2 channel. The equalizer maintap is set to FF vector tap 10. These filter lengths were selected after performing a number of simulations with various DFE architectures and establishing the minimum MSE. The SNR at the input of the antenna array is set to 20dB and the signal to interference ratio (SIR) is set to 5dB. The curves are obtained via Monte-Carlo simulations and averaging over 500 channel realizations is performed. A 2-element ULA with an element spacing of $10 \cdot \lambda$ is employed at the BS. The RLS algorithm is utilized to train the space-time DFEs for this situation, since the LMS algorithm converges far too slowly to be practical for a 2-user system. It should be noted that the 2-user system also requires longer space-time DFEs compared to that for the previous single user case. It is seen, that in all cases full convergence is achieved after 600 symbols. When SIC is performed (i.e. Fig. 6-7: curve b) and curve c)) the user₂ training is started 100 symbols after the user₁. This is to ensure that the detected symbols for user₁ are more reliable before training of the space-time DFE for user₂ commences. The MMSE of user₂ is worse than the MMSE of user₁ owing to the fact that the SNR of user₂ is only 15dB. Fig. 6-7: curve b) denoted 'corSIC' shows the convergence plot if the correlator channel estimate is used in the regeneration of the interference contribution due to user₁ and if the correlator is also used to estimate the received signal power. Curve c) denoted as 'idealSIC' shows the convergence plot if the ideal channel estimate is used in place of that from the correlator. It is seen that in both cases that the MMSE is improved though the use of SIC compared to a system without SIC, denoted as 'noSIC'.

The glitches evident in the figure are caused by error propagation when SIC is used. This effect has been also investigated in [Vande00]. Looking at each symbol decision when the glitches

occur reveals that each time the user₁ detector makes a symbol error, these errors also cause symbol errors in the user₂ detector. This is, because instead of cancelling interference one adds interference if the symbol decisions Y_l used to generate \tilde{X}_1 are incorrect. Note also that the error glitches in Fig. 6-7 appear smaller than they are in reality because the presented convergence rate curve is the average of 500 realizations. The actual squared error is around 1.5 when such a glitch occurs.

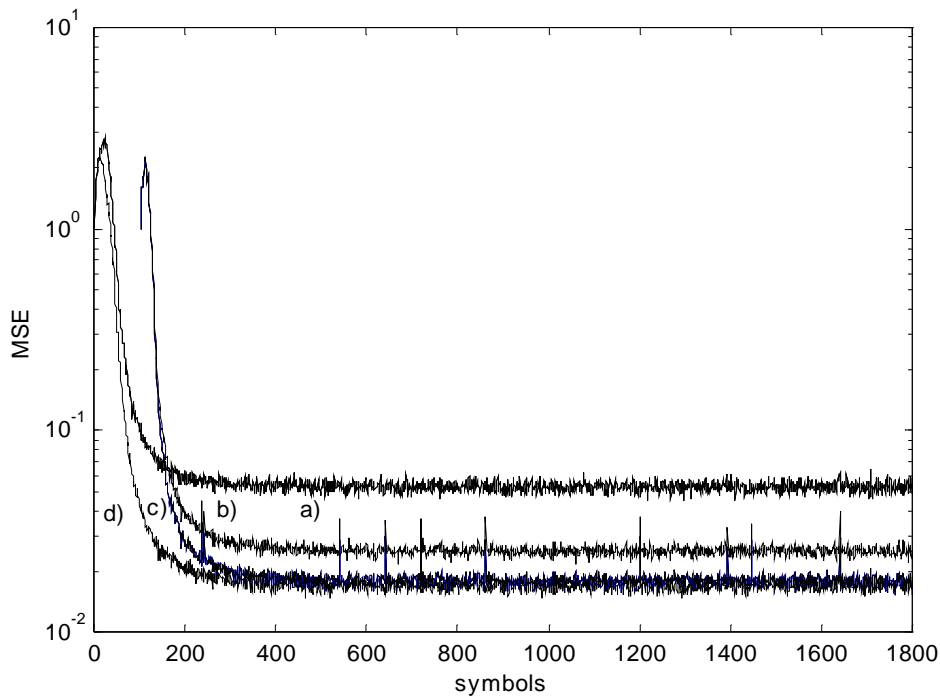


Fig. 6-7: Convergence plot for SUI-2, ULA(10λ spacing), DOA spread 3° :

a) noSIC user₂, b) corSIC user₂, c) idealSIC user₂ and d) noSIC user₁

Fig. 6-8 shows the convergence plot this time for the SUI-3 channel model. Once again longer space-time DFEs are necessary for the SUI-3 channel. The FF filter of the space-time DFE now has 21 symbol spaced vector taps and FB filter now has 14 symbol spaced taps. The maintap is set to FF vector tap 14. For this more hostile channel the RLS algorithm needs slightly longer to converge. However, in both cases full convergence is achieved after 600 symbols. The glitches seen in Fig. 6-7 are less evident in Fig. 6-8 owing to the higher MMSE, however as shown later in section 6.3.2.2, error propagation between the SIC stages still occurs. Again the MMSE of user₂ is improved through the use of SIC and a small performance penalty is paid when using the noisy correlator channel estimate. The MMSEs in Fig. 6-8 are slightly higher than those in Fig. 6-7.

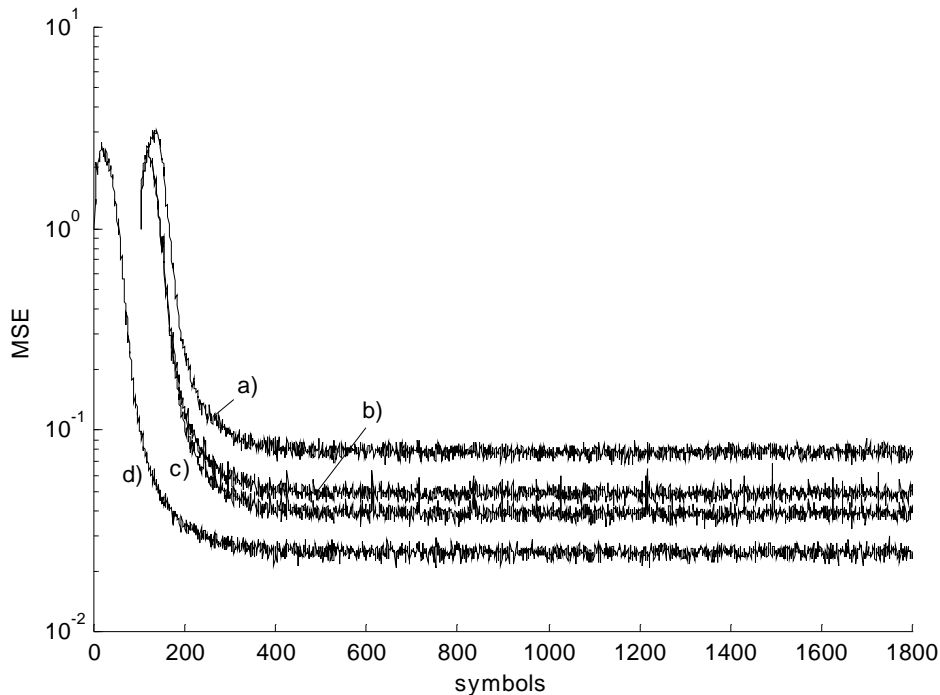


Fig. 6-8: Convergence plot for SUI-3, ULA(0.5λ spacing), DOA spread 40° :
 a) noSIC user₂, b) corSIC user₂, c) idealSIC user₂ and d) noSIC user₁

6.3.2.2 Error Propagation through the successive detection stages

In this section the error propagation effects evident in Fig. 6-7 are investigated. The burst structure and the space-time DFEs are the same as those used in the previous section. Additionally the error propagation effects for an ideal diversity channel are also investigated. In this case for each antenna the channel impulse response for an individual user channel is obtained through an independent realization using either the SUI-2 or SUI-3 power delay profile. These simulations are identified as i.i.d. SUI-2 and i.i.d. SUI-3, respectively. Again the SNR is 20dB and the SIR is 5dB. As in the convergence plots 500 packets (channel realizations) are transmitted. The error propagation effects for both the ideal channel estimation and cross-correlation channel estimation are investigated and as before these simulations are denoted as idealSIC and corSIC respectively.

In the simulation every detected packet for user₁ containing symbol errors is marked and the positions of every symbol error in these marked packets are also stored. Then the corresponding packets of the user₂ detector where the user₁ detector makes symbol errors are investigated. Again the positions of every symbol error in these packets are also stored. Subsequently the position of symbol errors in the user₁ detector is compared with the position of symbol errors in the user₂ detector and in this way the number of symbol errors, which propagate through from the user₁ detector to the user₂ detector is identified.

Table 6-3 shows the number of symbol errors, which propagate from the user₁ detector through to the user₂ detector, identified as *SymErrsProp* for various scenarios. $SymErrs_{user_1}$ denotes the total number of symbol errors made by the user₁ detector excluding packets where either the user₁ or the user₂ detector fails to converge. This means that the effects of convergence failures are eliminated from the statistics. In all the scenarios considered in Table 6-3 it turns out that the user₁ detector always converges, however the user₂ detector sometimes fails to converge and hence these packets are not included in the results. Similarly $SymErrs_{user_2}$ denotes the total number of symbol errors made by the user₂ detector (in only those packets where the user₁ detector makes symbol errors). The column headed *PerErrsProp* in Table 6-3 denotes the percentage of symbol errors, which propagate from the user₁ detector through to the user₂ detector.

scenario	$SymErrs_{user_1}$	$SymErrs_{user_2}$	<i>SymErrsProp</i>	<i>PerErrsProp</i>
SUI-3, 0.5λ , corSIC	234	2983	205	88%
SUI-3, 0.5λ , idealSIC	287	2321	280	98%
SUI-2, 10λ , corSIC	117	120	117	100%
SUI-2, 10λ , idealSIC	117	119	117	100%
i.i.d. SUI-3, corSIC	61	109	52	85%
i.i.d. SUI-3, idealSIC	61	98	50	82%
i.i.d. SUI-2, corSIC	398	406	381	96%
i.i.d. SUI-2, idealSIC	398	409	381	96%

Table 6-3: Investigation of error propagation through the SIC stages

For the scenarios considered almost all the symbol errors in the user₁ detector propagate through to the user₂ detector. For the case of SUI-2 with 2 antennas spaced 10λ apart, all user₁ errors propagate through to the user₂ detector, both when using an ideal or cross-correlation channel estimate. This error propagation behavior is observed with the RLS adaptation using symbol-by-symbol decisions. Sequence based algorithms such as the Viterbi algorithm may exhibit different behavior and may be more resilient to error propagation. Unfortunately, due to the computational complexity of sequence based algorithms (e.g. the Viterbi algorithm) for the FBWA scenario being considered, these algorithms could not be evaluated using a Monte Carlo simulation in a reasonable time and therefore this matter remains the subject of future work.

6.3.2.3 Probability of symbol error performance

For the P_s curves plotted in this section, the training sequence length is set to 600 symbols and the payload is 4000 data symbols. Again 200 symbols are reserved for timing synchronization and channel estimation. Fig. 6-9 shows the P_s for a 2-user SDMA/TDMA system with 2

antennas at the BS separated by $10\cdot\lambda$ over the SUI-2 channel. Curves labelled corSIC user₂ and idealSIC user₂ of Fig. 6-9 give the P_s of user₂ when SIC is employed using ideal and estimated channels respectively at an SIR of 5dB. For a system having an equal number of antennas and users, SIC shows a significant improvement. SIC is particularly effective if significant interference power remains after the space-time DFE, however the overall improvement is limited to that of the P_s of the strongest user (Fig. 6-9: noSIC user₁). The reason for this is that all the symbol errors from the user₁ detector propagate through to the user₂ detector and cause symbol errors to occur there (see section 6.3.2.2).

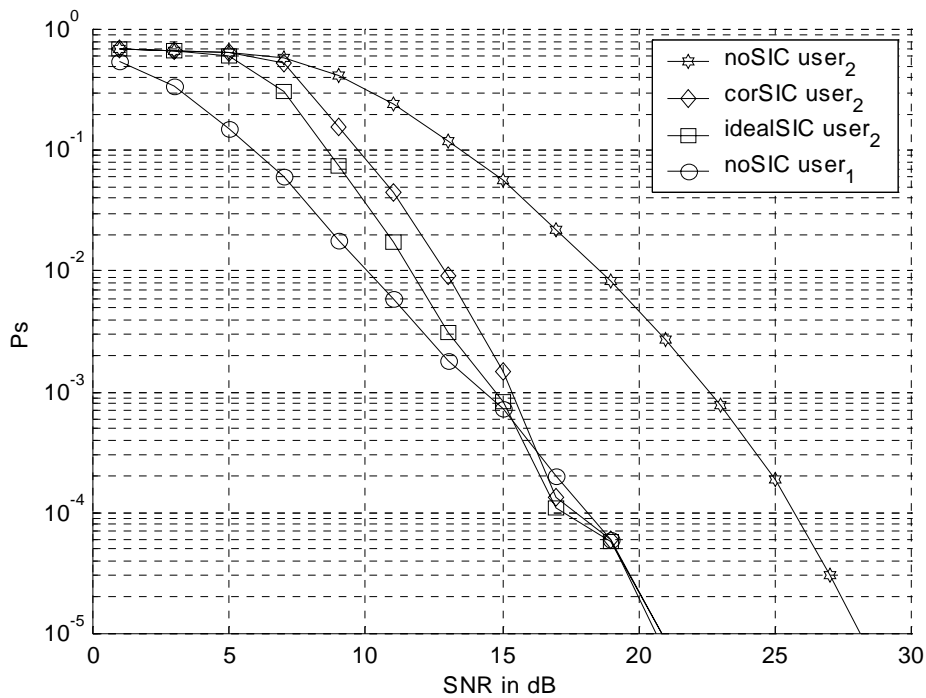


Fig. 6-9: P_s for SUI-2 channel, SIR=5dB, 2 antennas, $10\cdot\lambda$, 2 users

Note, the P_s of user₁ is the same for all 3 schemes (noSIC, corSIC and idealSIC), since the SIC stage does not affect the signal corresponding to the strongest user, user₁. Hence only one curve for user₁ is plotted in the sequel.

Unfortunately under some channel conditions convergence failures can occur even at high SNRs. However, such channel conditions occur very infrequently for typical fading channels [Ariya99]. Nonetheless, these convergence failures at high SNR will lead to misleading P_s curves. In a practical system such convergence failures would be detected by say a cyclic redundancy check (CRC) and would be overcome using an automated repeat request (ARQ) process. The ARQ function is typically implemented in the MAC protocol. Table 6-4 shows the number of convergence failures for the P_s curves of Fig. 6-9. For SNRs in excess of 25dB one has to check if there are convergence failures to simulate the effect of ARQ activity, since these convergence failures seriously degrade the P_s curve in the high SNR regime. In other words, the

P_s curve may be dominated by particularly unfavourable, but rare, channel conditions [Verdu98, chapter 3]. On the other hand at low SNR values, convergence failures are usual since the system gradually breaks down as the SNR decreases. This is evident in Table 6-4 for the noSIC user₂ results. At SNR values from 13 to 23 the number of convergence failures increases as the SNR decreases. The SNR for noSIC user₁, corSIC user₂ and idealSIC user₂ is high enough so that no convergence failures occur. However all the SNR points are checked and if a convergence failure does occur at high SNR values these packets are excluded from the results.

SNR	number of convergence failures			
	noSIC user ₂	corSIC user ₂	idealSIC user ₂	noSIC user ₁
13	163	0	0	0
15	73	0	0	0
17	32	0	0	0
19	11	0	0	0
21	2	0	0	0
23	1	—	—	—
25	0	—	—	—
27	0	—	—	—
29	0	—	—	—

Table 6-4: Number of convergence failures for Fig. 6-9

Fig. 6-10 depicts the P_s for the same configuration as before with the exception that an antenna spacing of only 0.5λ is used. Clearly, the P_s performance is significantly worse than when an antenna spacing of 10λ is used (see Fig. 6-9). Hence for the directional LOS SUI-2 channel, a large antenna spacing is required for good system performance.

Fig. 6-11 shows the P_s for a 2-user multi-detection SDMA/TDMA system with 2 antennas spaced 0.5λ apart employing space-time DFEs in the SUI-3 channel. For this more hostile radio channel, the P_s performance is not as good as for the SUI-2 channel. Unfortunately the performance improvement brought about through the use of SIC is not as marked as before. Nonetheless the P_s of the weaker user, user₂ can still be significantly improved with the use of SIC.

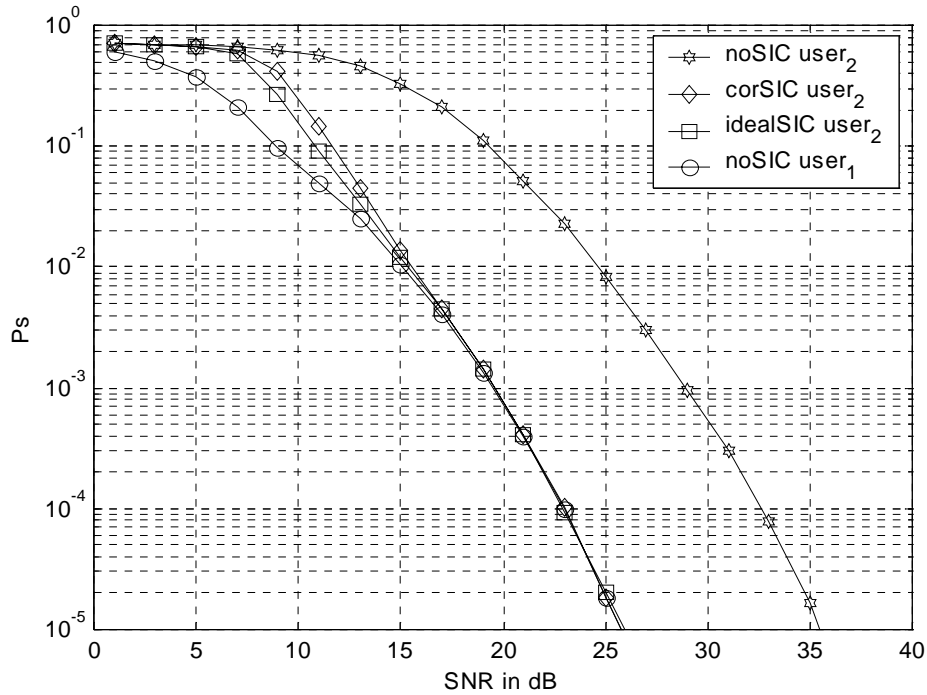


Fig. 6-10: P_s for SUI-2 channel, $SIR=5\text{dB}$, 2 antennas, $0.5\cdot\lambda$, 2 users

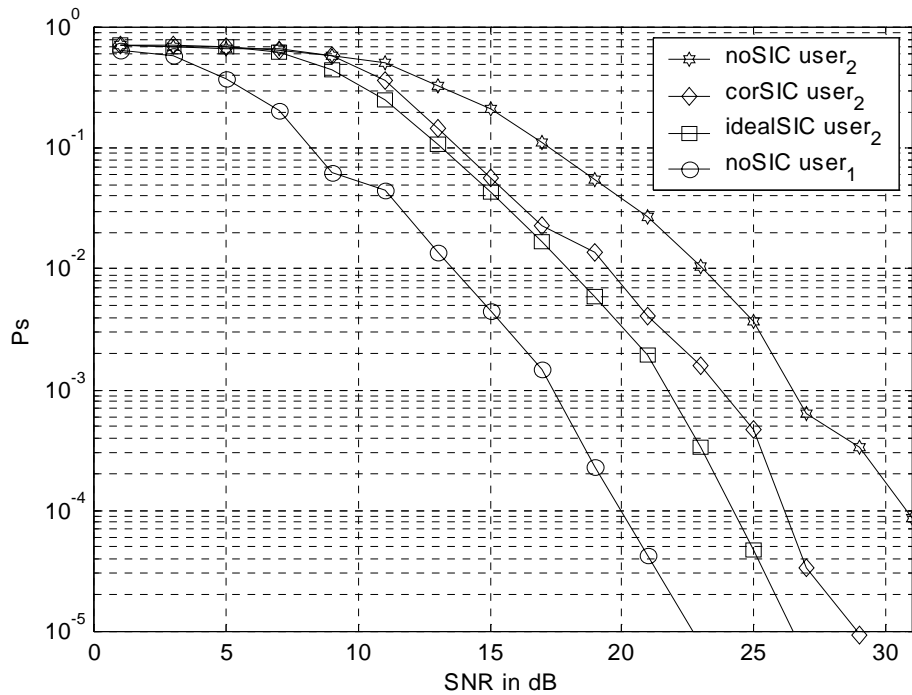


Fig. 6-11: P_s for SUI-3 channel, $SIR=5\text{dB}$, 2 antennas, $0.5\cdot\lambda$, 2 users

Fig. 6-12 and Fig. 6-13 show the P_s performance with the use of 4 antennas with spacings of $0.5\cdot\lambda$ and $10\cdot\lambda$ respectively for the SUI-2 channel. Again, two SDMA/TDMA users are detected jointly with space-time DFEs. Clearly an antenna spacing of $0.5\cdot\lambda$ is insufficient for the highly

directional SUI-2 channel. Consequently when the SUI-2 profile is used in the GWSSUS channel it is necessary to space the antennas $10 \cdot \lambda$ apart.

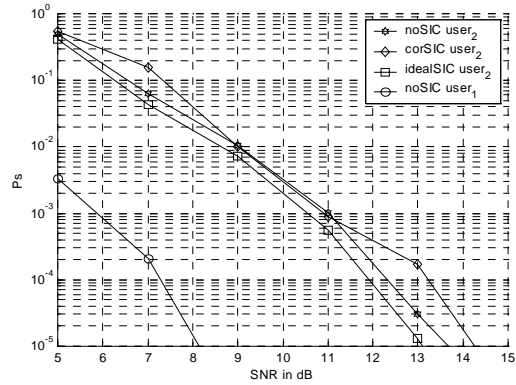
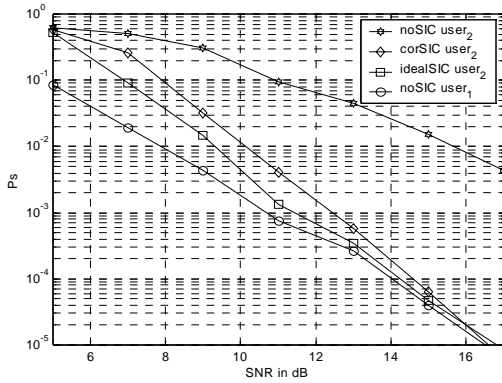


Fig. 6-12: P_s for SUI-2 channel, $SIR=5dB$, 4 antennas, $0.5 \cdot \lambda$, 2 users
 Fig. 6-13: P_s for SUI-2 channel, $SIR=5dB$, 4 antennas, $10 \cdot \lambda$, 2 users

In Fig. 6-12 the 4 antennas are too close together and the space-time DFE is incapable of significantly suppressing the MAI. Hence after the space-time DFE, MAI is still present and the SIC stage improves the performance of the weaker user₂. However, when the 4 antennas are spaced $10 \cdot \lambda$ apart (Fig. 6-13), the space-time DFEs greatly suppress the MAI. In this case virtually zero MAI remains for the SIC stage, and hence the performance is actually not improved by employing SIC, even though the user₂ signal is 5dB weaker than the user₁ signal.

Fig. 6-14 shows the P_s for that same configuration as used previously, with the exception that the SUI-3 power delay profile is used. The system uses 4 antennas spaced $0.5 \cdot \lambda$ apart with 2 SDMA/TDMA users. As before the SIC stage only marginally improves the P_s performance, because with 4 antennas and only 2 users the space-time DFEs are capable of suppressing the MAI leaving virtually nothing for the SIC stage.

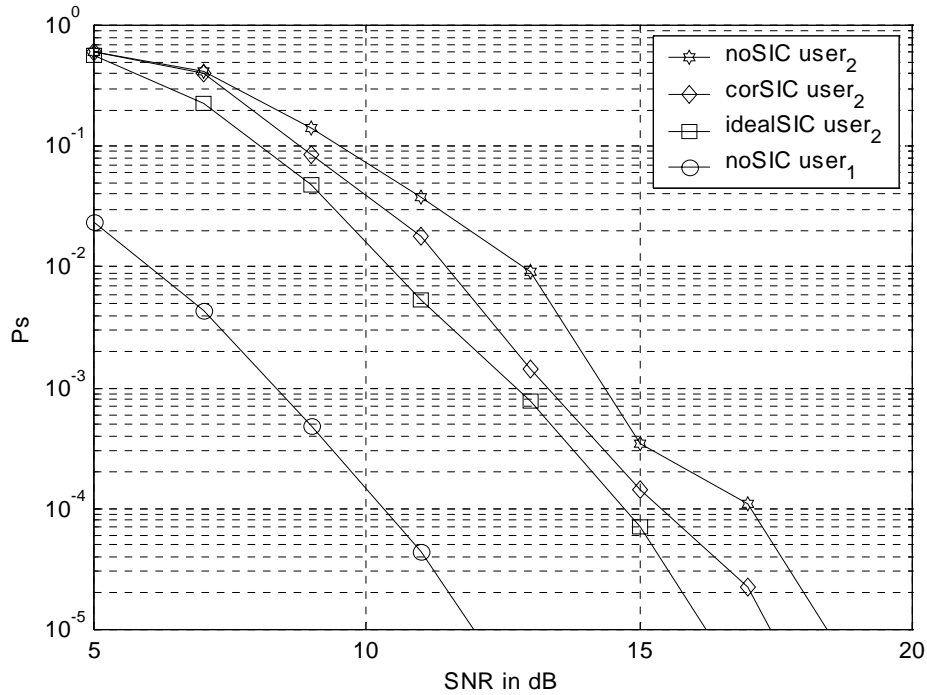


Fig. 6-14: P_s for SUI-3 channel, $SIR=5\text{dB}$, 4 antennas, $0.5 \cdot \lambda$, 2 users

For the scenarios simulated up to now, a significant power difference between the two user signals (i.e. the $SIR=5\text{dB}$) has existed. Now the P_s is investigated when both user signals have equal power (i.e. the $SIR=0\text{dB}$) and 2 antennas are employed at the BS. Fig. 6-15 shows the P_s for this scenario when using the SUI-2 power delay profile. Clearly there is no longer a stronger or a weaker user. Statistically sometimes user₁ is slightly stronger than user₂ and detected first or vice versa. Fig. 6-15 clearly shows that for situations where both users have similar signal powers, SIC does not improve the performance.

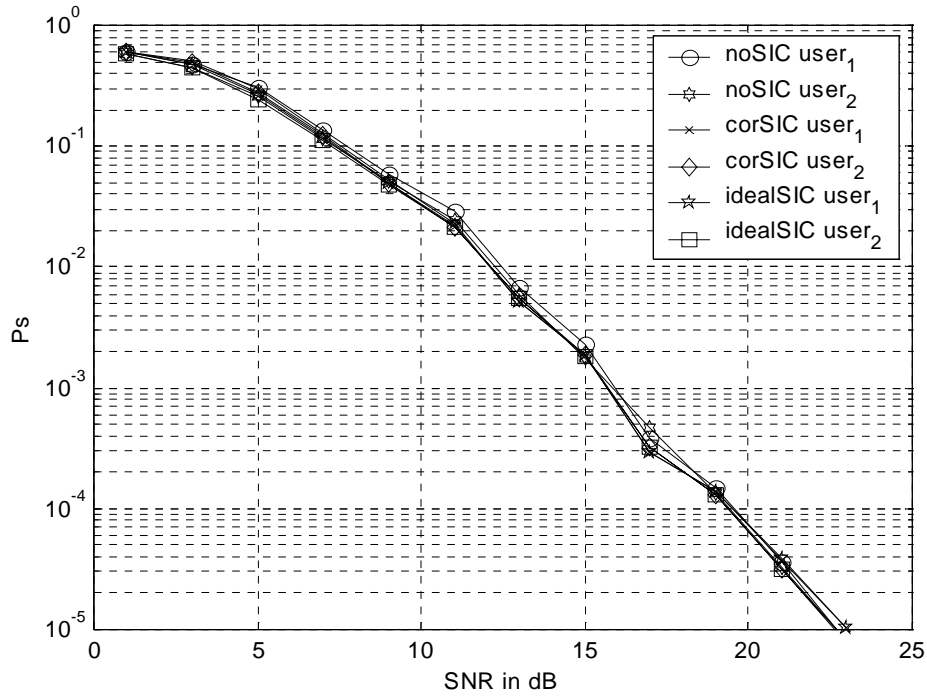


Fig. 6-15: P_s for SUI-2 channel, $SIR=0dB$, 2 antennas, $10 \cdot \lambda$, 2 users

Fig. 6-16 shows the P_s for a similar scenario to the previous one with the exception that the SUI-3 power delay profile is used.

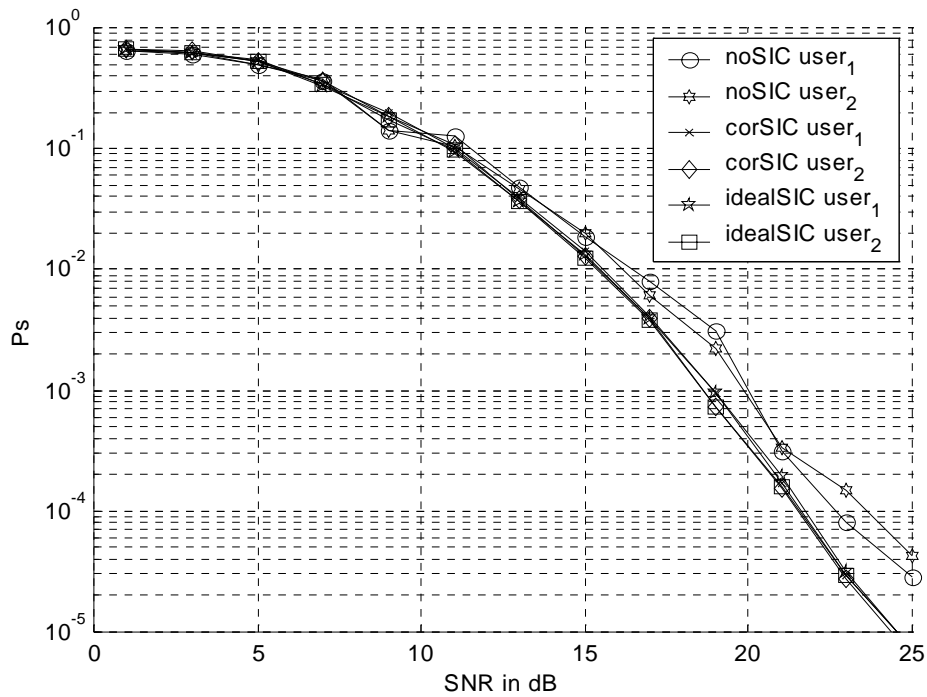


Fig. 6-16: P_s for SUI-3 channel, $SIR=0dB$, 2 antennas, $0.5 \cdot \lambda$, 2 users

At high SNR values the performance is slightly improved by employing the additional SIC stage after the space-time DFEs. However, the improvement is small and therefore it is probably better to detect the 2 user signals in parallel and not to employ SIC. Therefore a check on the received signal powers should be performed and only if the SIR exceeds a certain threshold should SIC be performed.

Finally in this section the system performance in an ideal diversity channel is investigated. These results are a benchmark for the best possible performances achieved in the channels having SUI-2 and SUI-3 power delay profiles. With an ideal diversity channel the Rayleigh component of the fading on each antenna is completely uncorrelated.

Fig. 6-17 shows the P_s performance for this situation when using the Rician SUI-2 channel delay profile, identified as i.i.d. SUI-2. Surprisingly, the performance in this situation is worse than that of the highly directional SUI-2 channel given previously in Fig. 6-9. The reason is that when one has independent fading on each antenna the situation can occur where the main cursor is not the same for each antenna. The space-time DFE has severe problems with such channels. A second version of the ideal diversity channel for a Rician SUI-2 power delay profiles is therefore devised. Here only the Rayleigh component on each antenna is i.i.d. and the Rician component is modelled as in the GWSSUS channel model (see section 3.3.2.2). This channel model is denoted as i.i.d. SUI-2 v2 and the results are given in Fig. 6-18. The Rician component is modelled for an antenna spacing of $10 \cdot \lambda$. It is seen that in this case the performance is slightly better than in Fig. 6-9, which is expected, because now the Rayleigh component is completely uncorrelated.

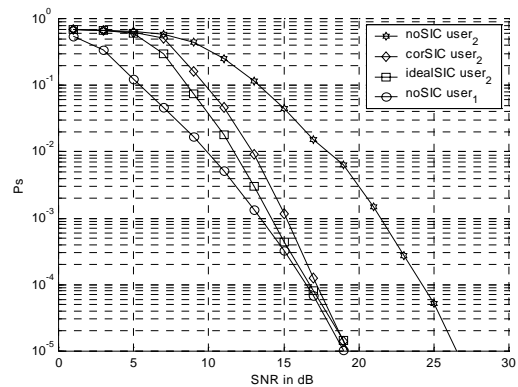
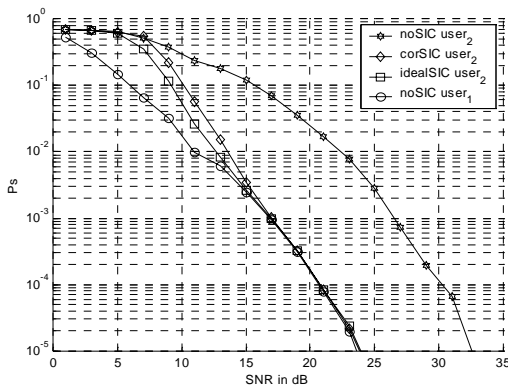


Fig. 6-17: P_s for i.i.d. SUI-2 channel, Fig. 6-18: P_s for i.i.d. SUI-2 v2 channel,
 $SIR=5dB$, 2 antennas, 2 users $SIR=5dB$, 2 antennas, $10 \cdot \lambda$,
 2 users

Fig. 6-19 shows the P_s results for the ideal diversity channel employing the SUI-3 power delay profile, identified as i.i.d. SUI-3. The P_s performances presented in Fig. 6-19 are slightly better than those in Fig. 6-11. So with an antenna spacing of only $0.5 \cdot \lambda$ and an azimuth spread of 40°

for the SUI-3 GWSSUS channel, the P_s performance is very close to that achievable in the ideal diversity channel.

Fig. 6-20 shows the P_s for the same arrangement as in Fig. 6-11, but with the exception that an antenna spacing of $10 \cdot \lambda$ is used. Clearly very little performance is gained by increasing the antenna spacing when using the SUI-3 profile with a 40° azimuth spread. This result is in contrast to the directional SUI-2 channel results of Fig. 6-9 where a large antenna spacing equal to $10 \cdot \lambda$ is necessary for good system performance.

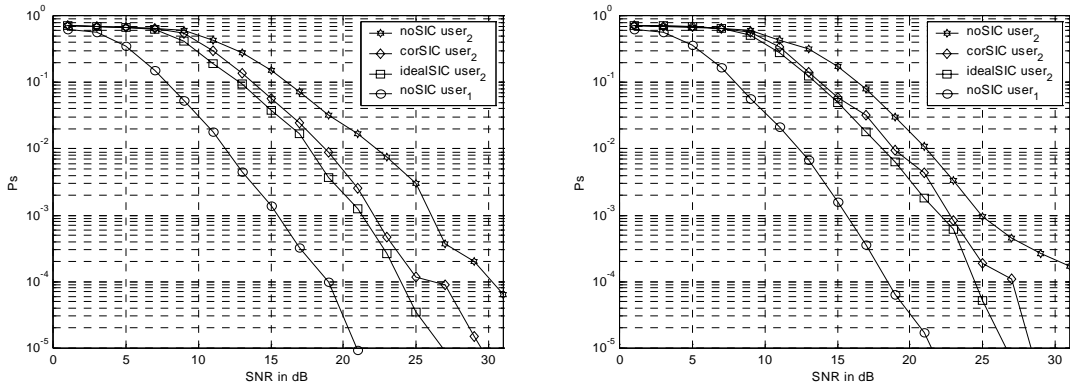


Fig. 6-19: P_s for i.i.d. SUI-3 channel, Fig. 6-20: P_s for SUI-3 channel, $SIR=5dB$, $SIR=5dB$, 2 antennas, 2 users
2 antennas, $10 \cdot \lambda$, 2 users

6.3.2.4 2 SIC stages for 2 users

In this section the performance of the proposed space-time DFE system this time employing 2 SIC stages is investigated. Again assuming a 2-user SDMA/TDMA FBWA system, with a BS employing a 2 element ULA and 2 SUs transmitting in the same time slot and at the same frequency. In this scheme the strongest user, namely user₁ is detected first and then the first SIC stage subtracts the interference contribution of user₁ from the received signal. This signal is named X_{rx2} . Then the second user, namely user₂ is detected. The second SIC stage generates the interference contribution of user₂ and subtracts it from X_{rx2} . Then the strongest user, namely user₁ is detected again. The results are denoted as corSIC user₁ or idealSIC user₁ depending whether the cross-correlation channel estimate is used or an ideal channel estimate is used respectively to generate the interference contribution. Again the SIR is 5dB and the antenna spacing is either $10 \cdot \lambda$ or $0.5 \cdot \lambda$, depending whether the SUI-2 or SUI-3 power delay profile is used.

Fig. 6-21 and Fig. 6-22 show the P_s curves for various scenarios using the SUI-2 and the SUI-3 power delay profiles respectively. Clearly, nothing is gained with the use of a second SIC stage. The reason again is that of error propagation through the SIC stages. Therefore it is best to

detect the strongest user $user_1$ directly from received antenna input and only perform a single stage of SIC for $user_2$.

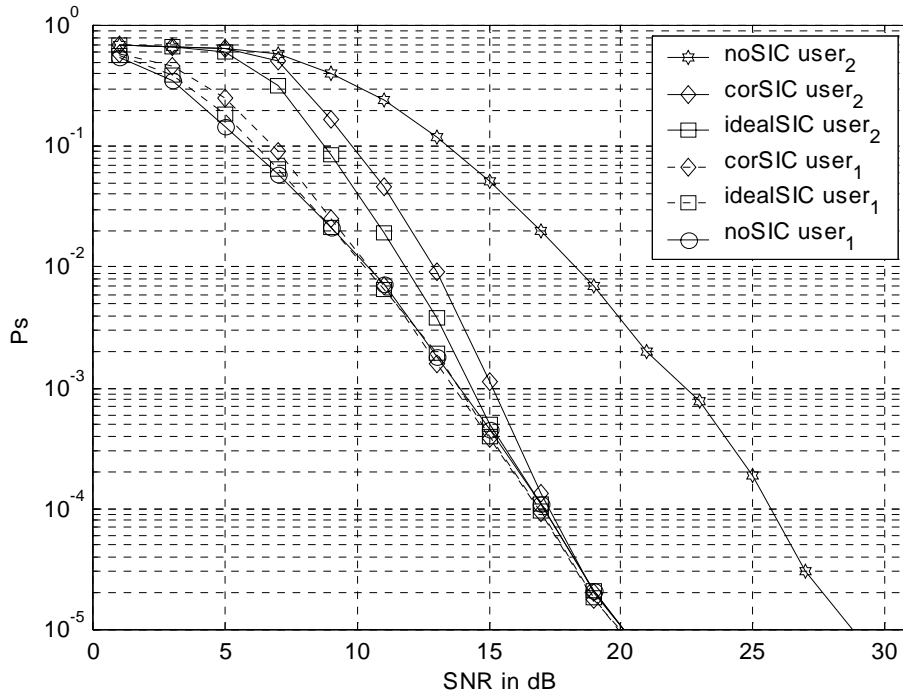


Fig. 6-21: P_s for SUI-2 channel, $SIR=5dB$, 2 antennas $10\cdot\lambda$ apart, 2 SIC stages, 2 users

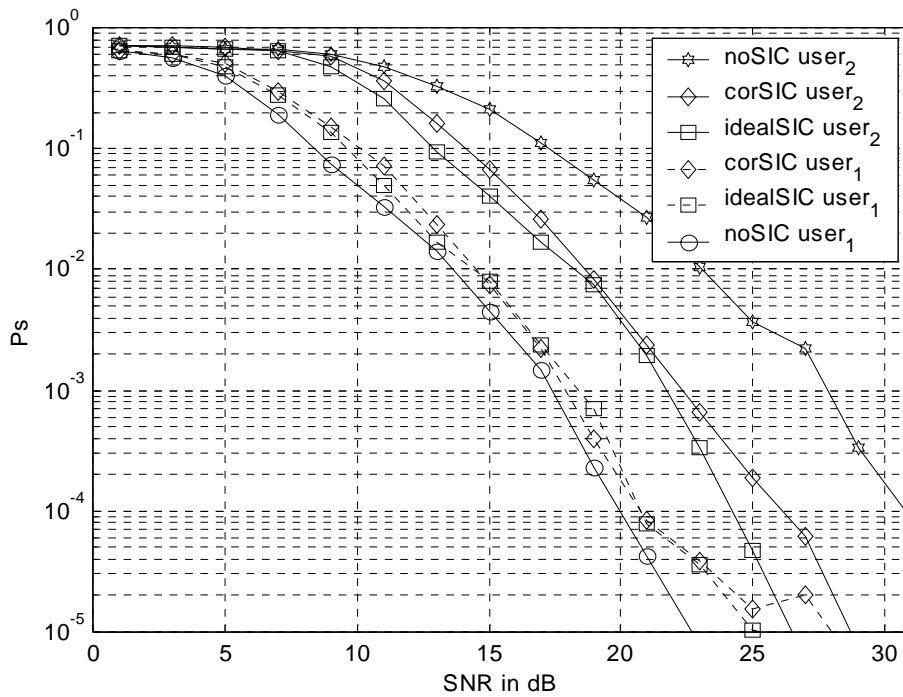


Fig. 6-22: P_s for SUI-3 channel, $SIR=5dB$, 2 antennas $0.5\cdot\lambda$ apart, 2 SIC stages, 2 users

6.3.2.5 Space-Time DFE/SIC compared with MIMO DFE

Finally, the proposed space-time DFE/SIC system of Fig. 6-1 is compared with a MIMO DFE. The MIMO DFE in this section is of the form shown in Fig. 2-5 where only previously detected symbols are available for the FBF [Al-Dha00]. Both the MIMO DFE and the space-time DFEs in the proposed system are trained with the RLS algorithm. The RLS algorithm for the MIMO DFE can be formulated in a compact matrix version [Kom02].

Fig. 6-23 shows the P_s of the MIMO DFE for the SUI-2 power delay profile overlaid with the space-time DFE results presented previously in Fig. 6-9. The MIMO DFE has a FF section of 2 times 15 vector taps, which corresponds to the FF section of the two space-time DFEs in the proposed 2-user SDMA/TDMA system. The FB matrix filter has a dimension of 10×4 , which correspond to the 2 FB filters each of 10 taps employed by the two space-time DFEs and 2 cross-decision FB filters each of 10 taps. The main tap is set to FF vector tap 10.

Fig. 6-23 shows that the MIMO DFE has the same performance as that achieved by the 2 space-time DFEs without SIC. However, the proposed space-time DFE/SIC system leads to a better P_s performance for the weaker user compared to that achieved by the MIMO DFE.

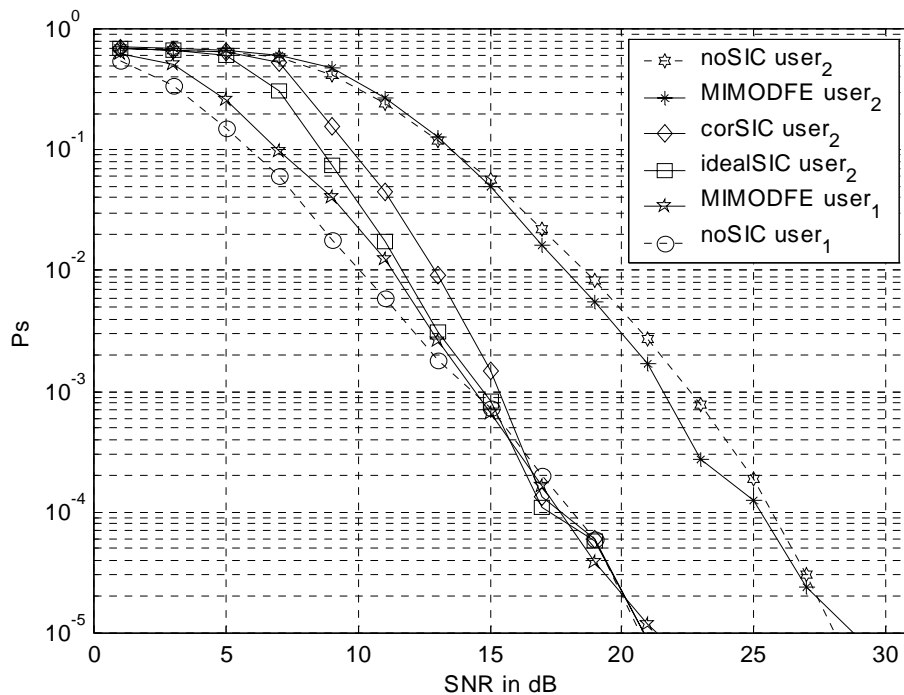


Fig. 6-23: Space-time DFE/SIC compared with MIMO DFE for SUI-2 channel, $SIR=5dB$, 2 antennas $10 \cdot \lambda$ apart, 2 users

Fig. 6-24 shows the P_s of the MIMO DFE for the SUI-3 power delay profile overlaid with the space-time DFE results presented previously in Fig. 6-11. For the SUI-3 delay profile a longer MIMO DFE is necessary. Here the FF section has 2 times 21 vector taps and the FB section is

of dimension 14×4 , which corresponds to 4 FB filters each of 14 taps. The main tap is FF vector tap 14.

For the SUI-3 profile the MIMO DFE has a better performance than the space-time DFE for the weaker user, user₂, when SIC is not used. However, the space-time DFE performs better than the MIMO DFE for the stronger user, user₁. The main result however is that the proposed space-time DFE system outperforms the MIMO DFE for both users when SIC is employed for the SUI-3 channel delay profile.

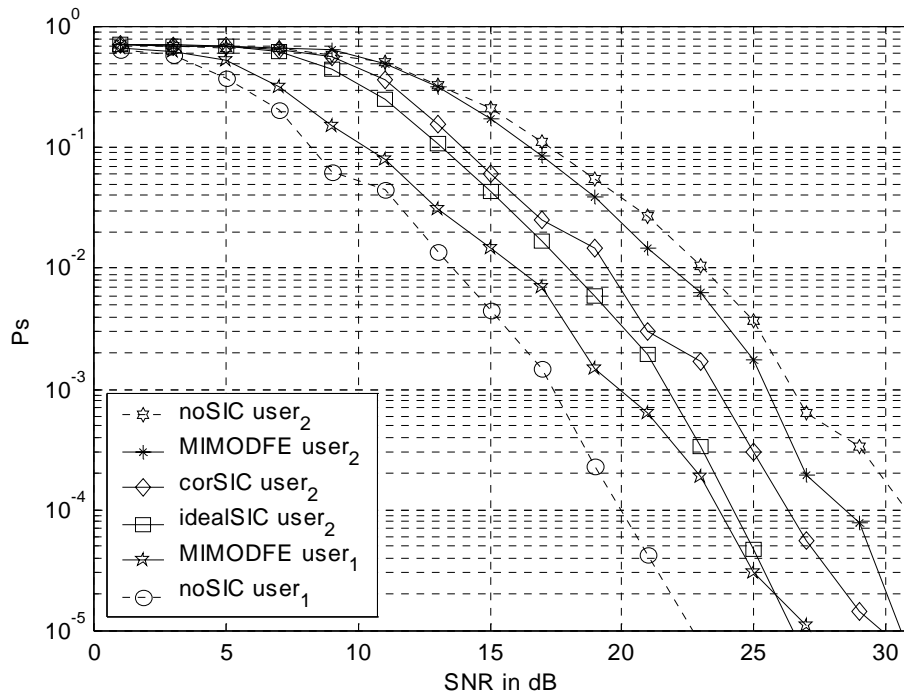


Fig. 6-24: Space-time DFE/SIC compared with MIMO DFE for SUI-3 channel, SIR=5dB, 2 antennas $0.5 \cdot \lambda$ apart, 2 users

6.4 Conclusions

Space-time processing in the uplink of a FBWA system is investigated in this chapter. First, a single space-time DFE is used to detect a single user employing multiple antennas at the BS and a single antenna at the SU. An antenna array at the BS improves the Ps performance considerably for typical FBWA channels, meaning that with multiple antennas at the BS, one can achieve a certain Ps at a considerably lower SNR. The improvement in Ps performance can be attributed to the antenna gain and to the diversity gain of the antenna array. The link quality is greatly improved through the use of multiple antennas at the BS. This can be exploited to either employ high-order modulation schemes (e.g. 64-QAM, 256-QAM) in order to increase the data rate, or else to increase the BS cell size leading to a reduction in the total number of

BSs required. In this chapter, QPSK modulation is used exclusively, and an investigation into the performance of high-order modulation schemes such as 64-QAM and 256-QAM remains a subject of future work. It is well known that the FF section of a DFE gives rise to noise enhancement. The space-time DFE appears particularly sensitive to the length of the FF section when a large number of antennas is employed. Thus noise enhancement is evident, particularly for the example using 8 antennas and the space-time DFE (15,10) in the SUI-3 channel (see section 6.3.1.2). In this situation the shorter space-time DFE (8,7) actually performs better owing to less noise enhancement. However, for the case when only 1 or 2 antennas are employed at the BS the longer space-time DFE(15,10) outperforms the shorter one.

The remainder of this chapter is devoted to multi-user detection in a SDMA/TDMA based FBWA system. Again, the SU has only a single antenna resulting in low-cost customer equipment. However, the BS uses an antenna array and is obviously more complex and expensive. Detecting U users in the same time slot and at the same frequency results in a U -fold bandwidth reuse. To achieve this a similar architecture to that of wideband V-BLAST of [Loza00] is proposed. In addition, this proposal combines space-time DFEs with SIC. The performance is shown for: a) detecting U users in parallel without SIC, b) detecting U users successively employing SIC with the cross-correlation channel estimate and c) detecting U users successively employing SIC with an ideal channel estimate. It is shown that SIC greatly improves the P_s of the weaker user in a 2-user SDMA/TDMA system when using a dual antenna array at the BS. Multiple antennas at the BS enable SDMA in the uplink and SDMA performance can be improved using SIC. Further, it is seen that the highly directional LOS SUI-2 channel demands a large antenna spacing to achieve good performance, whereas the NLOS SUI-3 channel which has a large azimuth spread achieves a good system performance with an antenna spacing of only $0.5 \cdot \lambda$.

However, the improvement achievable with SIC is limited by error propagation through the SIC stages as demonstrated in section 6.3.2.2. This is clearly seen in the example using the SUI-2 channel profile. In this case when SIC is employed all the errors from the first space-time DFE propagate through to the second space-time DFE where the weaker user, $user_2$ is detected. Therefore the improvement is limited by the P_s of the stronger user, namely $user_1$. The error propagation through the SIC stages is somewhat similar to the error propagation effect in the FB filter of a DFE. Unfortunately, both effects are hard to study analytically and hence the error propagation effect through the SIC stages is investigated empirically. The error propagation effect is seen to depend on the channel transfer function and on the difference in the received power of the two user signals (i.e. the SIR). Also it is shown that the error propagation through the SIC stages makes the use of more than one SIC stage for a 2-user SDMA/TDMA system not worthwhile.

Also SIC is shown to be effective if there is a significant difference in the received power of the two user signals. However, if both user signals have equal power, SIC does not offer any improvement. Therefore a check on the received signal powers should be performed at the outset, and only if the SIR exceeds a certain threshold should SIC be performed.

The signal ordering algorithm based on the input receive power works well when the number of antennas at the BS M and the number of SDMA/TDMA users U is the same. Additionally, a decision based on the measured received input powers to determine whether or not SIC should be used appears acceptable in this case. However, if the number of antennas exceeds the number of SDMA/TDMA users, the space-time DFE suppresses the MAI to such a degree that nothing is left for the SIC stage. In this situation it is best not to perform SIC. However, the measured input receive power can be misleading since a significant signal power difference at the input of the antenna array may not be the case after the space-time DFE. Hence, in these cases signal ordering and the SIC enabling decision should be based on the output SNR as employed in the BLAST systems. However, such an approach will be considerably more complex, since the evaluation of the pseudo-inverse of the matrix channel transfer function is necessary [Woln98], or in case of the wideband V-BLAST system, the inverse of the correlation matrix \mathbf{R} must be evaluated [Loza00].

Finally the performance of the proposed space-time DFE SDMA/TDMA architecture is compared with that of a MIMO DFE, where only previously detected symbols are available for the FB filter matrix. For the SUI-2 and the SUI-3 FBWA channel delay profiles investigated, the space-time DFE/SIC approach proposed in this chapter performs better than the MIMO DFE.

Chapter 7

Conclusions

Finally the findings in chapter 3, chapter 4, chapter 5 and chapter 6 are summarized.

Chapter 3 reviews spatial channel models for the uplink of a FBWA system. The original GWSSUS channel model from Zetterberg [Zet97] is modified to accommodate Rician fading. Rician fading occurs in FBWA environments, when there is a strong LOS component or when there is a strong specular component. The fading cross-correlation ρ is an important parameter in space-time processing systems since the performance of space-time equalization algorithms strongly depend on its value. The GWSSUS model enables the study of realistic FBWA scenarios and the effect of the fading cross-correlation.

A closed-form expression for the fading cross-correlation ρ is obtained via a trigonometric approximation. It is seen that this closed form expression holds when the DOA spread is small, which is the case for macrocells (i.e. the uplink in a FBWA system). The closed-form expressions presented here for Rician channels using the GWSSUS channel model have not been previously derived.

The ideal diversity channel is also discussed. This channel serves as a benchmark and represents a spatial channel with zero fading cross-correlation, i.e. $\rho = 0$.

In chapter 4 time-domain equalization techniques for a single-carrier FBWA system with single antennas at both SU and BS are studied. A computationally efficient RLS implementation, namely the LSL algorithm is investigated. The LSLDFE has not been considered previously for use in FBWA systems. Further, conventional LEs and DFEs trained with the LMS and the RLS algorithm are also studied. It is seen, that the LE always has an inferior P_s performance to all the DFEs. For the SUI-3 channel, the LE actually fails to deliver adequate performance. This is because the DFE outperforms the LE in the presence of spectral nulls. Error propagation in the FBF of the DFE is also studied. It is seen that this error propagation effect is more significant for the SUI-3 power delay profile than for the SUI-2 power delay profile.

An important result is that the lattice equalizer offers an excellent complexity-performance trade-off. The DFE trained with the LMS algorithm offers a similar P_s performance, however its convergence rate is far too slow for a bandwidth efficient FBWA system. Although the DFE trained with the RLS algorithm shows a slightly better performance than the LSLDFE, the

LSLDFE is much less computationally demanding than the DFE using the conventional RLS algorithm. For the SUI-3 channel the complexity of the LSL algorithm is nearly 3 times less than the RLS algorithm.

Chapter 5 presents a cross-correlation channel estimation technique for multi-user detection in SDMA/TDMA FBWA systems. Cross-correlation channel estimation is a common technique for single antenna systems employing single-user detection. However, for application to multiple antenna systems employing multi-user detection an extension to the original technique is needed. It is particularly interesting for FBWA applications, since its performance is the same as FR-ML channel estimation, but it has a much lower computational complexity, i.e. only one correlator is needed for each antenna. Multiple frequency-selective SDMA channels can be estimated using only one correlator per antenna branch when loaded with the mothersequence s_1 . The mothersequence s_1 is the first sequence in the set S and is furthermore an optimum sounding sequence [Ng98a].

Hence, the construction of the sequence set S for use in cross-correlation channel estimation is reduced to a number of cyclic shift operations on the mothersequence s_1 . In this way a ZCZ sequence set is constructed, which is optimal for cross-correlation channel estimation in a FBWA system having a number of simultaneously transmitting single antenna SUs and a BS with an antenna array performing multi-user detection. The application of the proposed ZCZ sequence set for cross-correlation channel estimation in a SDMA/TDMA FBWA system shows that highly accurate channel estimates can be obtained with this method.

Chapter 6 describes a low complexity space-time architecture for the uplink of SDMA/TDMA based FBWA systems. The FBWA system has SUs equipped with a single-antenna and BSs equipped with an adaptive antenna array. First, a conventional space-time DFE is used to detect a single SDMA/TDMA user. The antenna array at the BS improves the wireless link quality and opens the door to the use of high-order modulation schemes (e.g. 64-QAM, 256-QAM) leading to higher data rates. Alternatively if QPSK is retained the cell size can be extended and so fewer BSs will be necessary when deploying a FBWA network.

The remainder of this chapter is devoted to multi-user detection in a SDMA/TDMA based FBWA system employing a combination of space-time DFEs with SIC. Detecting U users in the same time slot and at the same frequency results in an U -fold bandwidth reuse. The performance is shown for: a) detecting U users in parallel without SIC, b) detecting U users successively employing SIC with the cross-correlation channel estimation technique of chapter 5 and c) detecting U users successively employing SIC with an ideal channel estimate. The performance of a 2-user SDMA/TDMA based FBWA system demonstrates that SIC improves the P_s of the

weaker user toward that of the stronger user. The penalty paid for using a realistic noisy cross-correlation channel estimate is shown to be small.

Unfortunately, the P_s performance improvement is limited by error propagation through the SIC stage. This is clearly seen in the example using the SUI-2 channel when employing SIC. In this case all the errors from the first space-time DFE propagate through to the second space-time DFE where the weaker user, $user_2$ is detected. Therefore the improvement is limited to the P_s of the stronger user, namely $user_1$.

When using SIC, performance is improved if there is a significant difference in the receive powers of the individual user signals. However, as seen in the performance study, if equal power users are detected, SIC does not improve the performance and it is better to detect the equal power users in parallel without SIC. The proposed architecture is flexible in the sense that SIC can be switched on or off depending whether or not a significant input power difference is detected.

SIC enabling and the signal ordering process can be based on the input receive power or on the post-detection SNR. However use of the post-detection SNR is likely to be more accurate but also more complex. The BLAST architecture uses post-detection SNR for signal ordering and could also be implemented in the proposed system at the cost of added complexity. However signal ordering and SIC enabling based on the input receive power is shown to be effective for a FBWA system where the number of SDMA/TDMA users is equal to the number of BS antennas.

When comparing the proposed space-time architecture with a MIMO DFE (where only previously detected symbols are available for the cross-feedback filters) it is seen that the proposed FBWA system outperforms the MIMO DFE.

The results in this chapter clearly demonstrate the advantages gained by installing an adaptive antenna array at the BS, specifically: a) the wireless link quality is improved and b) higher-data rates can be achieved through an U -fold reuse of system bandwidth. Clearly the capacity bottleneck in future FBWA systems can be ameliorated through the use of adaptive antenna array technology. However, computational complexity remains a burden, particularly when the number of antennas is large and/or antenna arrays are installed at both the SU and the BS. Complexity reduction for such MIMO systems remains the subject of future work.

Chapter 8

Future Work

The work presented in this thesis can be extended in many ways. The next obvious step is to extend the ideas in this thesis to the MIMO case. Multiple antennas at both the BS and the SU will give rise to even greater capacity and through-put improvements compared with multiple antennas at the BS alone. However, complexity issues need to be tackled in order to realize practical architectures. Future work is needed in the following areas.

8.1 Channel Modelling for FBWA MIMO channels

In Chapter 3, the GWSSUS model is used for SIMO channels, i.e. single antenna SUs and multi-antenna BSs. The proposed GWSSUS modelling approach can be extended to MIMO channels (i.e. multiple antennas at the SU and at the BS). Consequently this involves extending of the closed-form expression for the fading cross-correlation coefficient to the MIMO case.

8.2 Performance Study of the LSL algorithm

8.2.1 Fractionally symbol spaced taps

The equalization study in chapter 4 exclusively uses equalizers with symbol-spaced taps. Fractionally symbol spaced taps may offer a performance improvement. However, it has to be determined if the added complexity of the fractionally spaced equalizer is justified. It is likely that the performance improvement will not be too dramatic, since the system in chapter 4 already uses an oversampled correlator for symbol synchronization and sampling timing alignment. Since a fractionally spaced equalizer will have more taps than its symbol spaced counterpart, this will lead to a reduced convergence speed.

8.2.2 High-order modulation schemes

In chapter 4 the performance of the various equalizers is evaluated for QPSK modulation only. High-order modulation schemes such as 64-QAM or 256-QAM will offer much higher gross data rates. However, the SNR requirement for reliable data transfer needs to be investigated for such high-order schemes.

8.3 Cross-Correlation channel estimation for MIMO FBWA systems

The cross-correlation channel estimation method presented in chapter 5 can also be extended to a MIMO channel. Furthermore the problem of asynchronous users needs to be tackled. The method is shown to have the same performance as a FR-ML channel estimation, but does not require a computationally expensive matrix inversion. The performance study conducted in chapter 5 investigates a synchronous FBWA system. However an asynchronous FBWA system will require an increase in the sequence length (i.e. the size of the Z-zone).

8.4 Space-time processing for the FBWA downlink

8.4.1 MIMO pre-coding

In chapter 6, a SDMA/TDMA system has been proposed for the uplink. However, space-time processing in the downlink is not addressed. One area of interest therefore is MIMO pre-coding. Pre-coding has been investigated for single carrier time division duplex systems [Sell99b] and it may be possible to extend this scheme to MIMO FBWA systems. Pre-coding enables the BS to predistort the information symbols in such a way that the SU will receive the individual information sequences without ISI or MAI. This is possible when the uplink and downlink channels use the same frequency (i.e. the channel is reciprocal), as in e.g., a TDD system.

MIMO pre-coding has been investigated in [Choi99a, Choi99b, Dege01]. In these papers the pre-distortion is performed using a space-time linear equalizer. Extensions to MIMO pre-coding using a DFE could show interesting results.

The application of pre-coding at a BS, which is equipped with an antenna array shifts the equalization task toward the BS and consequently the SU can either operate without an equalizer or with one, which is much less complex (i.e., shorter). Somewhat related to the idea of pre-coding applied to an antenna array is that of space-time coding, which also has great potential for future research.

8.4.2 Space-time coding

Although the proposed space-time architecture of chapter 6 does not rely on the application of any coding, this does not mean that coding cannot be employed. It is expected that coding will improve system performance. For example, conventional coding could be applied to the individual user data streams. The improvement in terms of Ps can be explored in this context.

Space-time coding is a transmit diversity technique and the downlink of the proposed FBWA system in chapter 6 is an ideal candidate for the application of space-time coding techniques.

Space-time codes transmit the information symbols through an antenna array in such a way that both the coding gain and diversity gain at the receiver are maximized. Amongst the space-time codes available at the moment, space-time block codes appear to be the most appropriate for FBWA networks. Space-time block codes are designed (as with other space-time codes) to achieve the maximum diversity order for a given number of transmit and receive antennas, but subject to the constraint of having a simple decoding algorithm [Tar99c].

8.5 Improvements for the proposed SDMA/TDMA system

8.5.1 Signal ordering based on the post-detection SNR

As mentioned in chapter 6 signal ordering based on the input receive power can be misleading. Signal ordering and SIC enabling should be implemented based on the post-detection SNR as employed in BLAST [Fosch99].

8.5.2 Techniques for preventing error propagation through the SIC stages

The effect of error propagation through the SIC stages limits the performance of the proposed system in chapter 6. Techniques for preventing error propagation through the SIC stages are an interesting area of future research. In [Vande00] a state insertion technique is proposed, which improves the performance.

The scheme investigated in Chapter 6 employs symbol-by-symbol based detection, however it would be interesting to see if sequence based detection procedures (i.e. Viterbi algorithm) are more resilient to this error propagation effect. Unfortunately, due to the complexity of the Viterbi algorithm this could not be simulated in a reasonable time. However in the future with more powerful computers, such a study can be undertaken.

8.5.3 Antenna array at the SU and at the BS

By installing an antenna array at the SU, space-time coding in the uplink in connection with the multi-user detection scheme presented in chapter 6 can also be explored. This could lead to a BLAST like system with multi-user detection: Assuming that both the SUs and the BSs are equipped with antenna arrays, multiple SUs transmitting in the same time slot and at the same frequency (as in Chapter 6) could now also utilize space-time coding techniques during transmission. In general a MIMO system (multiple antennas at the BS and at the SU) will have a higher capacity than a SIMO system (a single antenna at the SU and multiple antennas at the BS).

Appendix A

Spatial fading cross-correlation for Rician channels using the GWSSUS channel model

Azimuth φ is defined along the array normal

Fading cross-correlation ρ_{diff} for the diffuse component

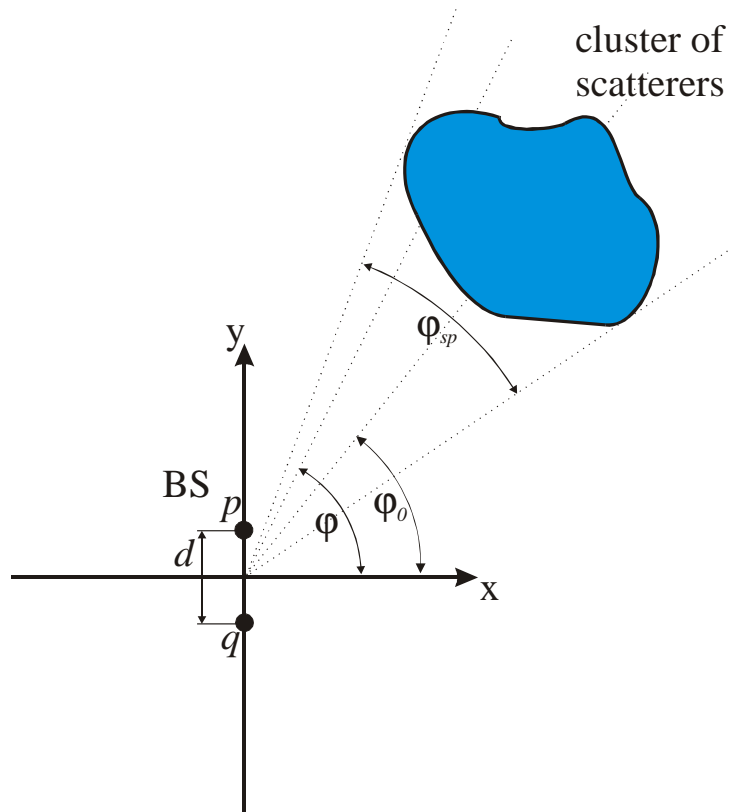


Fig. A-1: Fading cross-correlation ρ_{diff}

where: φ = azimuth

φ_0 = mean azimuth

φ_{sp} = azimuth spread or DOA spread defined as standard deviation of Gaussian pdf

d = antenna spacing

p and q are antenna indices, e.g. $p=1\dots 2$ and $q=1\dots 2$; $p \neq q$

Proof that

$$\varphi_i \sim N(0, \varphi_{sp}^2)$$

$$\rho_{diff} \approx \frac{1}{K+1} \cdot \exp\left\{j \cdot 2\pi \cdot (p-q) \frac{d}{\lambda} \cdot \sin(\varphi_0)\right\} \cdot \exp\left\{-\frac{1}{2} \left(2\pi \cdot (p-q) \frac{d}{\lambda} \cdot \cos(\varphi_0) \cdot \varphi_{sp}\right)^2\right\} \quad (\text{A-1})$$

using the following trigonometric approximation:

$$\sin(\varphi_0 + \varphi_i) = \sin(\varphi_0) \cdot \cos(\varphi_i) + \cos(\varphi_0) \cdot \sin(\varphi_i) \quad \text{and} \quad \cos(\varphi_i) = 1, \quad \sin(\varphi_i) = \varphi_i$$

$$\sin(\varphi_0 + \varphi_i) \approx \sin(\varphi_0) + \varphi_i \cdot \cos(\varphi_0) \quad (\text{A-2})$$

According to chapter 4 equation 3.22:

$$\begin{aligned} \rho_{diff} &= \sqrt{\frac{1}{(K_{mp}+1) \cdot (K_{mq}+1)}} \cdot E\left[\exp\left\{j \cdot 2 \cdot \pi \cdot (p-q) \cdot \frac{d}{\lambda} \cdot \sin(\varphi_0 + \varphi_i)\right\}\right] \\ \rho_{diff} &= \sqrt{\frac{1}{(K_{mp}+1) \cdot (K_{mq}+1)}} \cdot \int_{-\infty}^{\infty} \exp\left\{j \cdot 2 \cdot \pi \cdot (p-q) \cdot \frac{d}{\lambda} \cdot \sin(\varphi_0 + \varphi_i)\right\} \cdot \\ &\quad \frac{1}{\sqrt{2\pi} \cdot \varphi_{sp}} \cdot \exp\left\{-\frac{\varphi_i^2}{2 \cdot \varphi_{sp}^2}\right\} d\varphi_i \end{aligned} \quad (\text{A-3})$$

A-2 in A-3:

$$\begin{aligned} \rho_{diff} &= \sqrt{\frac{1}{(K_{mp}+1) \cdot (K_{mq}+1)}} \cdot \int_{-\infty}^{\infty} \exp\left\{j \cdot 2 \cdot \pi \cdot (p-q) \cdot \frac{d}{\lambda} \cdot \sin(\varphi_0)\right\} \\ &\quad \cdot \exp\left\{j \cdot 2 \cdot \pi \cdot (p-q) \cdot \frac{d}{\lambda} \cdot \cos(\varphi_0) \cdot \varphi_i\right\} \cdot \frac{1}{\sqrt{2\pi} \cdot \varphi_{sp}} \cdot \exp\left\{-\frac{\varphi_i^2}{2 \cdot \varphi_{sp}^2}\right\} d\varphi_i \end{aligned} \quad (\text{A-4})$$

introducing the constants: $a = -j \cdot 2\pi \cdot (p-q) \cdot \frac{d}{\lambda} \cdot \cos(\varphi_0)$ and $b = \frac{1}{2\varphi_{sp}^2}$

$$\begin{aligned} \rho_{diff} &= \sqrt{\frac{1}{(K_{mp}+1) \cdot (K_{mq}+1)}} \cdot \exp\left\{j \cdot 2 \cdot \pi \cdot (p-q) \cdot \frac{d}{\lambda} \cdot \sin(\varphi_0)\right\} \cdot \\ &\quad \frac{1}{\sqrt{2\pi} \cdot \varphi_{sp}} \cdot \int_{-\infty}^{\infty} \exp\{-a \cdot \varphi_i\} \cdot \exp\{-b \cdot \varphi_i^2\} d\varphi_i \end{aligned} \quad (\text{A-5})$$

completing the square inside the integral:

$$\begin{aligned} \Leftrightarrow \rho_{diff} &= \sqrt{\frac{1}{(K_{mp}+1) \cdot (K_{mq}+1)}} \cdot \exp\left\{j \cdot 2 \cdot \pi \cdot (p-q) \cdot \frac{d}{\lambda} \cdot \sin(\varphi_0)\right\} \cdot \\ &\quad \frac{1}{\sqrt{2\pi} \cdot \varphi_{sp}} \cdot \int_{-\infty}^{\infty} \exp\left\{-b \cdot \left(\varphi_i + \frac{a}{b} \varphi_i\right)\right\} d\varphi_i \\ \Leftrightarrow \rho_{diff} &= \sqrt{\frac{1}{(K_{mp}+1) \cdot (K_{mq}+1)}} \cdot \exp\left\{j \cdot 2 \cdot \pi \cdot (p-q) \cdot \frac{d}{\lambda} \cdot \sin(\varphi_0)\right\} \cdot \\ &\quad \frac{1}{\sqrt{2\pi} \cdot \varphi_{sp}} \cdot \int_{-\infty}^{\infty} \exp\left\{-b \cdot \left[\left(\varphi_i + \frac{a}{2b}\right)^2 - \left(\frac{a}{2b}\right)^2\right]\right\} d\varphi_i \end{aligned}$$

$$\begin{aligned}
 \Leftrightarrow \rho_{diff} &= \sqrt{\frac{1}{(K_{mp}+1)(K_{mq}+1)}} \cdot \exp\left\{j \cdot 2 \cdot \pi(p-q) \cdot \frac{d}{\lambda} \cdot \sin(\varphi_0)\right\} \cdot \exp\left\{b \left(\frac{a}{2b}\right)^2\right\} \\
 &\quad \frac{1}{\sqrt{2\pi} \cdot \varphi_{sp}} \cdot \int_{-\infty}^{\infty} \exp\left\{-b \cdot \left(\varphi_i + \frac{a}{2b}\right)^2\right\} d\varphi_i \\
 \Leftrightarrow \rho_{diff} &= \sqrt{\frac{1}{(K_{mp}+1)(K_{mq}+1)}} \cdot \exp\left\{j \cdot 2 \cdot \pi(p-q) \cdot \frac{d}{\lambda} \cdot \sin(\varphi_0)\right\} \\
 &\quad \exp\left\{-\frac{1}{2} \left(2\pi \cdot (p-q) \cdot \frac{d}{\lambda} \cdot \cos(\varphi_0) \cdot \varphi_{sp}\right)^2\right\} \cdot I
 \end{aligned} \tag{A-6}$$

where:
$$I = \frac{1}{\sqrt{2\pi} \cdot \varphi_{sp}} \cdot \int_{-\infty}^{\infty} \exp\left\{-b \cdot \left(\varphi_i + \frac{a}{2b}\right)^2\right\} d\varphi_i$$

$$\Leftrightarrow I = \frac{1}{\sqrt{2\pi} \cdot \varphi_{sp}} \cdot \int_{-\infty}^{\infty} \exp\left\{-\frac{\left[\varphi_i - \left(j \cdot 2\pi \cdot (p-q) \cdot \frac{d}{\lambda} \cdot \cos(\varphi_0) \cdot \varphi_{sp}^2\right)\right]^2}{2\varphi_{sp}^2}\right\} d\varphi_i \tag{A-7}$$

I is the integral from $-\infty$ to ∞ over a normalized Gaussian pdf with mean $\mu = j \cdot 2\pi \cdot (p-q) \cdot \frac{d}{\lambda} \cdot \cos(\varphi_0) \cdot \varphi_{sp}^2$, which is by definition 1. However the proof is continued and it is shown in the following that this is the case. Making the following change of variables in the integral:

$$x = [\varphi_i - \mu]^2$$

$$\Rightarrow I = \frac{1}{\sqrt{2\pi} \cdot \varphi_{sp}} \cdot \int_{-\infty}^{\infty} \exp\left\{-\frac{x^2}{2\varphi_{sp}^2}\right\} dx$$

Now instead solving I , the integral I^2 is evaluated. The reason for that will become apparent in equation A-8.

$$I^2 = \left(\frac{1}{\sqrt{2\pi} \cdot \varphi_{sp}}\right)^2 \cdot \int_{-\infty}^{\infty} \exp\left\{-\frac{x^2}{2\varphi_{sp}^2}\right\} dx \cdot \int_{-\infty}^{\infty} \exp\left\{-\frac{y^2}{2\varphi_{sp}^2}\right\} dy$$

Changing to polar coordinates ($x = r \cdot \cos(\alpha)$ and $y = r \cdot \sin(\alpha)$) leads:

$$I^2 = \left(\frac{1}{\sqrt{2\pi} \cdot \varphi_{sp}}\right)^2 \cdot \int_0^{2\pi} \int_0^{\infty} r \cdot \exp\left\{-\frac{r^2}{2\varphi_{sp}^2}\right\} dr \cdot d\alpha \tag{A-8}$$

$$\Leftrightarrow I^2 = \left(\frac{1}{\sqrt{2\pi} \cdot \varphi_{sp}}\right)^2 \cdot \int_0^{2\pi} \left[-\varphi_{sp}^2 \cdot \exp\left\{-\frac{r^2}{2\varphi_{sp}^2}\right\}\right]_0^{\infty} d\alpha$$

$$\Leftrightarrow I^2 = \left(\frac{1}{\sqrt{2\pi} \cdot \varphi_{sp}} \right)^2 \cdot 2\pi \cdot \varphi_{sp}^2 = 1$$

$$\therefore I = 1 \quad (\text{A-9})$$

A-9 in A-6:

$$\rho_{diff} = \sqrt{\frac{1}{(K_{mp}+1) \cdot (K_{mq}+1)} \cdot \exp\left\{j \cdot 2 \cdot \pi (p-q) \cdot \frac{d}{\lambda} \cdot \sin(\varphi_0)\right\} \cdot \exp\left\{-\frac{1}{2} \left(2\pi \cdot (p-q) \cdot \frac{d}{\lambda} \cdot \cos(\varphi_0) \cdot \varphi_{sp}\right)^2\right\}} \quad (\text{A-10})$$

Setting $K_{mp}=K_{mq}=K$ (i.e. the K-factor for each channel SU-BS channel is the same):

$$\rho_{diff} = \frac{1}{K+1} \cdot \exp\left\{j \cdot 2 \cdot \pi (p-q) \cdot \frac{d}{\lambda} \cdot \sin(\varphi_0)\right\} \cdot \exp\left\{-\frac{1}{2} \left(2\pi \cdot (p-q) \cdot \frac{d}{\lambda} \cdot \cos(\varphi_0) \cdot \varphi_{sp}\right)^2\right\} \quad (\text{A-11})$$

Fading cross-correlation ρ

$$\rho = \rho_{LOS} + \rho_{diff} \approx \frac{K}{K+1} \cdot \exp\left\{j \cdot 2 \cdot \pi (p-q) \cdot \frac{d}{\lambda} \cdot \sin(\varphi_{LOS})\right\} + \frac{1}{K+1} \cdot \exp\left\{j \cdot 2\pi \cdot (p-q) \cdot \frac{d}{\lambda} \cdot \sin(\varphi_0)\right\} \cdot \exp\left\{-\frac{1}{2} \left(2\pi \cdot (p-q) \cdot \frac{d}{\lambda} \cdot \cos(\varphi_0) \cdot \varphi_{sp}\right)^2\right\} \quad (\text{A-12})$$

$$\rho_{LOS} = \frac{K}{K+1} \cdot \exp\left\{j \cdot 2 \cdot \pi (p-q) \cdot \frac{d}{\lambda} \cdot \sin(\varphi_{LOS})\right\} \quad (\text{see chapter 4, equation 3.20})$$

p and q are antenna indices. Thus the fading cross-correlation between antenna 1 and antenna 2 is:

$$\rho = \rho_{LOS} + \rho_{diff} \approx \frac{K}{K+1} \cdot \exp\left\{-j \cdot 2 \cdot \pi \cdot \frac{d}{\lambda} \cdot \sin(\varphi_{LOS})\right\} + \frac{1}{K+1} \cdot \exp\left\{-j \cdot 2\pi \cdot \frac{d}{\lambda} \cdot \sin(\varphi_0)\right\} \cdot \exp\left\{-\frac{1}{2} \left(2\pi \cdot \frac{d}{\lambda} \cdot \cos(\varphi_0) \cdot \varphi_{sp}\right)^2\right\}$$

Azimuth φ is defined along the array axis

Now the azimuth is defined along the array axis like shown in Fig. A-2 and Fig. A-3. This definition of the azimuth was used in [Aszt96, Ert98]. Usually the azimuth is defined along the array normal [Salz94, Fuhl98, Monz80]. The analysis is similar like the one in the section where the ‘azimuth φ is defined along the array normal’ and is included here merely for completeness.

Fading cross-correlation ρ_{LOS} for the LOS component

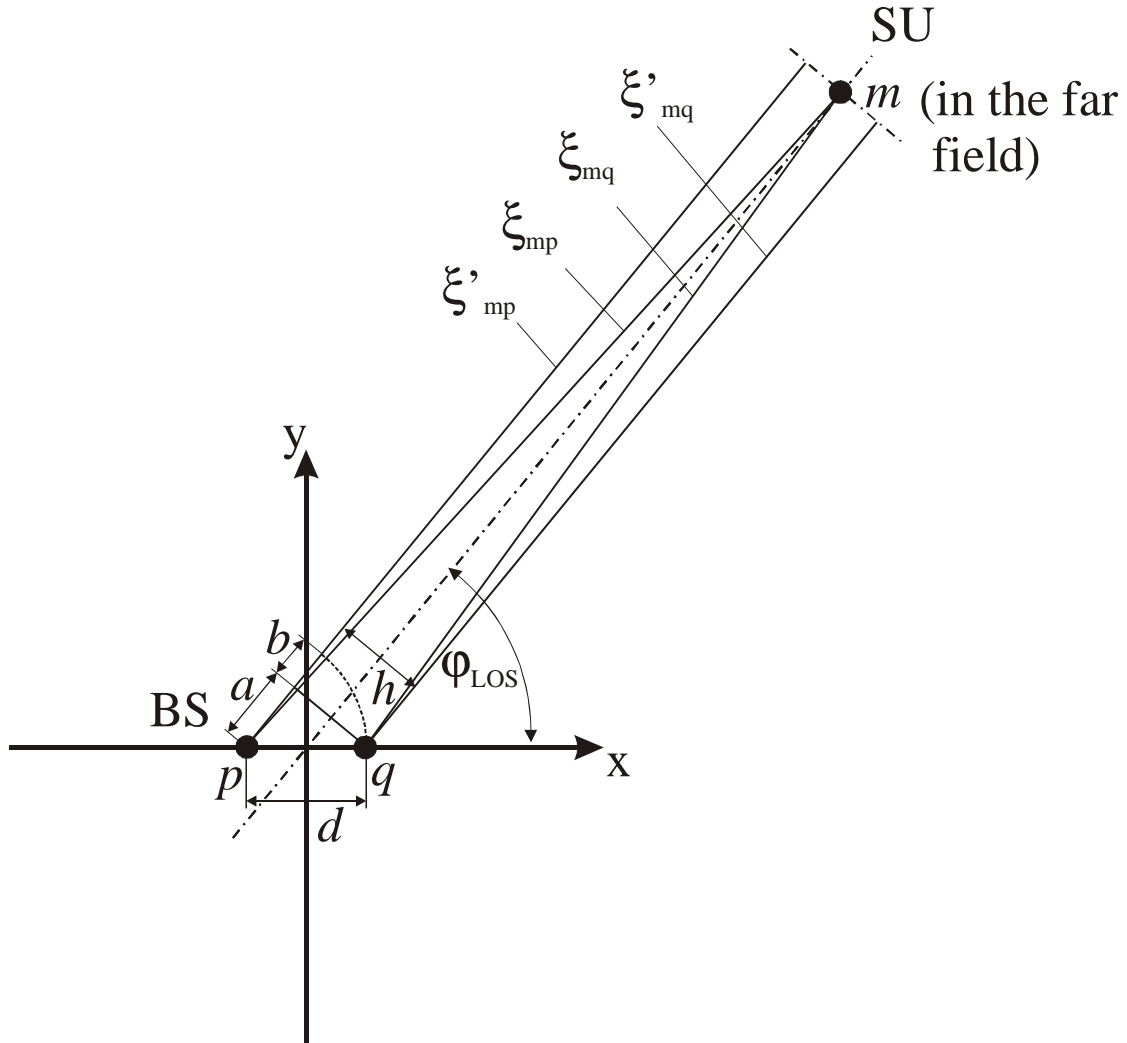


Fig. A-2: Fading cross-correlation ρ_{LOS}

where: φ_{LOS} = azimuth of LOS component

d = antenna spacing

p and q are antenna indices, e.g. $p=1 \dots 2$ and $q=1 \dots 2$; $p \neq q$

Again the fading cross-correlation of the LOS component is given by:

$$\rho_{mp,mq}^{LOS} = \sqrt{\frac{K_{mp} \cdot K_{mq}}{(K_{mp} + 1) \cdot (K_{mq} + 1)}} \cdot \exp\left\{-\frac{j \cdot 2\pi}{\lambda} [\xi_{mp} - \xi_{mq}]\right\} \quad (\text{A-13})$$

$$\xi_{mp} - \xi_{mq} \approx \xi'_{mp} - \xi'_{mq}$$

$$I : a = \xi'_{mp} - \xi'_{mq}$$

$$II : d = r \cdot \cos(\varphi_{LOS})$$

$$III : d^2 = r \cdot a$$

$$IV : r = a + b$$

$$III \text{ in } II: d = \frac{d^2}{a} \cdot \cos(\varphi_{LOS}) \Leftrightarrow a = d \cdot \cos(\varphi_{LOS})$$

$$\text{In } I: \xi'_{mp} - \xi'_{mq} = d \cdot \cos(\varphi_{LOS}) = (q - p) \cdot d \cdot \cos(\varphi_{LOS}) = -(p - q) \cdot d \cdot \cos(\varphi_{LOS})$$

Hence:

$$\rho_{LOS} = \sqrt{\frac{K_{mp} \cdot K_{mq}}{(K_{mp} + 1) \cdot (K_{mq} + 1)}} \cdot \exp\left\{j \cdot 2 \cdot \pi (p - q) \cdot \frac{d}{\lambda} \cdot \cos(\varphi_{LOS})\right\} \quad (\text{A-14})$$

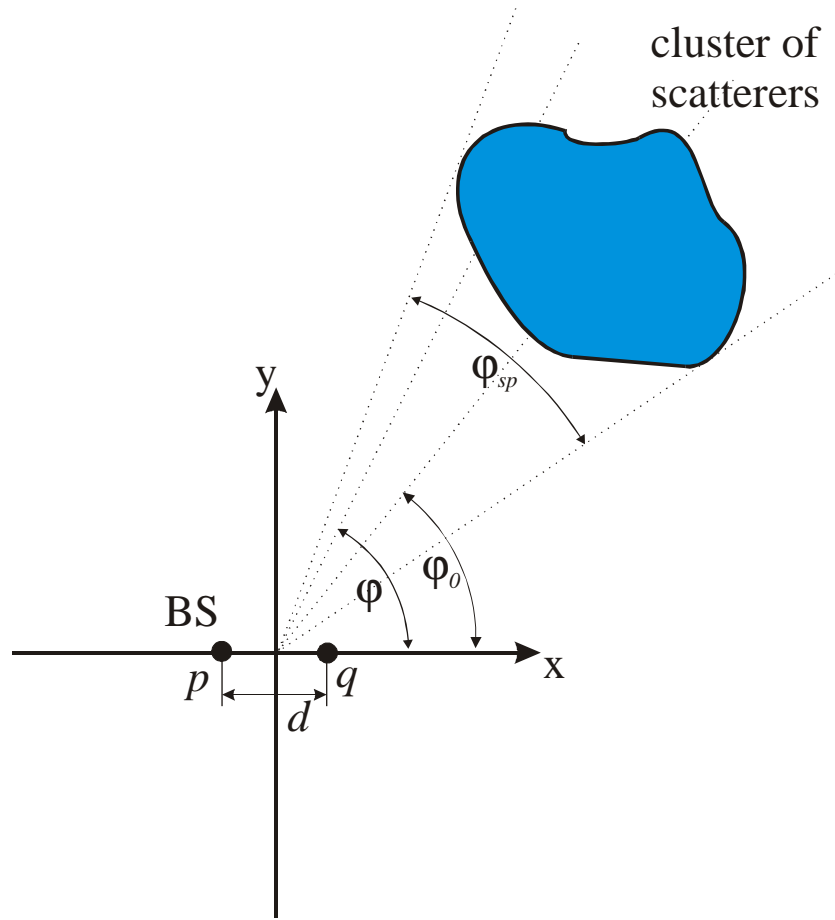
where: p = BS antenna index, e.g. dual antenna BS $p=1..2$

q = BS antenna index, e.g. dual antenna BS $q=1..2$

m = SU antenna index, e.g. equals 1 for SIMO channels

Letting the K-Factor for each spatial channel be the same, i.e. $K_{mp}=K_{mq}=K$:

$$\rho_{LOS} = \frac{K}{K+1} \cdot \exp\left\{j \cdot 2 \cdot \pi (p - q) \cdot \frac{d}{\lambda} \cdot \cos(\varphi_{LOS})\right\} \quad (\text{A-15})$$

Fading cross-correlation ρ for the diffuse component

 Fig. A-3: Fading cross-correlation ρ_{diff}

where: φ = azimuth
 φ_0 = mean azimuth
 φ_{sp} = azimuth spread or DOA spread defined as standard deviation of Gaussian pdf
 d = antenna spacing
 p and q are antenna indices, e.g. $p=1 \dots 2$ and $q=1 \dots 2$; $p \neq q$

Proof that

$$\varphi_i \sim N(0, \varphi_{sp}^2)$$

$$\rho_{diff} \approx \frac{1}{K+1} \cdot \exp\left\{j \cdot 2\pi \cdot (p-q) \frac{d}{\lambda} \cdot \cos(\varphi_0)\right\} \cdot \exp\left\{-\frac{1}{2} \left(2\pi \cdot (p-q) \frac{d}{\lambda} \cdot \sin(\varphi_0) \cdot \varphi_{sp}\right)^2\right\} \quad (\text{A-16})$$

using the following trigonometric approximation:

$$\cos(\varphi_0 + \varphi_i) = \cos(\varphi_0) \cdot \cos(\varphi_i) - \sin(\varphi_0) \cdot \sin(\varphi_i) \quad \text{and} \quad \cos(\varphi_i) = 1, \quad \sin(\varphi_i) = \varphi_i$$

$$\sin(\varphi_0 + \varphi_i) \approx \cos(\varphi_0) - \varphi_i \cdot \sin(\varphi_0) \quad (\text{A-17})$$

According to Asztely [Aszt96] and Abdi [Abdi02]:

$$\begin{aligned}\rho_{diff} &= \sqrt{\frac{1}{(K_{mp}+1)(K_{mq}+1)}} \cdot E \left[\exp \left\{ j \cdot 2 \cdot \pi (p-q) \cdot \frac{d}{\lambda} \cdot \cos(\varphi_0 + \varphi_i) \right\} \right] \\ \rho_{diff} &= \sqrt{\frac{1}{(K_{mp}+1)(K_{mq}+1)}} \cdot \int_{-\infty}^{\infty} \exp \left\{ j \cdot 2 \cdot \pi (p-q) \cdot \frac{d}{\lambda} \cdot \cos(\varphi_0 + \varphi_i) \right\} \cdot \\ &\quad \frac{1}{\sqrt{2\pi} \cdot \varphi_{sp}} \cdot \exp \left\{ -\frac{\varphi_i^2}{2 \cdot \varphi_{sp}^2} \right\} d\varphi_i\end{aligned}\tag{A-18}$$

In a similar fashion to the section where the ‘azimuth φ is defined along the array normal’ it can be shown that equation A-18 evaluates to equation A-19 by applying the trigonometric approximation A-17.

$$\begin{aligned}\rho_{diff} &= \sqrt{\frac{1}{(K_{mp}+1)(K_{mq}+1)}} \cdot \exp \left\{ j \cdot 2 \cdot \pi (p-q) \cdot \frac{d}{\lambda} \cdot \cos(\varphi_0) \right\} \cdot \\ &\quad \exp \left\{ -\frac{1}{2} \left(2\pi \cdot (p-q) \cdot \frac{d}{\lambda} \cdot \sin(\varphi_0) \cdot \varphi_{sp} \right)^2 \right\}\end{aligned}\tag{A-19}$$

Letting the K-Factor for each spatial channel be the same, i.e. $K_{mp}=K_{mq}=K$:

$$\rho_{diff} = \frac{1}{K+1} \cdot \exp \left\{ j \cdot 2 \cdot \pi (p-q) \cdot \frac{d}{\lambda} \cdot \cos(\varphi_0) \right\} \cdot \exp \left\{ -\frac{1}{2} \left(2\pi \cdot (p-q) \cdot \frac{d}{\lambda} \cdot \sin(\varphi_0) \cdot \varphi_{sp} \right)^2 \right\}\tag{A-20}$$

Cross-correlation ρ

Combining equation A-15 and A-20:

$$\begin{aligned}\rho = \rho_{LOS} + \rho_{diff} &\approx \frac{K}{K+1} \cdot \exp \left\{ j \cdot 2 \cdot \pi (p-q) \cdot \frac{d}{\lambda} \cdot \cos(\varphi_{LOS}) \right\} \\ &\quad + \frac{1}{K+1} \cdot \exp \left\{ j \cdot 2\pi \cdot (p-q) \cdot \frac{d}{\lambda} \cdot \cos(\varphi_0) \right\} \cdot \\ &\quad \exp \left\{ -\frac{1}{2} \left(2\pi \cdot (p-q) \cdot \frac{d}{\lambda} \cdot \sin(\varphi_0) \cdot \varphi_{sp} \right)^2 \right\}\end{aligned}\tag{A-21}$$

Thus, defining the azimuth along the array axis just changes the sin into cos and cos into sin compare to equation A-12.

p and q are antenna indices. Thus the fading cross-correlation between antenna 1 and antenna 2 is:

$$\begin{aligned}\rho = \rho_{LOS} + \rho_{diff} &\approx \frac{K}{K+1} \cdot \exp \left\{ -j \cdot 2\pi \cdot \frac{d}{\lambda} \cdot \cos(\varphi_{LOS}) \right\} + \frac{1}{K+1} \cdot \exp \left\{ -j \cdot 2\pi \cdot \frac{d}{\lambda} \cdot \cos(\varphi_0) \right\} \cdot \\ &\quad \exp \left\{ -\frac{1}{2} \left(2\pi \cdot \frac{d}{\lambda} \cdot \sin(\varphi_0) \cdot \varphi_{sp} \right)^2 \right\}\end{aligned}$$

Fading cross-correlation ρ when elevation is modelled

$$\rho_{LOS} = \frac{K}{K+1} \cdot \exp\left\{j \cdot 2\pi \cdot (p-q) \cdot \frac{d}{\lambda} \cdot \sin(\varphi_0) \cdot \cos(\theta_0)\right\} \quad (\text{see Chapter 3, equation 3.27})$$

Proof:

$$\begin{aligned} \rho_{diff} &\approx \frac{1}{K+1} \cdot \exp\left\{j \cdot 2\pi \cdot (p-q) \cdot \frac{d}{\lambda} \cdot \sin(\varphi_0) \cdot \cos(\theta_0)\right\} \cdot \\ &\exp\left\{-\frac{1}{2} \cdot \left[2\pi \cdot (p-q) \cdot \frac{d}{\lambda} \cdot \varphi_{sp}\right]^2 \cdot \cos^2(\varphi_0) \cdot \cos^2(\theta_0)\right\} \cdot \exp\left\{\frac{1}{2} \cdot \frac{\theta_{sp}^2 \cdot a'^2}{b'}\right\} \cdot \sqrt{\frac{1}{b'}} \end{aligned}$$

$$a' = 2 \cdot \cos^2(\varphi_0) \cdot \cos(\theta_0) \cdot \sin(\theta_0) + j \cdot 2\pi \cdot (p-q) \cdot \frac{d}{\lambda} \cdot \sin(\varphi_0) \cdot \cos(\theta_0)$$

where:

$$b' = 1 + \frac{1}{2} \cdot \left[2\pi \cdot (p-q) \cdot \frac{d}{\lambda} \cdot \varphi_{sp}\right]^2 \cdot \cos^2(\varphi_0) \cdot \sin^2(\theta_0) \cdot 2 \cdot \theta_{sp}^2$$

using the trigonometric approximation:

$$\sin(\varphi_0 + \varphi_i) = \sin(\varphi_0) \cdot \cos(\varphi_i) + \cos(\varphi_0) \cdot \sin(\varphi_i) \approx \sin(\varphi_0) + \varphi_i \cdot \cos(\varphi_0)$$

$$\cos(\theta_0 + \theta_i) = \cos(\theta_0) \cdot \cos(\theta_i) - \sin(\theta_0) \cdot \sin(\theta_i) \approx \cos(\theta_0) - \theta_i \cdot \sin(\theta_0)$$

and:

$$\varphi_i \sim N(0, \varphi_{sp}^2)$$

$$\theta_i \sim N(0, \theta_{sp}^2)$$

$$\rho_{diff} = \frac{1}{K+1} \cdot E\left[\exp\left\{j \cdot 2 \cdot \pi \cdot (p-q) \cdot \frac{d}{\lambda} \cdot \sin(\varphi_0 + \varphi_i) \cdot \cos(\theta_0 + \theta_i)\right\}\right]$$

$$\begin{aligned} \rho_{diff} &= \frac{1}{K+1} \cdot \int_{-\infty}^{\infty} \int_{-\infty}^{\infty} \exp\left\{j \cdot 2 \cdot \pi \cdot (p-q) \cdot \frac{d}{\lambda} \cdot \sin(\varphi_0 + \varphi_i) \cdot \cos(\theta_0 + \theta_i)\right\} \cdot \\ &\frac{1}{\sqrt{2\pi} \cdot \varphi_{sp}} \cdot \exp\left\{-\frac{\varphi_i^2}{2 \cdot \varphi_{sp}^2}\right\} \cdot \frac{1}{\sqrt{2\pi} \cdot \theta_{sp}} \cdot \exp\left\{-\frac{\theta_i^2}{2 \cdot \theta_{sp}^2}\right\} d\varphi_i d\theta_i \end{aligned}$$

$$\begin{aligned} \Leftrightarrow \rho_{diff} &= \frac{1}{K+1} \cdot \int_{-\infty}^{\infty} \int_{-\infty}^{\infty} \exp\left\{j \cdot 2 \cdot \pi \cdot (p-q) \cdot \frac{d}{\lambda} \cdot [\sin(\varphi_0) + \varphi_i \cdot \cos(\varphi_0)] \cdot [\cos(\theta_0) - \theta_i \cdot \sin(\theta_0)]\right\} \cdot \\ &\frac{1}{\sqrt{2\pi} \cdot \varphi_{sp}} \cdot \exp\left\{-\frac{\varphi_i^2}{2 \cdot \varphi_{sp}^2}\right\} \cdot \frac{1}{\sqrt{2\pi} \cdot \theta_{sp}} \cdot \exp\left\{-\frac{\theta_i^2}{2 \cdot \theta_{sp}^2}\right\} d\varphi_i d\theta_i \end{aligned}$$

$$\begin{aligned} \Leftrightarrow \rho_{diff} &= \frac{1}{K+1} \cdot \exp\left\{j \cdot 2\pi \cdot (p-q) \cdot \frac{d}{\lambda} \cdot \sin(\varphi_0) \cdot \cos(\theta_0)\right\} \cdot \\ &\int_{-\infty}^{\infty} \exp\left\{-j \cdot 2\pi \cdot (p-q) \cdot \frac{d}{\lambda} \cdot \theta_i \cdot \sin(\varphi_0) \cdot \sin(\theta_0)\right\} \cdot \\ &\int_{-\infty}^{\infty} \exp\left\{j \cdot 2 \cdot \pi \cdot (p-q) \cdot \frac{d}{\lambda} \cdot \varphi_i [\cos(\varphi_0) \cdot \cos(\theta_0) - \theta_i \cdot \cos(\varphi_0) \cdot \sin(\theta_0)]\right\} \cdot \\ &\frac{1}{\sqrt{2\pi} \cdot \varphi_{sp}} \cdot \exp\left\{-\frac{\varphi_i^2}{2 \cdot \varphi_{sp}^2}\right\} \cdot \frac{1}{\sqrt{2\pi} \cdot \theta_{sp}} \cdot \exp\left\{-\frac{\theta_i^2}{2 \cdot \theta_{sp}^2}\right\} d\varphi_i d\theta_i \end{aligned}$$

$$\begin{aligned}
 I_1 &= \frac{1}{\sqrt{2\pi} \cdot \varphi_{sp}} \cdot \int_{-\infty}^{\infty} \exp \left\{ j \cdot 2\pi \cdot (p-q) \cdot \frac{d}{\lambda} \cdot \varphi_i [\cos(\varphi_0) \cdot \cos(\theta_0) - \theta_i \cdot \cos(\varphi_0) \cdot \sin(\theta_0)] \right\} \\
 &\quad \cdot \exp \left\{ -\frac{\varphi_i^2}{2 \cdot \varphi_{sp}^2} \right\} \cdot d\varphi_i \\
 \Leftrightarrow \rho_{diff} &= \frac{1}{K+1} \cdot \exp \left\{ j \cdot 2\pi \cdot (p-q) \cdot \frac{d}{\lambda} \cdot \sin(\varphi_0) \cdot \cos(\theta_0) \right\} \cdot \\
 &\quad \int_{-\infty}^{\infty} \exp \left\{ -j \cdot 2\pi \cdot (p-q) \cdot \frac{d}{\lambda} \cdot \theta_i \cdot \sin(\varphi_0) \cdot \sin(\theta_0) \right\} \cdot I_1 \cdot \\
 &\quad \frac{1}{\sqrt{2\pi} \cdot \theta_{sp}} \cdot \exp \left\{ -\frac{\theta_i^2}{2 \cdot \theta_{sp}^2} \right\} \cdot d\theta_i
 \end{aligned} \tag{A-22}$$

solve for I_1 :

$$\Leftrightarrow I_1 = \frac{1}{\sqrt{2\pi} \cdot \varphi_{sp}} \cdot \int_{-\infty}^{\infty} \exp \{-a\varphi_i\} \cdot \exp \{-b\varphi_i^2\} \cdot d\varphi_i$$

$$\text{where: } a = -j \cdot 2\pi \cdot (p-q) \cdot \frac{d}{\lambda} \cdot [\cos(\varphi_0) \cdot \cos(\theta_0) - \theta_i \cdot \cos(\varphi_0) \cdot \sin(\theta_0)]$$

$$b = \frac{1}{2 \cdot \varphi_{sp}^2}$$

$$\Leftrightarrow I_1 = \exp \left\{ b \cdot \left(\frac{a}{2 \cdot b} \right)^2 \right\} \cdot \frac{1}{\sqrt{2\pi} \cdot \varphi_{sp}} \cdot \int_{-\infty}^{\infty} \exp \left\{ -b \cdot \left(\varphi_i + \frac{a}{2 \cdot b} \right)^2 \right\} \cdot \varphi_i$$

from equation A-7 to equation A-9, it can be deduced that:

$$\begin{aligned}
 I_1 &= \exp \left\{ b \cdot \left(\frac{a}{2 \cdot b} \right)^2 \right\} = \exp \left\{ -\frac{1}{2} \cdot \left[2\pi \cdot (p-q) \cdot \frac{d}{\lambda} \cdot (\cos(\varphi_0) \cdot \cos(\theta_0) - \theta_i \cdot \cos(\varphi_0) \cdot \sin(\theta_0)) \cdot \varphi_{sp} \right]^2 \right\} \\
 \Leftrightarrow I_1 &= \exp \left\{ b \cdot \left(\frac{a}{2 \cdot b} \right)^2 \right\} = \exp \left\{ -\frac{1}{2} \cdot \left(2\pi \cdot (p-q) \cdot \frac{d}{\lambda} \cdot \varphi_{sp} \right)^2 \cdot \left[\frac{\cos^2(\varphi_0) \cdot \cos^2(\theta_0) -}{2 \cdot \cos(\varphi_0) \cdot \cos(\theta_0) \cdot \theta_i \cdot \cos(\varphi_0) \cdot \sin(\theta_0) +} \right] \right\}
 \end{aligned} \tag{A-23}$$

A-23 in A-22:

$$\begin{aligned}
 \Leftrightarrow \rho_{diff} &= \frac{1}{K+1} \cdot \exp \left\{ j \cdot 2\pi \cdot (p-q) \cdot \frac{d}{\lambda} \cdot \sin(\varphi_0) \cdot \cos(\theta_0) \right\} \cdot \frac{1}{\sqrt{2\pi} \cdot \theta_{sp}} \cdot \\
 &\quad \int_{-\infty}^{\infty} \exp \left\{ -j \cdot 2\pi \cdot (p-q) \cdot \frac{d}{\lambda} \cdot \theta_i \cdot \sin(\varphi_0) \cdot \sin(\theta_0) \right\} \cdot I_1 \cdot \exp \left\{ -\frac{\theta_i^2}{2 \cdot \theta_{sp}^2} \right\} \cdot d\theta_i
 \end{aligned}$$

$$\begin{aligned}
 \Leftrightarrow \rho_{diff} &= \frac{1}{K+1} \cdot \exp\left\{j \cdot 2\pi \cdot (p-q) \cdot \frac{d}{\lambda} \cdot \sin(\varphi_0) \cdot \cos(\theta_0)\right\} \cdot \exp\left\{-\frac{1}{2} \cdot \left[2\pi \cdot (p-q) \cdot \frac{d}{\lambda} \cdot \varphi_{sp}\right]^2 \cdot \cos^2(\varphi_0) \cdot \cos^2(\theta_0)\right\} \\
 &\quad \frac{1}{\sqrt{2\pi} \cdot \theta_{sp}} \cdot \int_{-\infty}^{\infty} \exp\left\{-\left[j \cdot 2\pi \cdot (p-q) \cdot \frac{d}{\lambda} \cdot \sin(\varphi_0) \cdot \sin(\theta_0) + 2 \cdot \cos^2(\varphi_0) \cdot \cos(\theta_0) \cdot \sin(\theta_0)\right] \cdot \theta_i\right\} \\
 &\quad \exp\left\{-\frac{1}{2 \cdot \theta_{sp}^2} \cdot \theta_i^2 - \frac{1}{2} \cdot \left[2\pi \cdot (p-q) \cdot \frac{d}{\lambda} \cdot \varphi_{sp}\right]^2 \cdot \cos^2(\varphi_0) \cdot \sin^2(\theta_0) \cdot \theta_i^2\right\} \cdot d\theta_i
 \end{aligned} \tag{A-24}$$

$$I_2 = \frac{1}{\sqrt{2\pi} \cdot \theta_{sp}} \cdot \int_{-\infty}^{\infty} \exp\{-a' \cdot \theta_i\} \cdot \exp\left\{-\frac{b' \cdot \theta_i^2}{2 \cdot \theta_{sp}^2}\right\} \cdot d\theta_i$$

where: $a' = j \cdot 2\pi \cdot (p-q) \cdot \frac{d}{\lambda} \cdot \sin(\varphi_0) \cdot \sin(\theta_0) + 2 \cdot \cos^2(\varphi_0) \cdot \cos(\theta_0) \cdot \sin(\theta_0)$

$$b' = 1 + \frac{1}{2} \left[2\pi \cdot (p-q) \cdot \frac{d}{\lambda} \cdot \varphi_{sp}\right]^2 \cdot \cos^2(\varphi_0) \cdot \sin^2(\theta_0) \cdot 2 \cdot \theta_{sp}^2$$

Completing the square in the integral I_2 leads to:

$$I_2 = \exp\left\{\frac{1}{2} \cdot \frac{\theta_{sp}^2 \cdot a'^2}{b'}\right\} \cdot \frac{1}{\sqrt{2\pi} \cdot \theta_{sp}} \cdot \int_{-\infty}^{\infty} \exp\left\{-\frac{b' \cdot \left(\theta_i + \frac{\theta_{sp}^2 \cdot a'}{b'}\right)^2}{2 \cdot \theta_{sp}^2}\right\} \cdot d\theta_i$$

Changing the integration variable:

$$x = \theta_i + \frac{\theta_{sp}^2 \cdot a'}{b'}$$

$$\Rightarrow I_2 = \exp\left\{\frac{1}{2} \cdot \frac{\theta_{sp}^2 \cdot a'^2}{b'}\right\} \cdot \frac{1}{\sqrt{2\pi} \cdot \theta_{sp}} \cdot \int_{-\infty}^{\infty} \exp\left\{-\frac{b' \cdot x^2}{2 \cdot \theta_{sp}^2}\right\} \cdot dx$$

Solve for I_2^2 and change into polar coordinates ($x = r \cdot \cos(\alpha)$ and $y = r \cdot \sin(\alpha)$):

$$I_2^2 = \exp\left\{\frac{1}{2} \cdot \frac{\theta_{sp}^2 \cdot a'^2}{b'}\right\}^2 \cdot \left(\frac{1}{\sqrt{2\pi} \cdot \theta_{sp}}\right)^2 \cdot \int_{-\infty}^{\infty} \exp\left\{-\frac{b' \cdot x^2}{2 \cdot \theta_{sp}^2}\right\} \cdot dx \cdot \int_{-\infty}^{\infty} \exp\left\{-\frac{b' \cdot y^2}{2 \cdot \theta_{sp}^2}\right\} \cdot dy$$

$$\Leftrightarrow I_2^2 = \exp\left\{\frac{1}{2} \cdot \frac{\theta_{sp}^2 \cdot a'^2}{b'}\right\}^2 \cdot \left(\frac{1}{\sqrt{2\pi} \cdot \theta_{sp}}\right)^2 \cdot \int_0^{2\pi} \int_0^{\infty} r \cdot \exp\left\{-\frac{b'}{2 \cdot \theta_{sp}^2} \cdot r^2\right\} \cdot dr \cdot d\alpha$$

$$\Leftrightarrow I_2^2 = \exp\left\{\frac{1}{2} \cdot \frac{\theta_{sp}^2 \cdot a'^2}{b'}\right\}^2 \cdot \left(\frac{1}{\sqrt{2\pi} \cdot \theta_{sp}}\right)^2 \cdot \int_0^{2\pi} \left[-\frac{\theta_{sp}^2}{b'} \cdot \exp\left\{-\frac{b'}{2 \cdot \theta_{sp}^2} \cdot r^2\right\}\right]_0^{\infty} \cdot d\alpha$$

$$\Leftrightarrow I_2^2 = \exp\left\{\frac{1}{2} \cdot \frac{\theta_{sp}^2 \cdot a'^2}{b'}\right\}^2 \cdot \left(\frac{1}{\sqrt{2\pi} \cdot \theta_{sp}}\right)^2 \cdot 2\pi \cdot \frac{\theta_{sp}^2}{b'}$$

$$\Leftrightarrow I_2 = \exp\left\{\frac{1}{2} \cdot \frac{\theta_{sp}^2 \cdot a'^2}{b'}\right\} \cdot \sqrt{\frac{1}{b'}} \quad (\text{A-25})$$

A-25 in A-24:

$$\rho_{diff} = \frac{1}{K+1} \cdot \exp\left\{j \cdot 2\pi \cdot (p-q) \cdot \frac{d}{\lambda} \cdot \sin(\varphi_0) \cdot \cos(\theta_0)\right\} \cdot \exp\left\{-\frac{1}{2} \cdot \left[2\pi \cdot (p-q) \cdot \frac{d}{\lambda} \cdot \varphi_{sp}\right]^2 \cdot \cos^2(\varphi_0) \cdot \cos^2(\theta_0)\right\} \cdot \exp\left\{\frac{1}{2} \cdot \frac{\theta_{sp}^2 \cdot a'^2}{b'}\right\} \cdot \sqrt{\frac{1}{b'}} \quad (\text{A-26})$$

where: $a' = 2 \cdot \cos^2(\varphi_0) \cdot \cos(\theta_0) \cdot \sin(\theta_0) + j \cdot 2\pi \cdot (p-q) \cdot \frac{d}{\lambda} \cdot \sin(\varphi_0) \cdot \sin(\theta_0)$

$$b' = 1 + \frac{1}{2} \cdot \left[2\pi \cdot (p-q) \cdot \frac{d}{\lambda} \cdot \varphi_{sp}\right]^2 \cdot \cos^2(\varphi_0) \cdot \sin^2(\theta_0) \cdot 2 \cdot \theta_{sp}^2$$

References

- [Abdi02] A. Abdi and M. Kaveh, "A Space-Time Correlation Model for Multielement Antenna Systems in Mobile Fading Channels", *IEEE Journal on Selected Areas in Communications*, Vol. 20, No. 3, April 2002, pp. 550-560
- [Abend70] K. Abend, "Statistical Detection for Communication Channels with Intersymbol Interference", *Proceedings of the IEEE*, Vol. 58, No. 5, May 1970, pp. 779-785
- [Ada86] F. Adachi, M.T. Feeney, A.G. Williamson and J.D. Parsons, "Crosscorrelation between the envelopes of 900MHz signals received at a mobile radio base station site", *IEE Proceedings F: Radar and Signal Processing*, Vol. 133, No. 6, October 1986, pp. 506-512
- [ADAP99] Adaptive Broadband, "AB Access", Adaptive Broadband, <http://www.adaptivebroadband.com/datasheets/abflyer2.pdf>, visited: July 26, 1999
- [Albert67] A.E. Albert and L.S. Gardner, "Stochastic Approximation and Nonlinear Regression", MIT Press, Cambridge, 1967
- [Alamo98] S.M. Alamouti, "A Simple Transmit Diversity Technique for Wireless Communications", *IEEE Journal on Selected Areas in Communications*, Vol. 16, No. 8, October 1998, pp. 1451-1458
- [Al-Dha00] N. Al-Dhahir, "The Finite-Length Multi-Input Multi-Output MMSE-DFE", *IEEE Transactions on Signal Processing*, Vol. 48, No. 10, October 2000, pp. 2921-2936
- [And91] S. Anderson, M. Millnert, M. Viberg and B. Wahlberg, "An Adaptive Array for Mobile Communication Systems", *IEEE Transactions on Vehicular Technology*, Vol. 40, No. 1, February 1991, pp. 230-236
- [Ariya99] S. Ariyavisitakul, J.H. Winters and I. Lee, "Optimum Space-Time Processors with Dispersive Interference: Unified Analysis and Required Filter Span", *IEEE Transactions on Communications*, Vol. 47, No. 7, July 1999, pp. 1073-1083
- [Ariya97a] S. Ariyavisitakul, N.R. Sollenberger and L.J. Greenstein, "Tap-Selectable Decision-Feedback Equalization", *IEEE Transactions on Communications*, Vol. 45, No. 12, December 1997, pp. 1497-1500
- [Ariya97b] S. Ariyavisitakul and L.J. Greenstein, "Reduced-Complexity Equalization Techniques for Broadband Wireless Channels", *IEEE Journal on Selected Areas in Communications*, Vol. 15, No. 1, January 1997, pp. 5-15
- [Aszt96] D. Asztély, "On Antenna Arrays in Mobile Communication Systems, Fast Fading and {GSM} Base Station Receiver Algorithms", Royal Institute of Technology, Signals, Sensors and Systems Technical Report IR-S3_SB_9611, Stockholm, Sweden, March 1996

- [Aus67] M.E. Austin, "Decision-feedback equalization for digital communication over dispersive channels", MIT Lincoln Lab., Lexington, MA, USA, Technical Report 437, August 1967
- [Benv84] N. Benvenuto, "Distortion analysis on measuring the impulse response of a system using a cross-correlation method", AT&T Technical Journal, Vol. 63, December 1984, pp. 2171-2192
- [Beny00] A. Benyamin-Seeyar, "Initial PHY Layer System Proposal for Sub 11 GHz BWA", IEEE 802.16 proposal 802.16.3c-00/40r1, 02.11.2000
- [Bitm80] R.R. Bitmead and B.D.O. Anderson, "Performance of adaptive estimation algorithms in dependent random environments", IEEE Transactions on Automated Control, Vol. AC-25, No. 4, August 1980, pp. 788-794
- [Bou02] N. Boubaker, K.B. Letaief and R.D. Murch, "Performance of BLAST Over Frequency-Selective Wireless Communication Channels", IEEE Transactions on Communications, Vol. 50, No. 2, February 2002, pp. 196-199
- [Bull99] Y. Sun, A.R. Nix, D.R. Bull, D. Milford, H. de Beauchesne, R. Sperling and Ph. Rouzet, "Design of a Novel Delayed LMS Decision Feedback Equaliser for HIPERLAN/1 FPGA Implementation", IEEE Vehicular Technology Conference, 1999, Vol. 1, pp. 300-304
- [COST89] COST 207, "Digital land mobile radio communications", COST 207 Final Report, ISBN 92-825-9946-9, 1989
- [Chen93] S. Chen, B. Mulgrew and S. McLaughlin, "Adaptive Bayesian Equalizer with Decision Feedback", IEEE Transactions on Signal Processing, Vol. 41, No. 9, September 1993, pp. 2918-2927
- [Chen95a] S. Chen, S. McLaughlin, B. Mulgrew and P.M. Grant, "Adaptive Bayesian Decision Feedback Equalizer for Dispersive Mobile Radio Channels", IEEE Transactions on Communications, Vol. 43, No. 5, May 1995, pp. 1937-1946
- [Chen95b] S. Chen, S. McLaughlin, P.M. Grant and B. Mulgrew, "Multi-Stage Blind Clustering Equaliser", IEEE Transactions on Communications, Vol. 43, No. 2/3/4, February/March/April 1995, pp. 701-705
- [Chen98] W.Y. Chen, "DSL: Simulation Techniques and Standards Development for Digital Subscriber Line Systems", Macmillan Technical Publishing, ISBN 1-57870-017-5, 1998
- [Chuah00] C-N. Chuah, G. J. Foschini, R. A. Valenzuela, D. Chizhik, J. Ling, and J. M. Kahn, "Capacity Growth of Multi-Element Arrays in Indoor and Outdoor Wireless Channels", IEEE Wireless Communication and Networking Conference, Chicago, IL, USA, September 2000

- [Choi99a] I.T. Lu and J.S. Choi, "Space-Time Processing for Broadband Multi-Channel Communication Systems Using Smart Antennas at Both Transmitter and Receiver", IEEE International Conference on Communications (ICC), Vancouver, Canada, Vol. 1, June 1999, pp. 1-5
- [Choi99b] I.T. Lu and J.S. Choi, "Broadband Smart Antenna Technique for both Transmitter and Receiver Using Generalized Zero Forcing Approach", IEEE Vehicular Technology Conference (VTC), Houston, Texas, USA, Vol. 1, May 1999, pp. 632-636
- [Choi98] J.S. Choi, "Multiple Access Smart Antenna Systems at Both Transmitter and Receiver for TDD and FDD Wireless Communications", PhD dissertation, Polytechnic University, Brooklyn, New York, USA, December 1998
- [Cros00] D. Crosby, "Propagation modelling for directional fixed wireless access systems", PhD thesis, University of Cambridge, Department of Engineering, U.K., January 2000
- [Dane96] B. Daneshrad and L.J. Cimini, "Equalization Requirements for 30 MBPS Indoor Wireless Data Transmission", IEEE Vehicular Technology Conference (VTC), Vol. 1, Atlanta, Georgia, USA, April 1996, pp. 71-75
- [Dege01] C.M. Degen, C.M. Walke, A. Lecomte and B. Rembold, "Adaptive MIMO Techniques for the UTRA-TDD Mode", IEEE Vehicular Technology Conference (VTC), Vol. 1, Rhodes, Greece, May 2001, pp. 108-112
- [Dou98] S.C. Douglas, Q. Zhu and K.F. Smith, "A Pipelined LMS Adaptive FIR Filter Architecture Without Adaptation Delay", IEEE Transactions on Signal Processing, vol. 46, No. 3, March 1998, pp. 775-779
- [Duel92] A. Duel-Hallen, "Equalizers for Multiple Input/Multiple Output Channels and PAM Systems with Cyclostationary Input Sequences", IEEE Journal on Selected Areas in Communications, Vol. 10, No. 3, April 1992, pp. 630-639
- [Duel95] A. Duel-Hallen, "A Family of Multiuser Decision-Feedback Detectors for Asynchronous Code-Division Multiple-Access Channels", IEEE Transactions on Communications, Vol. 43, No. 2/3/4, February/March/April 1995, pp. 421-434
- [Dut99] A. Dutta-Roy, "Bringing home the internet", IEEE Spectrum, Vol. 36, No. 3, March 1999, pp. 32-38
- [Ekl02] C. Eklund, R.B. Marks, K.L. Standwood and S. Wang, "IEEE Standard 802.16: A Technical Overview of the WirelessMANTM Air Interface for Broadband Wireless Access", IEEE Communications Magazine, June 2002, pp. 98-107
- [Erceg01] V. Erceg, K.V.S. Hari, M.S. Smith, K.P. Sheikh, C. Tappenden, J.M. Costa, D.S. Baum and C. Bushue, "Channel Models for Fixed Wireless Applications", IEEE 802.16. proposal 802.16.3c-01/29, 19.01.2001

- [Erceg99] L.J. Greenstein and V. Erceg, "Gain Reductions Due to Scatter on Wireless Paths with Directional Antennas", *IEEE Communications Letters*, Vol. 3, No. 6, June 1999, pp. 169-171
- [Erceg97] V. Erceg, S. Fortune, J. Ling, A. Rustako, R. Valenzuela, "Comparisons of a Computer-Based Propagation Prediction Tools with Experimental Data Collected in Urban Microcellular Environments", *IEEE Journal on Selected Areas in Communications*, Vol 15., No. 4, May 1997, pp. 667-676
- [Ert98] R.B. Ertel, P. Cardieri, K.W. Sowerby, T.S. Rappaport and J.H. Reed, "Overview of Spatial Channel Models for Antenna Array Communication Systems", *IEEE Personal Communications Magazine*, Vol. 5, No. 1, February 1998, pp. 10-22
- [Evans01] J.V. Evans, "Communication Satellite Systems for High-Speed Internet Access", *IEEE Antennas and Propagation Magazine*, Vol. 43, No. 5, October 2001, pp. 11-22
- [Falc78] D.D. Falconer and L. Ljung, "Application of fast Kalman estimation to adaptive equalization", *IEEE Transactions on Communications*, Vol. COM-26, No. 10, October 1978, pp. 1439-1446
- [Falc99] D. Falconer and R. Saini, "Equalization Requirements for Millimeter Wave Fixed Broadband Wireless Access Systems", Contribution to IEEE 802.16 working group, IEEE802.16pc-99/28, Aug. 18, 1999
- [Far97] C. Farsakh, "Raummultiplex mit intelligenten Antennen in zellularen Mobilfunksystemen", (in German), PhD Dissertation, TU-München, München, Germany, ISBN 3-933083-20-6, December 1997
- [Fech94] S.A. Fechtel and H. Meyr, "Optimal Parametric Feedforward Estimation of Frequency-Selective Fading Radio Channels", *IEEE Transactions on Communications*, Vol. 42, No. 2/3/4, February/March/April 1994, pp. 1639-1650
- [Fev98] I.J. Fevrier, S.B. Gelfand and M.P. Fitz, "Fast Computation of Efficient Decision Feedback Equalizers for High Speed Wireless Communications", *IEEE Int'l Conf. on Acoustic, Speech and Signal Processing*, Vol. 4, 1998, pp. 3493-3496
- [Fev99] I.J. Fevrier, S.B. Gelfand and M.P. Fitz, "Reduced Complexity Decision Feedback Equalization for Multipath Channels with Large Delay Spreads", *IEEE Transactions on Communications*, Vol. 47, No. 6, June 1999, pp. 927-937
- [Forn72] G.D. Forney, "Maximum-Likelihood Sequence Estimation of Digital Sequences in the Presence of Intersymbol Interference", *IEEE Transactions on Information Theory*, Vol. It-18, No. 3, May 1972, pp. 363-378
- [Fort95] S.J. Fortune, D.M. Gay, B.W. Kernighan, O. Landron, R.A. Valenzuela and M.H. Wright, "WISE design of indoor wireless systems: practical computation and optimization", *IEEE Computational Science and Engineering*, Vol. 2, No. 1, Spring, 1995, pp. 58-68

- [Fosch96] G.J. Foschini, "Layered Space-Time Architecture for Wireless Communication in a Fading Environment When Using Multiple Antennas", Bell Labs Technical Journal, Vol. 1, No. 2, Autumn 1996, pp. 41-59
- [Fosch98] G.J. Foschini and M.J. Gans, "On Limits of Wireless Communications in a Fading Environment when using Multiple Antennas", Wireless Personal Communications, Vol. 6, 1998, pp. 311-335
- [Fosch99] G.J. Foschini, G.D. Golden, R.A. Valenzuela and P.W. Wolniansky, "Simplified Processing for High Spectral Efficiency Wireless Communication Employing Multi-Element Arrays", IEEE Journal on Selected Areas in Communications, Vol. 17, No. 11, November 1999, pp. 1841-1852
- [Fuhl98] J. Fuhl, A.F. Molish, E. Bonek, "Unified channel model for mobile radio systems with smart antennas", IEE Proc. Radar, Sonar Navigation, Vol. 145, No. 1, February 1998, pp. 32-41
- [Gib97] J.D. Gibson, "The Communications Handbook", CRC Press, ISBN 0-8493-8349-8, 1997
- [Gold99] G.D. Golden, C.J. Foschini, R.A. Valenzuela and P.W. Wolniansky, "Detection algorithm and initial laboratory results using V-BLAST space-time communication architecture", Electronics Letters, Vol. 35, No. 1, January 1999, pp. 14-16
- [Goda74] D.N. Godard, "Channel Equalization Using a Kalman Filter for Fast Data Transmission", IBM Journal of Research and Development, Vol. 18, May 1974, pp. 267-273
- [Goda80] D.N. Godard, "Self-Recovering Equalization and Carrier Tracking in Two-Dimensional Data Communication Systems", IEEE Transactions on Communications, Vol. COM-28, No. 11, November 1980, pp. 1867-1875
- [Godar97] L.C. Godara, "Application of Antenna Arrays to Mobile Communications, Part II: Beam-Forming and Direction-of-Arrival Considerations", Proceedings of the IEEE, Vol. 85, No. 8, August 1997, pp. 1195-1245
- [Ham99] J.S. Hammerschmidt, A.A. Hutter and C. Drewes, "Comparison of Single Antenna, Selection Combining, and Optimum Combining Reception at the Vehicle", IEEE Vehicular Technology Conference (VTC) Fall, Amsterdam, Netherland, September 1999, pp. 11-16
- [Ham00] J.S. Hammerschmidt, "Adaptive Space and Space-Time Signal Processing for High-Rate Mobile Data Receivers", PhD Dissertation, TU-München, München, Germany, June 2000
- [Hay96] S. Haykin, "Adaptive Filter Theory – Third Edition", Prentice Hall, ISBN 0-13-322760-X, 1996
- [IEEE802] IEEE WirelessMAN 802.16, <http://www.ieee802.org/16/>, visited 01.01.2002

- [IEEE8022] IEEE WirelessMAN 802.16 task group 2 (coexistence), <http://www.ieee802.org/16/tg2/index.html>, visited 11.04.2002
- [Kav85] M Kavehrad and J. Salz, "Cross-Polarization Cancellation and Equalization in Digital Transmission Over Dually Polarized Multipath Fading Channels", AT&T Technical Journal, Vol. 64, No. 10, December 1985, pp. 2211-2245
- [Khat01] B.S. Khatri, "Effect on Capacity of Clustering in Indoor MIMO Channels", IEE Seminar MIMO: Communications Systems from Concept to Implementations, December 2001, pp. 15/1-15/7
- [Kim99] B. Kim, N.K. Shankaranarayanan, P.S. Henry, K. Schlosser and T. Fong, "The AT&T Labs broadband fixed wireless field experiment", IEEE Communications Magazine, Vol. 37, No. 10, October 1999, pp. 56-62
- [Kom02] C. Kominakis, C. Fragouli, A.H. Sayed and R.D. Wesel, "Multi-Input Multi-Output Fading Channel Tracking and Equalization Using Kalman Estimation", IEEE Transactions on Signal Processing, Vol. 50, No. 5, May 2002, pp. 1065-1076
- [Lee73] W.C.Y. Lee, "Effects on Correlation Between Two Mobile Radio Base-Station Antennas", IEEE Transactions on Communications, Vol. COM-21, No. 11, November 1973, pp. 1214-1224
- [Lee81] D.T.L. Lee, "Recursive least squares ladder estimation algorithms", IEEE Transactions on Acoustic, Speech and Signal Processing, Vol. ASSP-29, No. 3, June 1981, pp. 627-641
- [Lee97] Y. Lee, "Adaptive Equalization and Receiver Diversity of Indoor Wireless Data Communications", PhD dissertation, Stanford University, Stanford, CA, USA, August 1997
- [Lee98a] W.C.Y. Lee, "Spectrum and technology of a wireless local loop system", IEEE Personal Communications, Vol. 5, No. 1, February 1998, pp. 49-54
- [Lee98b] I. Lee, "Optimization of Tap Spacings for the Tapped Delay Line Decision Feedback Equalizer", IEEE Int'l Conf. on Communications, Vol. 1, June 1998, pp. 11-15
- [Lind99] E. Lindskog, "Space-Time Processing and Equalization For Wireless Communications", PhD dissertation, Uppsala University, Signals and Systems, Sweden, June 1999
- [Ling01] J. Ling, D. Chizhik, R. Valenzuela, "Predicting Multi-Element Receive & Transmit Array Capacity Outdoors with Ray Tracing", IEEE Vehicular Technology Conference, Rhodes, Greece, May 2001, pp. 392-394
- [Ling85] F. Ling and J.G. Proakis, "Adaptive Lattice Decision-Feedback Equalizers – Their Performance and Application to Time-Variant Multipath Channels", IEEE Transactions on Communications, Vol. COM-33, No. 4, April 1985, pp. 348-356

- [Lo93] T. Lo, J. Litva and H. Leung, "Estimating the impulse response of indoor radio channels using signal subspace techniques", *IEE Proceedings I: Communications, Speech and Vision*, Vol. 140, No. 3, June 1993, pp. 203-209
- [Lo95] N.W.K. Lo, D.D. Falconer and A.U.H. Sheikh, "Adaptive Equalization for Co-Channel Interference in a Multipath Fading Environment", *IEEE Transactions on Communications*, Vol. 43, No. 2/3/4, February/March/April 1995, pp. 1441-1453
- [Long89] G. Long, F. Ling, J.G. Proakis, "The LMS Algorithm with Delayed Coefficient Adaptation", *IEEE Transactions on Acoustics, Speech and Signal Processing*, Vol. 37, No. 9, September 1989, pp. 1397-1405
- [Loza00] A. Lozano and C. Papadias, "Space-Time Receiver for Wideband BLAST in Rich-Scattering Wireless Channels", *IEEE Vehicular Technology Conference (VTC)*, Vol. 1, Tokyo, Japan, Spring 2000, pp. 186-190
- [Luck65] R.W. Lucky, "Automatic Equalization for Digital Communications", *Bell System Technical Journal*, Vol. 44, No. 4, April 1965, pp. 547-588
- [Luck66] R.W. Lucky, "Techniques for Adaptive Equalization of Digital Communications", *Bell System Technical Journal*, Vol. 45, pp. 255-286
- [Mede99] K.R. Medepalli and N. Mandayam, "Combined Equalization and Cochannel Interference Cancellation for the Downlink Using Tentative Decisions", *IEEE Vehicular Technology Conference (VTC)*, Vol. 1, May 1999, pp. 637-641
- [MeshN02] MeshNetworks Inc, <http://www.meshnetworks.com/>
- [Monz80] R.A. Monzingo and T.W. Miller, "Introduction to Adaptive Arrays", Wiley, ISBN 0-471-05744-4, 1980
- [Mulg96] B. Mulgrew, "Applying Radial Basis Functions", *IEEE Signal Processing Magazine*, Vol. 13, No. 2, March 1996, pp. 50-65
- [Nagu67] J.I. Nagumo and A. Noda, "A learning method for system identification", *IEEE Transactions on Automated Control*, Vol. AC-12, No. 3, June 1967, pp. 282-287
- [Naray96] K.R. Narayanan and L.J. Cimini, "Equalizer Adaptation Algorithms for High-Speed Wireless Communications", *IEEE Vehicular Technology Conference (VTC)*, Vol. 2, 1996, pp. 681-685
- [Ng98a] J.C.L. Ng, K.B. Letaief and R.D. Murch, "Complex Optimal Sequences with Constant Magnitude for Fast Channel Estimation Initialization", *IEEE Transactions on Communications*, Vol. 46, No. 3, March 1998, pp. 305-308
- [Ng98b] J.C.L. Ng, K.B. Letaief and R.D. Murch, "Antenna Diversity Combining and Finite-Tap Decision Feedback Equalization for High-Speed Data Transmission", *IEEE Journal on Selected Areas in Communications*, Vol. 16, No. 8, October 1998, pp. 1367-1375

- [Nicol01] M. Nicoli and U. Spagnolini, "Reduced rank channel estimation and rank order selection for CDMA systems", IEEE International Conference on Communications (ICC), Vol. 9, June 2001, pp. 2737-2741
- [Nix96a] R. Perry, D.R. Bull, A. Nix, "High throughput adaptive DFR for HIPERLAN", IEEE International Symposium on Circuits and Systems, v 2, 1996, p 301-304
- [Nix96b] R. Perry, D.R. Bull, A. Nix, "Adaptive DFE for high data rate applications", IEEE Vehicular Technology Conference, Vol. 2, 1996, pp. 686-690
- [Pap99] Z. Papir and A. Simmonds, "Competing for Throughput in the Local Loop", IEEE Communications Magazine, Vol. 37, No. 5, May 1999, pp. 61-66
- [Par91] J.D. Parsons, A.M.D. Turkmani, "Characterisation of mobile radio signals: model description", IEE Proceedings I: Communications, Speech and Vision, Vol. 138, No. 6, December 1991, pp. 549-556
- [Pir84] G. Pirani and V. Zingarelli, "Adaptive Multiplication-Free Transversal Equalizers with Application to Digital Radio Systems", IEEE Transactions on Communications, Vol. Com-32, No. 9, September 1984, pp. 1025-1033
- [Port00] J.W. Porter and J.A. Thweatt, "Microwave Propagation Characteristics In The MMDS Frequency Band", IEEE International Conference on Communications, New Orleans, LA, USA, June 2000, pp. 1578-1582
- [Press92] W.H. Press, S.A. Teukolsky, W.T. Vetterling and B.P. Flannery, "Numerical Recipes in C – The Art of Scientific Computing – Second Edition", Cambridge University Press, 1992, ISBN 0-521-43108-5
- [Pro91] J.G. Proakis, "Adaptive Equalization for TDMA Digital Mobile Radio", IEEE Transactions on Vehicular Technology, Vol. 40, No. 2, May 1991, pp. 333-341
- [Pro95] J.G. Proakis, "Digital Communications – Third Edition", McGraw-Hill, ISBN 0-07-051726-6, 1995
- [Qure85] S.U.H. Qureshi, "Adaptive Equalization", Proceedings of the IEEE, Vol. 73, No. 9, September 1985, pp. 1349-1387
- [Radia02] Radiant Networks Plc, <http://www.radiantnetworks.com/>
- [Rag93] S.A. Raghavan, J.K. Wolf, L.B. Milstein, L.C. Barbosa, "Nonuniformly spaced tapped-delay-line equalizers", IEEE Transactions on Communications, Vol. 41, No. 9, September 1993, pp. 1290-1295
- [Sal87] A.A.M. Saleh and R.A. Valenzuela, "A Statistical Model for Indoor Multipath Propagation", IEEE Journal on Selected Areas in Communications, Vol. SAC-5, No. 2, February 1987, pp. 128-137
- [Salz94] J. Salz and J.H. Winters, "Effect of Fading Correlation on Adaptive Arrays in Digital Mobile Radio", IEEE Transactions on Vehicular Technology, Vol. 43, No. 4, November 1994, pp. 1049-1057

- [Sar80] D.V. Sarwate and M.B. Pursley, "Crosscorrelation Properties of Pseudorandom and Related Sequences", Proceedings of the IEEE, Vol. 68, No. 5, May 1980, pp. 593-620
- [Say94] A.H. Sayed and T. Kailath, "A State-Space Approach to Adaptive RLS Filtering", IEEE Signal Processing Magazine, Vol. 11, July 1994, pp. 18-60
- [Schulz89] H. Schulze, "Stochastische Modelle und digitale Simulation von Mobilfunkkanälen", (in German), Proc. Kleinheubacher Berichte, Vol. 32, 1989, pp. 473-483
- [Sei94] S.Y. Seidel and T.S. Rappaport, "Site-Specific Propagation Prediction for Wireless In-Building Personal Communication System Design", IEEE Transactions on Vehicular Technology, Vol. 43, No. 4., November 1998, pp. 879-891
- [Sell99a] M.P. Sellars, S.D. Greaves, J. Porter, A. Hopper and W.J. Fitzgerald, "Performance of a fast start-up equalizer for indoor radio", IEEE Symposium on Personal, Indoor & Mobile Radio Communications (PIMRC), Osaka, Japan, September 1999, Vol. 3, pp. 1124-1128
- [Sell99b] M.P. Sellars, "Low Complexity Equalization Techniques for Broadband Indoor Radio", PhD dissertation, University of Cambridge, Department of Engineering, December 1999
- [Shuk91] P.K. Shukla and L.F. Turner, "Channel-estimation-based adaptive DFE for fading multipath radio channels", IEE Proceedings-I: Communications, Speech and Vision, Vol. 138, No. 6, December 1991, pp. 525-543
- [Smee97] J.E. Smee and N.C. Beaulieu, "On the Equivalence of the Simultaneous and Separate MMSE Optimization of a DFE FFF and FBF", IEEE Transactions on Communications, Vol. 45, No. 2, February 1997, pp. 156-158
- [Stein94] B. Steiner and P. Jung, "Optimum and Suboptimum Channel Estimation for the Uplink of CDMA Mobile Radio Systems with Joint Detection", European Transactions on Telecommunications, Vol. 5, No. 1, January-February 1994, pp. 39-50
- [Sue94] N. Suehiro, "A Signal Design without Co-Channel Interference for Approximately Synchronized CDMA Systems", IEEE Journal on Selected Areas in Communications, Vol. 12, No. 5, June 1994, pp. 837-841
- [Tame98] E.K. Tameh and A.R. Nix, "The Use of Measurement Data to Analyse the Performance of Rooftop Diffraction and Foliage Loss Algorithms in a 3-D Integrated Urban/Rural Propagation Model", IEEE Vehicular Technology Conference, Ottawa, Canada, May 1998, pp. 303-307

- [Tar99a] V. Tarokh, A. Naguib, N. Seshadri and A.R. Calderbank, "Combined Array Processing and Space-Time Coding", *IEEE Transactions on Information Theory*, Vol. 45, No. 4, May 1999, pp. 1121-1128
- [Tar99b] V. Tarokh, A. Naguib, N. Seshadri and A.R. Calderbank, "Space-Time Codes for High Data Rate Wireless Communication: Performance Criteria in the Presence of Channel Estimation Errors, Mobility, and Multiple Paths", *IEEE Transactions on Communications*, Vol. 47, No. 2, February 1999, pp. 199-207
- [Tar99c] V. Tarokh, H. Jafarkhani and A.R. Calderbank, "Space-Time Block Codes from Orthogonal Designs", *IEEE Transactions on Information Theory*, Vol. 45, No. 5, July 1999, pp. 1456-1467
- [Tide99] C. Tidestav, "The Multivariable Decision Feedback Equalizer", PhD dissertation, Uppsala University, Signals and Systems, Sweden, 1999
- [Turk91] A.M.D. Turkmani, J.D. Parsons, "Characterisation of mobile radio signals: base station crosscorrelation", *IEE Proceedings I: Communications, Speech and Vision*, Vol. 138, No. 6, December 1991, pp. 557-565
- [UBS01] UBS Product – Fixed Broadband Wireless Access System – MMDS, <http://www.uniquesys.com/res11-broadband-wireless-access.htm>, visited 17.09.2001
- [Usya01] M. Usyal and C.N. Georghiadis, "Effect of spatial fading correlation on performance of space-time codes", *IEE Electronics Letters*, Vol. 37, No. 3, February 2001, pp. 181-183
- [Vande00] P. Vandenameele, L. Van Der Perre, M.G.E. Engels, B. Gyselinckx and H.J. De Man, "A Combined OFDM/SDMA Approach", *IEEE Journal on Selected Areas in Communications*, Vol. 18, No. 11, November 2000, pp. 2312-2321
- [Veen88] B.D. Van Veen and K.M. Buckley, "Beamforming: A Versatile Approach to Spatial Filtering", *IEEE Acoustics, Speech and Signal Processing Magazine*, April 1988, pp. 4-24
- [Ver02a] A. Verstak, J. He, L.T. Watson, N. Ramakrishnan, C.A. Shaffer, T.S. Rappaport, C.R. Anderson, K. Bae, J. Jiang and W.H. Tranter, "S⁴W: Globally Optimized Design of Wireless Communication Systems", *Proceedings of the Next Generation Software (NGS) Workshop, 16th International Parallel and Distributed Processing Symposium (IPDPS'02)*, Fort Lauderdale, FL, Apr 2002
- [Ver02b] J. He, A. Verstak, L.T. Watson, T.S. Rappaport, C.R. Anderson, N. Ramakrishnan, C.A. Shaffer, W.H. Tranter, K. Bae and J. Jiang, "Global Optimization of Transmitter Placement in Wireless Communication Systems", *Proceedings of the High Performance Computing Symposium, Advanced Simulation Technologies Conference*, San Diego, CA, USA, Apr 2002

- [Verdu98] S. Verdu, "Multiuser Detection", Cambridge University Press, ISBN 0-521-59373-5, 1998
- [Vit67] A.J. Viterbi, "Error Bounds for Convolutional Codes and an Asymptotic Optimum Decoding Algorithm", IEEE Transactions on Information Theory, Vol. It-13, No. 2, April 1967, pp. 260-269
- [Wid66] B. Widrow, "Adaptive Filters, I: Fundamentals", Stanford Electronics Laboratory, Stanford University, Standord, CA, Technical Report No. 6764-6, December 1966
- [Wid67] B. Widrow, P.E. Mantey, L.J. Griffiths and B.B. Goode, "Adaptive Antenna Systems", IEEE Proceedings, Vol. 55, No. 12, December 1967, pp. 2143-2159
- [Wint84] J.H. Winters, "Optimum Combining in Digital Mobile Radio with Cochannel Interference", IEEE Journal on Selected Areas in Communications, Vol. SAC-2, No. 4, July 1984, pp. 528-539
- [Wint87a] J.H. Winters, "On the Capacity of Radio Communications Systems with Diversity in a Rayleigh Fading Environment", IEEE Journal on Selected Areas in Communications, Vol. SAC-5, No. 5, June 1987, pp. 871-878
- [Wint87b] J.H. Winters, "Optimum Combining for Indoor Radio Systems with Multiple Users", IEEE Transactions on Communications, Vol. COM-35, No. 11, November 1987, pp. 1222-1230
- [Woln98] P.W. Wolniansky, G.J. Foschini, G.D. Golden and R.A. Valenzuela, "V-BLAST: An Architecture for Realizing Very High Data Rates Over the Rich-Scattering Wireless Channel" Proceedings of the International Symposium on Signals, Systems and Electronics (ISSSE), Pisa, Italy, September 1998, pp. 295-300
- [Wright98] Margaret H. Wright, "Optimization methods for base station placement in wireless applications", IEEE Vehicular Technology Conference (VTC), Ottawa, Ontario, Canada, May 1998, pp. 387-391
- [Yos99] H. Yoshimura, K. Sato and N. Takachio, "Future Photonic Transport Networks Based on WDM Technologies", IEEE Communications Magazine, Vol. 37, No. 2, February 1999, pp. 74-81
- [Yoon93] Y.C. Yoon, R. Kohno and H. Imai, "A Spread-Spectrum Multiaccess System with Cochannel Interference Cancellation for Multipath Fading Channels", IEEE Journal on Selected Areas in Communications, Vol. 11, No. 7, September 1993, 1067-1075
- [Young52] W.R. Young, "Comparison of mobile radio transmission at 150, 450, 900 and 3700 MC", Bell System Technical Journal, Vol. 31, No. 6, 1952, pp. 1068-1085
- [Zet97] P. Zetterberg, "Mobile Cellular Communications with Base Station Antenna Arrays: Spectrum Efficiency, Algorithms and Propagation Models", PhD Dissertation, Royal Institute of Technology, Stockholm, Sweden, June 1997